

Insight into physicochemical structure of soil organic matter by cation interaction and nanothermal properties

by

Yamuna Kunhi Mouvenchery (MSc.)
from Kerala, India

Accepted Dissertation thesis for the partial fulfilment of the requirements for a
Doctor of Natural Sciences
Fachbereich 7: Natur- und Umweltwissenschaften
Universität Koblenz-Landau

Thesis Examiners:

Prof. Dr. Gabriele E. Schaumann (University Koblenz-Landau, Germany)

Prof. Dr. Sören Thiele-Bruhn (University Trier, Germany)

PD Dr. Marko Bertmer (University Leipzig, Germany)

Supervisor: Prof. Dr. Gabriele E. Schaumann (University Koblenz-Landau, Germany)

Co-supervisor: PD Dr. Jiri Kucerik (Universität Koblenz-Landau, Germany)

Date of the oral examination: 20-08-2013

Declaration

I hereby declare that I autonomously conducted the work shown in this Ph.D thesis entitled “Insight into physicochemical structure of soil organic matter by cation interaction and nanothermal properties”. All used assistances and involved contributors are clearly declared.

This thesis has never been submitted elsewhere for an exam, as thesis or for evaluation in a similar context; to any department of this university or any scientific institution.

Place, Date	Signature
-------------	-----------

The following parts of this thesis are published or submitted for publications.

Chapter 2 has been published:

Kunhi Mouvenchery, Y., Kucerik, J., Diehl, D., Schaumann, G.E. (2012) *Cation-mediated cross-linking in natural organic matter: a review*. Reviews in Environmental Science and Biotechnology 11: 41-54

Chapter 3 has been published:

Kunhi Mouvenchery, Y., Jäger, A., Aquino, A.J.A., Tunega, D, Diehl, D., Bertmer, M., Schaumann, G.E. (2013) *Restructuring of a peat in interaction with multivalent cations: Effect of cation type and aging time*. PLoS ONE 8(6): e65359. doi:10.1371/journal.pone.0065359

Chapter 6 has been published:

Schaumann, G.E., Kunhi Mouvenchery, Y. (2012) *Potential of AFM–nanothermal analysis to study the microscale thermal characteristics in soils and natural organic matter (NOM)*. Journal of Soils and Sediments 12 (1): 48-62

Chapter 7 has been submitted to the journal, Geochimica et Cosmochimica Acta:

Kunhi Mouvenchery, Y., Miltner, A., Schurig, C., Kästrner, M, Schaumann, G.E. (submitted, 2013) *Linking Atomic Force Microscopy with nanothermal analysis to assess microspatial distribution of materials in young soils*. Geochimica et Cosmochimica Acta

Acknowledgements

I gratefully acknowledge Prof. Dr. G.E. Schaumann for her excellent guidance, without which I would not have been able to finish this doctoral work. I extend my gratitude to Dr. Jiri Kucerik, my second supervisor, also for being a good friend to me. This work was funded by German Research Foundation (DFG) within the priority program, SPP 1315, Biogeochemical Interfaces in Soils.

I would like to thank current and previous colleagues in the Department of Environmental and Soil Chemistry for their invaluable helps and discussions. Special thanks go to Dr. Dörte Diehl, Mrs. Priya Mary Abraham, Mrs. Karin Mayer and Dr. Wolfgang Fey and to our secretary Mrs. Angelika Horderle for her innumerable helps and concerns.

It is beyond words to express my gratitude to the families of Kulendrarajah and Ravichchandran, for their affection and care during my days in Landau. Last, but not least, I would like to acknowledge the unutterable support and encouragement from my family.

To my teachers

Table of contents

1. GENERAL INTRODUCTION.....	11
1.1 SOIL ORGANIC MATTER AND ITS STRUCTURE.....	12
1.2 PRINCIPLES OF NANOTHERMAL ANALYSIS.....	26
1.3 WORKING HYPOTHESIS.....	27
1.4 STRUCTURE OF THE THESIS.....	30
2. CATION-MEDIATED CROSS-LINKING IN NATURAL ORGANIC MATTER: A REVIEW.....	38
3. RESTRUCTURING OF A PEAT IN INTERACTION WITH MULTIVALENT CATIONS: EFFECT OF CATION TYPE AND AGING TIME.....	53
4. CATION MEDIATED CROSS LINKING IN SOIL ORGANIC MATTER: ROLE OF HYDRATION SHELL.....	80
4.1 INTRODUCTION.....	81
4.2 MATERIALS AND METHODS.....	82
4.3 RESULTS AND DISCUSSIONS.....	84
4.4 CONCLUSIONS.....	93
5. ORGANO-MINERAL ASSOCIATIONS IN ARTIFICIAL SOIL SAMPLES: CHEMICAL QUALITY OF ORGANIC MATTER AND DEVELOPMENT OF PHYSICOCHEMICAL STRUCTURE.....	94
5.1 INTRODUCTION.....	95
5.2 MATERIALS AND METHODS.....	95
5.3 RESULTS AND DISCUSSIONS.....	97
5.4 CONCLUSIONS.....	102

6.	POTENTIAL OF AFM–NANOTHERMAL ANALYSIS TO STUDY THE MICROSCALE THERMAL CHARACTERISTICS IN SOILS AND NATURAL ORGANIC MATTER (NOM).....	104
7.	LINKING ATOMIC FORCE MICROSCOPY WITH NANOTHERMAL ANALYSIS TO ASSESS MICROSPATIAL DISTRIBUTION OF MATERIALS IN YOUNG SOILS.....	122
8.	CONCLUSIONS AND SYNTHESIS.....	154
	8.1 CATION-MEDIATED CROSS-LINKING IN SOM: FURTHER IMPLICATIONS.....	155
	8.2 AFM-NTA TO TRACE THERMAL PROPERTIES RELEVANT TO OM IN LOW-ORGANIC SOILS.....	157
	8.3 THE ‘CATION EXPERIMENTAL STRATEGY’.....	160
	8.4 IMPLICATIONS OF STRUCTURAL REORGANISATION IN OM DURING CATION TREATMENT.....	160
	8.5 ONGOING RESERACH AND OPEN QUESTIONS.....	166
9	ANNEX.....	170

Abstract

Structure of soil organic matter (SOM) is a hot topic of discussion among scientific community for several decades. The mostly discussed models, among many, are polymer model and supramolecular model. While the former considers SOM as macromolecules consisting of amorphous and crystalline domains, the latter explains SOM as a physicochemical entity dominated by weak hydrophobic and H-bond interactions in the secondary level, which holds individual molecules of primary structure together. The weak forces in secondary level impart characteristic mobility of SOM. Very important consequence of this multidimensional formulation is that physicochemical structure plays a crucial role in most biogeochemical functions of SOM, apart from the chemical composition. Recently introduced concept of cation and water molecule mediated bridges between OM molecular segments (CaB and WaMB, respectively) evolved from physicochemical understanding of SOM structure. Even though several indirect evidences were produced for CaB and WaMB during last years, no clear-cut understanding of these processes has been achieved yet. Experimental difficulty due to overlapping effects of equally important CaB-governing parameters such a pH and competing cations raises huge challenge in investigating CaB-related influences. This thesis, therefore, aims to validate an experimental set-up for inducing CaB within OM structures and assessing it from various chemical and physicochemical aspects.

The method involved removal of omnipresent cations and adjustment of pH before cation addition. This helped to separate pH effects and cation effects. Based on results obtained on two different types of organic matter, it can be deduced that multivalent cations can cross-link SOM, given that functional group density of the SOM material is enough for the functional groups to be arranged in sufficient spatial proximity to each other. Physicochemical structural reorganisation during aging causes formation of more and/or stronger CaB and WaMB. As for inducing CaB directly after cation treatment, cationic size and valency were found determinant also for aging effect. A strongly cross-linked system in the beginning is less vulnerable to structural changes and undergoes aging with lower intensity, than an initially weakly cross-linked system. Responsible for the structural changes is, the inherent mobility of SOM within its physicochemical assemblage. Thus the information on structural requirement of CaB and its consequences on OM matrix rigidity will help to obtain insight into the physicochemical SOM structure. Additionally, organic matter quality (assessed by thermal analysis) and pore structure of SOM formed in a set of

artificial soils showed that mineral materials are important for the chemical nature of SOM molecules, but not for the physical structure of organo-mineral associations, at least after several months of SOM development.

Furthermore, nanothermal analysis using atomic force microscopy (AFM-nTA) was implemented in soils for the first time to reveal nanoscale thermal properties and their spatial distribution in nano- and micrometer scales. This helped to identify physicochemical processes, such as disruption of WaMB, in low-organic soils, in which bulk methods fail due to their low sensitivity. Further, various types of materials constituting in soils were distinguished with high resolution by advanced application of the method, in combination with other AFM parameters. Attempts were done to identify various materials, with the usage of defined test materials. Above all, the method is potent to reveal microspatial heterogeneity on sample surfaces, which could help understanding process-relevant hotspots, for example.

This thesis thus contributes to the scientific understanding on physicochemical structural dynamics via cross-linking by cations and via nanoscale thermal properties. Direct investigation on CaB demonstrated here will potentially help making a big leap in knowledge about the interaction. The observed aging effects add well to the understanding of supramolecular consideration of SOM. By introducing nanothermal analysis to the field of soil science, it is made possible to face the problem of heterogeneity and spatial distribution of thermal characteristics. Another important achievement of AFM-nTA is that it can be used to detect physicochemical processes, which are of low intensity.

Zusammenfassung

Die Struktur der organischen Bodensubstanz (OBS) ist ein seit Jahrzehnten unter Wissenschaftlern viel diskutiertes Thema. Die wichtigsten Modelle sind unter anderem das Polymer Modell und das Supramolekulare Modell. Während ersteres die OBS als Makromoleküle betrachtet, die amorphe und kristalline Bereiche enthält, erklärt letzteres die OBS als physikochemische Verbindung in der durch schwache hydrophobe Wechselwirkungen und Wasserstoffbrückenbindungen individuelle Moleküle primärer Struktur in einer Sekundärstruktur zusammengehalten werden. Die schwachen Wechselwirkungen innerhalb der Sekundärstruktur gewähren der OBS ihre charakteristische Mobilität. Eine wichtige Konsequenz dieses mehrdimensionalen Aufbaus ist es, dass abgesehen von der chemischen Zusammensetzung, die physikochemische Struktur der OBS eine entscheidende Rolle für ihre biogeochemischen Funktionen spielt. Aus diesem physikochemischen Verständnis der OBS Struktur heraus entstand das kürzlich eingeführte Konzept der durch Kationen und Wassermoleküle vermittelten Brücken zwischen OBS Segmenten (CaB und WaMB). Obwohl es in den letzten Jahren einige indirekte Anhaltspunkte für die Ausbildung von CaB und WaMB gab, gibt es bis heute kein klar umrissenes Verständnis dieser Prozesse. Experimentelle Probleme aufgrund sich überlagernder Effekte von wichtigen ebenfalls CaB beeinflussenden Parametern, wie pH und der Konzentration konkurrierender Kationen, erschweren die Untersuchung der CaB-bezogenen Einflüsse. Daher zielte diese Arbeit darauf ab, eine experimentelle Herangehensweise zu entwickeln um CaB innerhalb der OBS zu erzeugen und diese hinsichtlich verschiedener chemischer und physikochemischer Aspekte zu beurteilen. Dazu wurden zuerst die in den Proben schon vorhandenen Kationen entfernt und der pH Wert definiert eingestellt, bevor die Proben erneut mit bestimmten Kationen beladen wurden. So konnten pH- und Kationen-Effekte voneinander getrennt beobachtet werden.

Aus den Ergebnissen, die mit zwei unterschiedlichen Typen organischer Substanz erzielt worden sind, kann folgender Rückschluss gezogen werden: Unter der Voraussetzung, dass die Dichte der funktionellen Gruppen in der OBS hoch genug ist, so dass diese in ausreichender räumlicher Nähe zueinander arrangiert sind, können Kationen die OBS quervernetzen. Eine physikochemische strukturelle Umorientierung findet auch in Alterungsprozessen statt, die die Bildung von mehr und/oder stärkeren CaB und WaMB verursachen. Kationengröße und -ladung bestimmen sowohl die Erzeugung von CaB direkt bei der Kationenbehandlung, als auch die Effekte der Alterungsprozesse. Ein anfänglich

stärker quervernetztes System ist weniger anfällig für strukturelle Änderungen und unterliegt weniger starken Alterungsprozessen als ein anfänglich schwächer quervernetztes. Verantwortlich für die strukturellen Veränderungen ist die der OBS innewohnende Mobilität innerhalb ihres physikochemischen Verbundes. Information über die strukturellen Voraussetzungen zur Bildung von CaB und deren Konsequenzen für die Matrixstabilität der OBS können helfen, Einblicke in die physikochemische Struktur der OBS zu erhalten. Außerdem zeigten die Qualität der OBS (bestimmt mithilfe thermischer Analytik) und deren Porenstruktur, die sich in einer Reihe von künstlich hergestellten Böden nach einigen Monaten der OBS Entwicklung gebildet hatten, dass die mineralischen Ausgangsmaterialien zwar eine Bedeutung für die chemische Natur der OBS Moleküle hatten, nicht jedoch für die physikalische Struktur der organisch-mineralischen Verbindungen.

In der vorliegenden Arbeit wurde außerdem erstmals die nanothermische Analyse mithilfe der Rasterkraftmikroskopie (AFM-nTA) für Boden eingesetzt, um thermische Eigenschaften und deren räumliche Verteilung im Nano- und Mikrometerbereich zu erfassen. Diese Methode ermöglichte es, physikochemische Prozesse, wie z.B. das Aufbrechen von WaMB in humusarmen Böden zu identifizieren, bei denen herkömmliche Methoden aufgrund zu niedriger Empfindlichkeit scheiterten. Weiterhin konnten durch eine verbesserte Anwendung der Methode und die Kombination mit anderen AFM-Parametern einige in Böden vorkommende Materialien in hoher räumlicher Auflösung unterschieden werden. Durch die Verwendung definierter Testmaterialien wurde versucht, diese Bodenmaterialien zu identifizieren. Das größte Potential dieser Methode liegt allerdings darin, die mikroskopische Heterogenität von Probenoberflächen zu quantifizieren, was z.B. dabei helfen kann, Prozess-relevante Hotspots aufzudecken.

Durch die Einbindung der AFM-nTA Technologie trägt die vorliegende Arbeit zum wissenschaftlichen Verständnis der Änderungen der physikochemischer Struktur der OBS durch Kationenquervernetzung bei. Die hier demonstrierte direkte Untersuchung der CaB kann möglicherweise zu einem großen Wissenssprung hinsichtlich dieser Wechselwirkungen verhelfen. Der beobachtete Alterungsprozess ergänzt gut das supramolekularen Verständnis der OBS. Die Einführung der nanothermischen Analyse in die Bodenkunde ermöglicht es, dem Problem der Heterogenität und der räumlichen Verteilung thermischer Eigenschaften zu begegnen. Ein anderer wichtiger Erfolg der AFM-nTA ist, dass sie genutzt werden kann um physikochemische Prozesse sehr geringer Intensität zu detektieren.

Chapter 1

Introduction

1. General Introduction

1.1 Soil organic matter and its structure

Soil organic matter (SOM) is an important constituent of soils with its abundance ranging from 0.5-5 % (w/w, in mineral soils) up to 100 % in organic soils (histosols). It imparts characteristics such as cation exchange capacity (CEC) (Essington 2003), nutrient- and contaminant binding (Tipping 2004), water retention potential (Sparks 1995) and many others. Further, it helps to maintain soil aggregate structure by OM-mineral associations and acts as source of micro- and macronutrients and C to the terrestrial flora (Sparks 1995).

SOM consists of fresh plant and animal debris and their microbial decomposition products. The undecayed and partly decayed materials form substrates for microorganisms and have short mean residence time ($\sim 0.1-1$ year) (Six et al. 2002). They consist of low-molecular weight precursor molecules such as organic acids, lipids, nucleic acids, lignin fragments, simple carbohydrates, amino sugars, etc. (Essington 2003). Products of microbial decomposition having relatively high molecular weight ranging from several thousands of daltons to several hundred kilodaltons form humic fraction of SOM (humic substances, HS) (Stevenson 1994). They are very stable in the environment, with long turnover times and are operationally categorized into humic acids (HA), fulvic acids (FA) and humins, depending on solubility in water at different pH. Humins are the insoluble fraction whereas FA is soluble at all pH ranges and HA dissolve in very acidic pH (Tipping 2004). Owing to the least solubility and extractability, humins are the least studied whereas the other two compartments are being investigated for their molecular structure, chemical composition, and molecular weight along with a large spectrum of environmentally relevant properties, interactions and reactions.

Even though, up to now, scientists did not reach a universal consensus about the chemical composition and molecular structure of SOM (and natural organic matter (NOM), in general) because of high heterogeneity and chemical complexity. Moreover, their properties change from sample to sample depending on the source, formation and further physical and chemical interactions they had undergone and the method used in studying them (Egeberg and Alberts 2002). Owing to the molecular weight distribution, SOM expresses a continuum of properties. However, due to the outbreak of development in preparative and analytical techniques (e.g. nuclear magnetic resonance (NMR), X-ray absorption spectroscopy (XAS), mass spectroscopy (MS)) and in experimental approaches, chemical structure of HS is almost resolved (Wershaw 2004; Kleber and Johnson 2010). Moreover, a new approach called

humeomics, introduced recently by Nebbioso and Piccolo (2012), in which sequential fractionation is coupled with advanced analytical techniques like NMR, is promising for further chemical characterization of highly complex and heterogeneous SOM structure.

It has been found that apart from chemical structure, physicochemical structure of SOM is very important for SOM functionalities such as aggregate formation (Lishtvan 1977), C sequestration (Six et al. 2002), wettability (Schaumann and Hurraß 2003) binding of organic contaminants (Schneckenburger et al. 2012), water molecules and cations (Schaumann and Thiele-Bruhn 2011) and soil aging (Schneckenburger et al. 2012). Physicochemical structure is defined by the abundance and spatial distribution of molecular segments, inter- and intramolecular interactions, mobility of structural constituents, crystalline, glassy or rubbery character of molecular segments and porosity. Therefore, it becomes essential to understand SOM structure in physicochemical point of view. There is a lack of complete understanding of SOM structure in this perspective and currently existing models, individually, cannot fully account for SOM properties and functionalities (Schaumann 2006). Several structural models have been proposed for SOM, among which the most discussed are polymer model and supramolecular model.

1.1.1 Polymer model

The polymer model considers SOM as amorphous matrix composed of macromolecules of different chain mobility (LeBoeuf and Weber 1997; Xing and Pignatello 1997). They behave like flexible linear polymer in dilute solutions and get densely coiled into globular conformation as solution concentration, ionic strength and acidity increase (Ghosh and Schnitzer 1980; Swift 1989). The concept was first proposed by Kononova (1961) based on the observed high molecular weight of alkaline extracts of HS (up to 300 kDa) (Flaig 1958), functional group distribution and elemental composition. Secondary synthetic reactions, e.g. by phenol-quinone pathway (Smith and March 2007), are believed to lead to the formation of covalently linked humic-like materials by condensation and oxidation of simple precursor molecules (Kononova and Belchikova 1961; Stevenson 1994). Such products have unique chemical structure, different from the initial precursors (Stevenson 1994), but similar to natural polymers. This enzyme-catalysed polymerization reaction accounts well for the polydispersity of HS (Stevenson 1994).

Colloidal characteristics of HS such as flocculation and dispersion were found similar to that of polymers (Stevenson 1994). Sorption in HS was described by two-step mechanism in

polymer-like humic matrix, with the formation of voids in the matrix followed by occupying the voids by the sorbent molecules (ten Hulscher and Cornelissen 1996). The void formation and diffusion within OM depend on the glassy/rubbery character of the OM (Xia and Pignatello 2001). This dual mode sorption to interconnected voids, by physical entrapment is energetically favored, as assessed in computational studies (Schulten and Leinweber 2000). Further, long residence time (250-3000 years) of humic materials (Stevenson 1994) was attributed to the intrinsic stability of covalently linked polymeric structure. Also crystalline or partly crystalline micro fibrils formed by carbohydrates, mainly cellulose (Wershaw 2004), and lipids (Chilom and Rice 2005) are believed to provide resistance to microbial attack.

Despite its acceptance to explain many of the NOM characteristics (Stevenson 1994; LeBoeuf and Weber 1997; Xing and Pignatello 1997), many recent studies contradict the polymer model based on concerns regarding reliance of molecular weight values and the idea of synthetic processes in the formation of NOM (Haider and Martin 1967; Schnitzer and Khan 1972; Jenkinson 1981; Clapp and Hayes 1999; Haberhauer et al. 2001; Spaccini et al. 2001; Piccolo 2002; Simpson et al. 2002; Sutton and Sposito 2005; Kleber and Johnson 2010). Advancement of instrumental techniques in last decades provided more sophisticated fractionation and analytical techniques which lead to an outbreak in the number of studies on humic materials. Most of them reported much lower molecular weight for fractionated humic materials and found evidences against synthetic intermediates in the decomposition path way of plant and animal debris (see e.g. Piccolo 2002).

1.1.2 Supramolecular model

As an alternative overcoming the above-mentioned demerits of polymer model, Wershaw (1986) suggested aggregate formation involving hydrophobic interactions between small humic molecules, accounting for the observed low molecular weight. Those smaller units organize in a micelle-like fashion with their hydrophobic moieties centered to the interior and hydrophilic domains protruding outwards, leading to a highly ordered system (Wershaw 2004). But such an ordered state is less favorable in heterogeneous system of SOM. Highly ordered crystalline domains are suggested to exist in SOM, but less ordered semicrystalline and amorphous structures are more prominent (Hu et al. 2003).

Later, Piccolo (Piccolo and Conte), based on low- and high pressure size exclusion chromatography (LPSEC and HPSEC, respectively) experiments, proposed that HS (and NOM, in general) constitute small molecules that are aggregated via weak interaction forces

such as hydrophobic, van der Waals, π - π and CH- π interactions, along with H-bonds. Apparently high molecular size of HS aggregates is considered to arise from weak interactions between small molecules. In the light of supramolecular theory, SOM is suggested to be formed in three steps — degradation, aggregation of degradation products and degradation of aggregation products (Lou et al. 2004). OM formation takes place via partial degradation of dead cell materials, mainly caused by microorganisms, in which fresh plant- and animal remains follow thermodynamic gradient downwards to a least energy state (Piccolo 2002). Mixing of degradation products induces new supramolecular associations, resulting in the structure of NOM (Wershaw 2004). Multidimensional liquid state NMR techniques and LC-NMR identified the following major structural components in HS from a wide range of soils: aliphatic acids, ethers, esters and alcohols and aromatic lignin-derived fragments, polysaccharides and polypeptides. Low molecular weight values ranging from 500-2000 Da, which is in agreement with previous observations (e.g. Schnitzer and Khan 1972), were noted. Aggregate formation by these components was suggested (Simpson et al. 2002). Based on this structural information, the authors proposed a schematic model of humic aggregates that are held together by weak forces, see Simpson et al. (2002).

Supramolecular assembly is characterized by condition-dependant dynamicity in both levels of structural organization, tending to approach minimal energy state (Steed and Atwood 2000). Molecules undergo conformational changes to reach energetic stability and aggregates are constantly formed and disrupted, even in solid state (Lou 2004). This would create new physicochemical structure, affecting sorptive properties, mobility of molecular segments, etc. The inherent tendency to attain low energy state via self-reorganisation causes aging of SOM (Schneckenburger et al. 2012). Aging alters its physicochemical structure and properties. Conformational reorganization and disruption are enthalpy driven whereas stabilization of smaller, disrupted fractions is entropy driven (Piccolo 2001).

Aggregation and disaggregation

Small aggregates were proposed to undergo further aggregation, forming self-assembled units of apparently high molecular weight (Piccolo 2002). Several experimental evidences are available in favor of aggregate stabilization via hydrophobic interactions (e.g., Tarasevich et al. 2013). Even very large size fractions of 500 kD were found to dominate in week interactions with higher abundance of hydrophobic moieties than in low molecular weight fractions (Piccolo 2002). Aggregate stability was found to be increased in an OM-free soil by

addition of hydrophobic compounds, either HA or stearic acid, whereas addition of hydrophilic polysaccharide gum decreased the aggregate stability (Piccolo and Mbagwu 1999). This was attributed to the weak interactions between hydrophobic moieties than to the hydrophilic binding agents (Piccolo and Mbagwu 1999). Recently, supramolecular structural stabilisation was found to occur via chemical reactions, e.g. oxidative degradation of oxygen-containing functional groups of OM molecules (Patrakov et al. 2012).

Aggregation is reversible and hence disruption of aggregate structures occurs, owing to the dynamicity of supramolecular structure and interference of external factors. High molecular weight conformation of HS was easily broken, via organic acids (Piccolo et al. 1996; Conte and Piccolo 1999; Kucerik et al. 2009). Such conformational changes might be reversible as the weak, non-covalent bonds can be easily formed and disrupted. Acids decrease the pH, causing the disaggregation of dissolved NOM to form smaller aggregates (reduction in size from 100 kD to 25 kD) which are stabilized by H-bonds (Piccolo and Conte 1999). Unlike the mineral acids, addition of an organic acid causes additional restructuring of dispersed aggregates (Piccolo and Nardi 1996). Piccolo's (Piccolo and Nardi 1996) findings would indicate that the organic acids induce mainly physical effects on NOM structural compactness, which was later supported by other group (Kucerik et al. 2009). Disruption of aggregate structures by H-bonding was found to be caused also by reduction in pH of a purified humic solution (Miano et al. 1992) and of FA and HA solutions (Mazzei and Piccolo 2012) by the addition of glyphosate herbicide. The fact that these conceding results were obtained on different types of humic materials, by using independent methods - Fluorescence and IR spectroscopy by Miano et al. (1992) and NMR spectroscopy by Mazzei and Piccolo (2012) - denotes consistency of the observation. It suggests that disaggregation and hence aggregation are universal and characteristic features of NOM. Similar result was obtained when active H atoms were replaced with trimethylsilyl groups and reducing the degree of H-bonding in molecular aggregates (Haider et al. 2000).

The largest fraction excluded from HPSEC columns of various humic materials were found to contain mainly aliphatic alkyl groups, as studied by ^{13}C NMR spectra and by GC-MS analysis of fractions (Conte et al. 2007). Smaller size fractions were dominated by hydrophilic and mobile molecular associations (Conte et al. 2007). This was further supported by the humeomics approach (Nebbioso and Piccolo 2012) in which size fractions eluted from HPSEC column were further qualitatively analysed by advanced analytical methods (NMR and GC-MS) for chemical characterization of the fractions. Thus aliphatic

domains were found to exist in humic solutions as larger aggregates through hydrophobic interactions whereas the hydrophilic moieties occurred as smaller units; plausibly their aggregation is prevented by repulsive electrostatic interactions. This could impart different stability for humic materials possessing different chemical composition, as observed by Conte and Piccolo (1999) in a HPSEC study of four HA samples. The HA samples revealed different elution patterns which was attributed to difference in their chemical composition, provided that possibilities of artifacts due to column materials were excluded.

Consequences of supramolecular structure

Primary (1°) structure, defined by chemical nature of small molecules which are formed by covalent and electrostatic bonds and secondary (2°) structure defined by the weak interactions between the small molecules constitute together to form the humic structure. Intermolecular forces within 2° structure determine the conformational structure and complexity of multiple non-covalent bonds within 1° structure are decisive for the environmental activity (Piccolo 2002).

1° structure is characterized by dynamic nature and flexibility, owing to side chain mobility, changes in H-bonding and formation of voids (Schulten 1997), which are decisive for supramolecular structure. Type and stability of weak interactions in 2° structure are dependent on abundance and distribution of hydrophilic and hydrophobic components of molecules that constitute 1° structure. Further, relative spatial distribution of individual small molecules, their distance of separation and packing density would decide the strength and degree of weak interactions in suprastructure.

Binding of non-extractable residue (NER) occur by covalent and ionic bonds assured by 1° structure as well as by physical entrapment caused by 2° structure (Burauel and Fuhr 2000). The former two mechanisms would happen according to the chemical nature of organic backbone. Certain xenobiotics (e.g. 2,4-DP-P, terbuthylazine, fluoranthene, etc.) and their degradation intermediates were found linked with SOM molecules, via covalent bonds between C atoms or between C and N atoms (Burauel and Fuhr 2000). This is obviously dependent on the chemical nature of humic molecules and that of the sorbent. Such reactions can form new 1° structure, ultimately creating a new 2° structure. Similarly, cation exchange capacity (CEC), which is one of the decisive features for NOM functioning, depends on cation binding status which in turn depends on the abundance and deprotonation status of hydrophilic functional groups belonging to the 1° structure. Further, removal of cations from

HS causes alterations in 2° structure (Wrobel et al. 2003), as better described in a following section. Similarly, fractionation of HA by change in pH (e.g. by acid addition (Piccolo and Nardi 1996; Conte and Piccolo 1999)) is owing to protonation of functional groups, which belong to the 1° structure. Thus 1° structure induces direct and indirect effects on sorptive and exchange capacities of NOM.

2° structure is constantly formed, reorganized and disrupted, owing to the inherent dynamicity, by changing interaction partner, change in spatial occupancy of interacting molecules (Lou et al. 2004) and under the influence of external interferences (Piccolo and Conte 2000). Hydrophobic associations provide surfactant properties (Hayase and Tsubota 1983), water repellency (Adhikari and Chakrabarti 1976) and protection against quenching of fluorescent-active molecules (e.g. pyrene (von Wandruszka et al. 1999)). Amphiphilic moieties in 2° structure undergo self-reorganisation in presence of water molecules and cations forming higher molecular weight fractions, as shall be seen in next section. Difference in degree of segment mobility imparts crystalline, glassy and rubbery nature to SOM. It is important to state that not only polymers but also small organic molecules such as for example organic pigments (David et al. 2011) can exhibit glass transition: change from glassy state to rubbery state at glass transition temperature, T_g .

Sorption of xenobiotics may undertake via physical entrapment within supramolecular 2° structure, which is characterized by weak interactions, depending also on polarity of the sorbent (Burauel and Fuhr 2000; Schaumann and Thiele-Bruhn 2011). Enhanced dissolution of acetophenone in methanol by FA was observed and assigned as due to hydrophobic regions that have expelled water out (Nanny et al. 1997). The retention and bioavailability of such contaminant molecules will in turn be a function of weak interactions forming the 2° suprastructure.

Further, disaggregation by reaction of carboxylic, (Piccolo and Conte 1999; Piccolo et al. 2003), hydroxyl, keto and sulfonic acids can impart direct effects in soils (Cozzolino et al. 2001). Since root exudation and microbial transformations can produce these organic acids (Cozzolino et al. 2001; Piccolo et al. 2003), root activity can be influenced by alteration in size of humic materials in soil solutions (Nardi et al. 1996). This was demonstrated in a laboratory scale experiment on root growth of maize, by Vlckova et al. (Vlckova et al.) using physically and chemically modified lignite humic acid samples, by organic acids and mineral acids, respectively.

Weak interactions create microdomains characterised by hydrophilic or hydrophobic nature, within the humic matrix, which are isolated from each other (Engebretson and von Wandruszka 1994; von Wandruszka et al. 1999). Existence of such microdomains suggests spatial heterogeneity of NOM structure, inclusive of microregions of differing polarity and inter- and intramolecular interactions. Each region is dominated by potential for individual type of interaction and undergoes different interactions with apolar and polar moieties including water and cations. In other words, this will lead to a system of heterogeneously distributed hotspots, relevant for each type of process. For example, sorption of organic molecules and thus their fate and transport in natural systems including soil and water would be influenced by the presence of sorption-relevant hotspots. Discrete microregions of different polarity were attributed to cause diffusion of polar organic compounds in humic matter (Aochi and Farmer 1997; Chien et al. 1997; Kohl et al. 2000).

Hydrophobic domains would expel out water due to less favored solvation, in energetical terms, and end up in partial precipitation of humic materials in solution (Baalousha, et al. 2006). Putting it differently, aggregation of small molecules caused by weak interactions leads to precipitation of dissolved organic matter (DOM). This would indicate that molecular size is a key factor for OM solubility, beyond chemical structure. i.e., weak forces dominating in 2° structure would influence solubility via aggregation or by forming ‘water-free’ microdomains. Kucerik et al. (2012) named such domains as ‘hydrophobic scaffold’. Thus supramolecular concept suggests that the classical distinction of HS based on solubility should be reconsidered. In the light of above discussions, solubility is a function of molecular size and hydrophilicity of individual microdomain, rather than merely of chemical composition in 1° structure. Thus Piccolo’s (2002) view of HA and FA in light of supramolecular model can be understood as originating from combination of 1° and 2° structures of humic associations and it reads as follows: “HA are made of associations of predominantly hydrophobic compounds (poly)methylene chains, fatty acids, steroid compounds) which are stabilized at neutral pH by hydrophobic dispersive forces (van der Waals, π - π , and CH- π bondings). Their conformations grow progressively in size when intermolecular hydrogen bonds are increasingly formed at lower pH, until they flocculate” (Piccolo 2002) and FA are “associations of small hydrophilic molecules in which there are enough acidic functional groups to keep the fulvic structures dispersed in solution at any pH” (Piccolo 2002). However, this new definition itself is not fully convincing, for example, Drastik et al. (Drastik et al. 2009) observed aggregation of FA even at low concentration.

Fractionation of humic materials in presence of organic acids (Piccolo 2002; Piccolo et al. 2005), owing to their suprastructure, suggests that bulk humic samples can be separated into single molecules by simple methods. This provides more homogeneous samples, especially useful for pharmaceutical and other industrial applications, with less chemical complexity and with less polydispersity (700-1200 Da). Moreover, it would add efficiently to the attempts to elucidate the chemical structure of NOM materials.

Altogether, the two levels of structural organization and humic functions can be assumed to form a triangular relationship between each other. Interrelation between 1° and 2° structures form one side of the triangle and implications of the two levels of organization on their environmental functionalities form the other two sides (see the schematic diagram, figure 1).

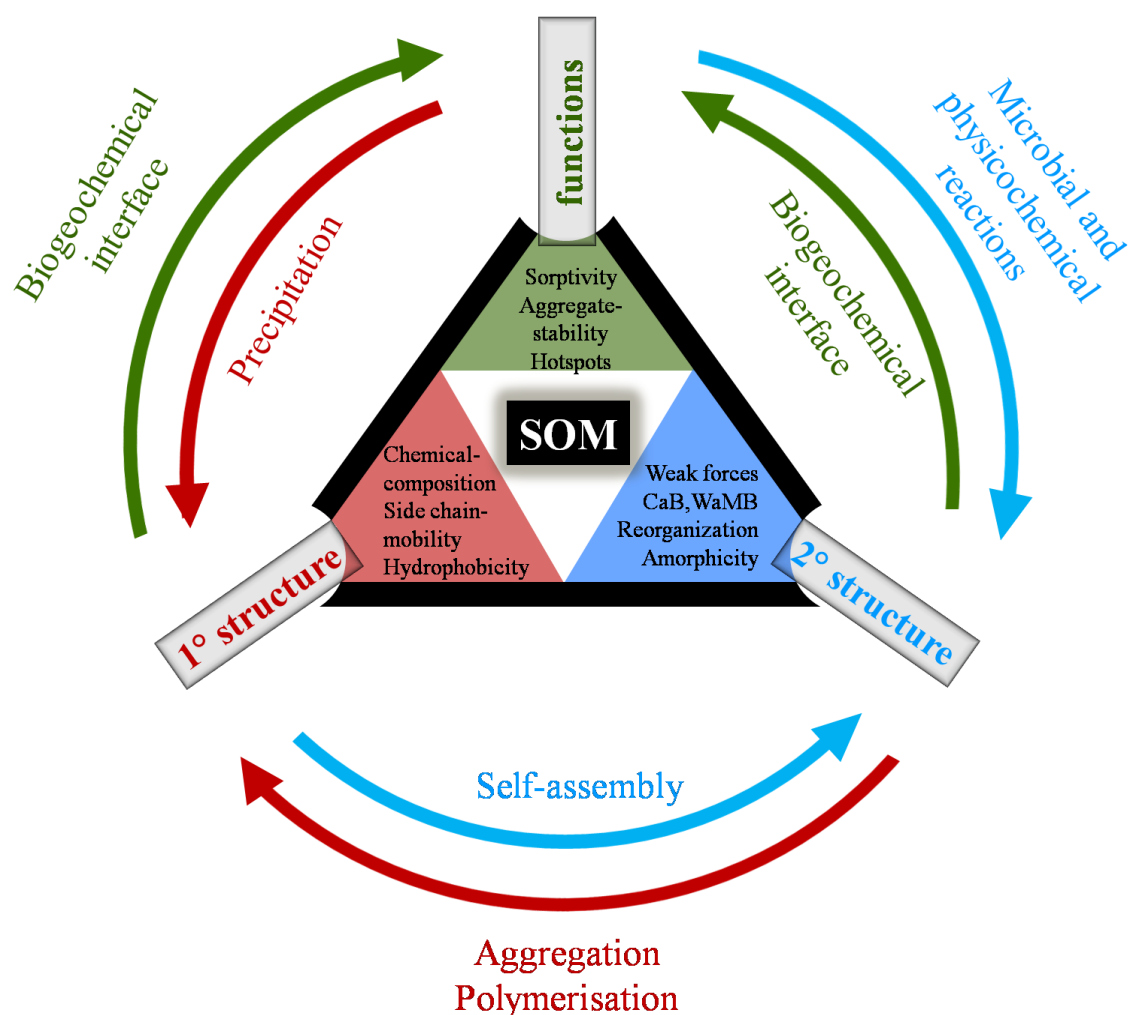


Figure 1. Sketch showing triangular relationship between 1° and 2° structure of SOM and SOM functions. The arrows indicate the direction of the dependence, via the responsible interactions indicated in the same colour.

Cations and water molecules

Water (e.g. Kucerik et al. 2012) and cations (e.g. Gaiffe et al. 1984) may act to aggregate small molecules and small aggregate structures to form larger aggregates. Conformational rearrangement and aggregation evoked by water and/or metal cations may depend on hydrophobic associations, charge interactions, cation- and/or water bridging (CaB and WaMB, respectively) and H-bonding. The balance between negative charges on OM molecules formed by dissociation of functional groups and the amount of cations is important for the aggregation process (Baalousha et al. 2006). Two mechanisms of NOM-cation interaction were proposed – complexation at separated functional groups and cross-linking between adjacent functional groups (Buurman et al. 2002). Complexation, in this context, addresses electrostatic interaction between charged functionalities and cations. It occurs mainly in case of monovalent cations, especially when active functional groups in OM are situated far away from each other.

Several evidences were shown for cations inducing supramolecular structural stabilization, via cross-linking (Lu and Pignatello 2004; Rudolph and Schaumann 2006; Schaumann et al. 2006; Wang et al. 2009; Aquino et al. 2011; Schaumann and Thiele-Bruhn 2011; Kalinichev et al. 2011). Calcium chloride was found to cause dramatic increase in the size of HS, as observed under transmission electron microscope (TEM), which slowed down at CaCl₂ concentrations above 0.2M. This has implications that a part of charges is less accessible, probably due to steric factors (Baalousha et al. 2006). Ca²⁺-enhanced aggregation to a higher extent than Na⁺, causing aggregate size of 1800 nm and 120 nm, respectively was noted in a HS sample (Baalousha et al. 2006). In line with this, it was also reported that bivalent cations decelerated the dissolution of a humic acid sample by intervening the intermolecular forces (Brigante et al. 2009). Cation bridges between clay and OM fractions were found to stabilize organomineral associations (Gaiffe et al. 1984; Leinweber et al. 1993; Ahmed et al. 2002). Inversely, chelating agents are known to mobilize OM, as suggested, because of disruption of cation bridges between small OM molecules, causing disruption of aggregate structure (Wrobel et al. 2003).

Lowering in energy content of bridged OM structure could make it less dynamic to have reduced flexibility and therefore the aggregate structure after CaB/WaMB formation would undergo conformational changes to lower extent than was before. These bridges can be disrupted at higher temperature by breakage of the relatively weak bonds between the water molecules and bridged moieties. On the other hand, direct CaB via inner sphere complexation

would not be as vulnerable to disruption as outer sphere complexes would do, due to stronger ionic bond. A system with outer sphere CaB (CaB-WaMB) and WaMB undergoes step-transition when heated to characteristic temperature, imparting higher molecular mobility (Hurrass and Schaumann 2005; Schneckenburger et al. 2012). Further, restructuring would be induced by aging and by drying, resulting in a different quality of CaB and/or WaMB (Schaumann et al. submitted 2013). A detailed review on CaB and CaB-WaMB associations in SOM is given in chapter 2 of this thesis.

Supramolecular structure of soil organic matter (SOM) - major concerns

Almost all the existing evidences for supramolecular model are obtained in studies using fractionated or purified HS, HA or FA. But SOM constitute other important components that were overlooked by these studies. Humins and freshly entered biopolymers are the least studied, in this respect, as in many other discussions on NOM. Based on literature, Schaumann (2006) pointed out that the humic fractionation procedure addresses only low molecular mass fractions. Therefore, one might not blindly accept the reports available on model NOM systems such as humic acids, to whole SOM. However, the effects due to individual components in whole soil may overlap each other to make it challenging to investigate particular SOM properties and processes. This demands model systems where individual properties are identifiable.

Majority of the investigations were focused on molecular weight and size determination and chemical characterization. As seen before, physicochemical nature of 2° structure demands more attention and hence it needs to be focused. There is a lack of direct investigation on the nature of suprastructure in SOM and its effects on SOM properties (e.g. CEC, sorptivity etc.) and processes (e.g. formation and disruption of CaB and WaMB).

Schaumann (2006) argued that major and introducing evidences for supramolecular concept were based on extracted humic acids in H-form, exclusive of omnipresent cations. Thus the role of chelation, cross-linking and cation exchange in intermolecular interactions were overlooked. This can have serious ill-effects when considering that cations instigate aggregation in HS (Simpson et al. 2002) and removal of cations caused disaggregation (Wrobel et al. 2003). One might argue that LPSEC and HPSEC studies conducted by Piccolo (2002) utilized HA in Na⁺ rich eluent, hence cations were also considered. Still, a lack of knowledge on the type and degree of Na⁺-HA interaction exists and other cations, especially

multivalent cations, induce different types of interactions within NOM, which were overlooked.

Nevertheless, supramolecular model does not explain sorption non-linearity, desorption hysteresis and conditioning/history effects up to now, as discussed by Schaumann (2006). This points to the absence of a model system representing supramolecular structure of SOM. It makes the understanding of physical structure and functions of SOM (and generally, NOM) challenging. Equally important is that the inherent recalcitrance of NOM is not yet explained by this model. A weakly bound dynamic system, tending to achieve low energy state would be very unstable, resulting in low retention time; but this is obviously not the case for SOM. SOM recalcitrance in association with inorganic compartments such as Al and Fe species and crystalline Fe oxides was already suggested (Mikutta et al. 2006; Kleber et al. 2007). However, recalcitrance of non-mineral stabilized OM remains unexplained yet. Recently, Kucerik et al. (2012) suggested that formation of ‘hydrophobic scaffold’ would separate some SOM component molecules from water and they remain unaffected by microbial degradation. This might explain the supramolecular view of SOM recalcitrance, but needs to be verified further.

1.1.3 (supra)macromolecular structure

Owing to the fact that NOM is partly explained by polymer model and partly by supramolecular model, Schaumann (2006) suggested that both type of structures co-exist. According to her, both low molecular weight supramolecular matrix and high molecular weight polymer matrix coexist, leading to polydisperse mixture. Individual polymeric structural segment may also exhibit supramolecular characteristics to certain degree, by undergoing weak interactions with similar segment or with neighboring supramolecular entity of small molecules. The (supra)macromolecular matrix will, thus, be stabilized by hydrophobic interactions, H-bonds and cation- and water- mediated cross-linking. Langford and Melton (2005) had suggested a combinatorial model in which humic molecules are treated as complex supramolecular assembly of small molecules, oligomers and polymers, aggregated into supramolecular assemblies by non-covalent forces. Further, Senesi et al. (2009) suggested SOM as supramolecular assemblies of monomers to macromolecules, including a continuum of biomolecules to highly transformed carbonaceous materials, with polymer-like properties. All these proposals obey the general consideration that supramolecular associations are independent of molecular weight (Steed and Atwood 2000).

Decomposition fragments of plant polymers are mostly oligomers or monomers vulnerable to all types of non-covalent interactions as the original polymer did. Exceptions are polyphenolic tannins which can undergo oxidative coupling reactions to form polymerized structures (Wershaw 2004). This implies that also polymers self-assemble and form secondary structure (e.g. crystalline micro fibrils of cellulose (Horii 2001)). Moreover, the observation of Mikutta et al. (2006) that the inherently recalcitrant OM fraction constitute mainly aliphatic structures is suggestive for the presence of polymeric and/or crystalline aliphatic structures that contribute to recalcitrance of the whole OM, along with mineral-stabilized small molecules.

Further, polymerization of supramolecular aggregates via enzymatic oxidative coupling reactions was found to oligomerise or polymerise small molecules such as phenols and anilines forming new covalent bonds (Kim et al. 1997). Piccolo et al. (2000) showed that small heterogeneous molecules present in humic aggregates can be polymerized covalently by oxidative coupling reactions, in HPSEC and diffuse reflectance IR spectroscopy (DRIFT) studies. The extent of polymerization depends on the number of humic molecules (phenolic and benzene carboxylic acids from lignins and from biosynthesis). Such polymerization products were more stable to fractionation via organic acids, than the original aggregate structures (Piccolo et al. 2000). Moreover, structural reorganization on aggregated humic structure was found to cause energy minimization by 20 kcal mol^{-1} , when calculated by computational means while the respective polymeric structure reduced its energy only by 10 kcal mol^{-1} , without showing significant physical changes (Schulten et al. 1998). This suggests that polymeric molecules will undergo conformational changes in presence of acetic acid to much lower extent than the supramolecular association of small molecules, as observed by the group of Piccolo (Piccolo and Nardi 1996; Piccolo et al. 1996). Polymerization in humic materials was assessed by synthetic Fe-porphyrin complex and the product was found to have increased motional rigidity, as assessed by proton spin-lattice relaxation in rotating frame ($T1\rho$) (Piccolo et al. 2005).

Irrespective of small or macro molecules, SOM is regarded to constitute molecular assemblies held together via weak, non-covalent interactions (Schaumann 2006). SOM matrix constitutes aggregates with structures of several tens and hundreds of nanometers, as revealed by TEM and SEM analysis, resulting from a multilevel organization of fulvic and humic supramolecular structures (Fedotov et al. 2008). Such nanoscale structures of SOM may constitute microphase stratification of supramolecular humic matrix. Hence nano- and

microstructures of SOM, including existence of hydrophilic and hydrophobic microdomains and certain process-relevant hotspots are dependent on 2° level physicochemical organization and chemical composition within 1° structure. This would imply that the microdomains possess individual physicochemical properties as distinctive feature, along with chemical composition. For example, intensity of WaMB transition temperature was found to be in accordance with the abundance of H-bonding sites in SOM (Hurrass and Schaumann 2005), indicating that microdomains with pronounced H-bonds show strong WaMB and probably the other domains to less extent. The microdomains, supposedly, constitute different types of molecules with different types of interactions. This automatically induces difference in energy content of hydrophilic and hydrophobic microdomains. Based on this, it can be expected that thermal stability of hydrophobic and hydrophilic domains differ from each other and can be distinguished by thermal-analytical techniques.

Thus spatial distribution of such physicochemical structures and related heterogeneity (ranging from nano- to macroscales) are important for the bulk soil properties, for example, thermal stability, expression of WaMB and CaB (and hence matrix rigidity) and sorption of organic contaminants and their bioavailability. SOM-relevant properties are mostly unidentified in low organic soils, either due to their irrelevance in defining the whole soil or due to low detectability/undetactability by applied methodology. For example, Hurass and Schaumann (2005) assessed glass transition-like step transition (WaMB transition, according new terminology) in a large set of soils with varying OM content, using DSC. They found that the particular transition was absent in anthropogenically altered soils, owing to their low OM content. Further, when OM was removed from soils from natural sites below 10 %, step-transition was decreased below the detectability of DSC (Hurrass and Schaumann 2005).

A microscale methodology which can explore material characteristics (e.g. thermal behavior) would be helpful to investigate structural features acting behind SOM properties and processes. This will further allow identifying the relevant hotspots. Therefore, focus of this thesis was laid also on implementing a suitable nanoscale methodology that benefits research in this direction. We selected atomic force microscopy-assisted nanothermal analysis (AFM-nTA), which was already proven in the field of polymer and pharmaceutical science, to be useful to identify and distinguish materials in nano- and macroscales, based on thermal characteristics such as glass transition temperature, (Chiou et al. 2006; Harding et al. 2007; Duvigneau et al. 2011).

1.2 Principles of AFM-nTA

Nanothermal analysis provides information on localised thermal behavior in sample materials, with a spatial resolution of up to sub-100 nanometers. Sample specific thermal features such as phase transition, melting etc. can be observed in desired localities (Chiou, et al. 2006; Harding et al. 2007; Duvigneau et al. 2011). It uses the commonly used AFM instrument, with additional thermal analysis unit and specially designed probe. During imaging, the probe having a cantilever on the end moves along the surface either in contact (contact mode) or without contacting (non-contact or tapping mode) the sample surface. Vertical and angular deflections of the probe are recorded using a reflected laser beam from the back top of the tip. An array of photodiode detector senses the reflected beam. Angular direction of the reflected laser beam changes according to the probe-deflections and falls on one or the other detector. Relative intensity of laser in each detector is then processed by electronic output unit in the form of images. Contact mode provides height images, showing vertical topography (Rossini et al. 2001). In tapping mode AFM, cantilever oscillates with a defined amplitude, phase and frequency. Changes in these oscillation parameters are additionally recorded to give respective images, which are informative about frictional and viscoelastic properties of materials under investigation (Namjesnik-Dejanovic and Maurice 1997). Sample-tip force mapping is another possible augmentation, which is informative about chemical and mechanical properties: interaction forces, material hardness and Young's modulus (Tielemans et al. 2012).

In nanothermal analysis a temperature-calibrated cantilever is kept constantly at the point of interest and is heated. Sample gets heated locally, due to thermal conduction from the cantilever. Vertical cantilever deflections that reflect the thermal expansion or compression of the sample material, are recorded to give thermogram (figure 2A). Upward deflections result due to thermal expansion and when the surface undergoes softening, for example by melting, a downward deflection is noted. Other characteristic thermal properties such as phase transition would cause change in slope of the expansion phase, due to softening of the material. Thus the slopes of expansion and compression regimes in thermograms characterize coefficients of thermal expansion or compression (α and κ , respectively). α , κ and characteristic temperatures are specific for each material. AFM-nTA can thus be considered as a nanoscale analogue to thermomechanical analysis (TMA). Figure 2B is an example showing melting of two polymers, polyethylene terephthalate (PET) and high density polyethylene (HDPE).

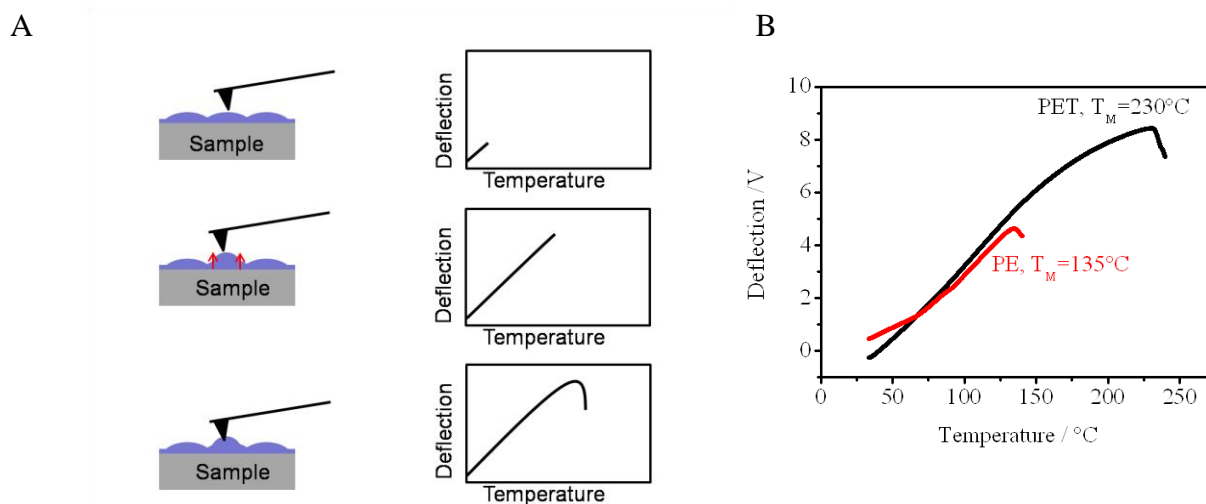


Figure 2. Schematic diagram showing development of nanothermogram, as sample undergoes heating (A) and example of thermogram showing melting of different polymers- PET and HDPE (B)

Thus AFM-nTA promises to explore spatial distribution of material characteristics with a resolution of up to sub-100 nm. Typically, the lateral reach of heating depends on the tip radius and also on thermal conductivity of the sample. Vertical heat conduction through the sample from the surface layer to the bottom heats up the layers under the surface. Therefore the observed tip deflection will reflect a sum of thermal properties of the vertically heated materials. Depending on heat conductivity, it can range up to a micrometer. This is a crucial point needs to be aware of, when analysing surface features. Nevertheless, with the containment of additional AFM parameters such as nanomorphological and nanomechanical properties, one might be able to locate material characteristics and to picturise their heterogeneous distribution in nano- and microscale.

1.3 Working hypothesis and objectives

Even though cross-linking by multivalent cations is a widely discussed topic in recent years, with evidences from a large variety of studies (Lu and Pignatello 2004; Schaumann et al. 2006), there is still a lack of detained understanding on CaB. Availability of only limited number of studies on CaB might be because that formation, functional features and disruption of cross-linking are affected by a number of overbalancing factors, which makes it challenging to identify requirements for and characteristics of CaB.

Therefore, this thesis aims to design and validate a new experimental strategy which involves inducing CaB within SOM materials and assessing the aftereffects on various SOM functions. It is hypothesised that characteristic features of SOM and cations, in general, and

external conditions at the time of interaction and during aging are decisive for CaB. pH is one of the key factors since the extent and mode of cation-SOM interaction depend on the degree of deprotonation of OM functional groups. Further, change in pH of SOM due to uptake of cations or due to other environmental reasons could influence the degree of expression of cation-SOM associations in many SOM functions. Therefore, the pH at which cations come in contact with the OM and the pH at which specific OM function is expressed should be distinguished while attempting to study CaB. Cation type and amount are decisive for the mode and degree of interaction, via cationic strength and size. Moreover, the effects due to a particular cation could get overlaid or masked by effects of other, omnipresent cations. Thus, one of the main objectives of this thesis is to evaluate the hypothesis that properties of SOM, cations and surroundings at which the two interact are determinant for CaB. A well-designed experiment helps to separate the effects of individual CaB-relevant parameters and should also be able to identify the effects of CaB on structure and functions of SOM among alterations caused by other factors.

It is further hypothesised, based on the supramolecular model of SOM, that relative spatial organization of molecular segments maintained via weak interactions play a key role in determining whether CaB exists or not. This has been already demonstrated by computational means by Aquino et al. (2011), under restricted structural conditions. However, experimental validation of this hypothesis is required since the assumptions defined in modelling seem to be very ideal, when bringing to reality. Part of this thesis is dedicated for validation of this hypothesis.

Large distances are not expected to be bridged solely by cations or by associations of CaB and WaMB. But water molecules in hydration shell and confined water in the outer sphere of hydrated cations can help bridging smaller distances. The more water molecules are confined around the cation, the larger the distance it can bridge. But the bridging can be weaker than in case of a less hydrated cation of similar valency. Thus it is hypothesised that the size of hydration shell and hence the number of water molecules takes a determinant role in defining CaB. Verification of this hypothesis is another important objective of this thesis.

Aging-induced physicochemical restructuring within supra- and hence superstructure of SOM is hypothesised to bring the potential bridging sites of SOM closer. This leads to the formation of new CaB and strengthening of existing CaB, increasing the supramolecular matrix rigidity. Effect of such restructuring will be depended also on mobility of water

molecules confined around the cation. Therefore, the objective is to monitor the structural changes brought about by aging, using matrix rigidity as a tool, with special focus on the effect of CaB and WaMB.

An additional objective of this thesis was to demonstrate the proposed triangle relation between primary and secondary structural levels and SOM functions at biogeochemical interface. Microbial-mineral associations were found to be decisive for the quality of OM in soils (Kleber and Johnson 2010). Based on this, it was hypothesised that characteristics of minerals (e.g. chemical composition, grain size, etc.) are determinant for primary structure of SOM. The newly formed OM molecules interact with each other and with mineral surfaces in secondary level to provide structure of the whole soil.

As has been hypothesised based on the modelling results (Aquino et al. 2011), structural complexity and heterogeneity are other important SOM features that control CaB and holds back relevant information, as in case of most NOM investigations. Additionally, the existence of hydrophilic and hydrophobic microdomains within the SOM superstructure would lead to the formation of CaB-relevant hotspots, by bunching of active functional groups. Therefore, it is important to be informed about the structural complexity, heterogeneity and spatial distribution of various structural regimes, in microscale. Currently, the lack of suitable instrumental techniques raises a huge challenge in this field. Acknowledging this technical lack, we aimed to bring proved potentials of AFM-nTA into the system of soils to be able to shed light on spatial heterogeneity in distribution of materials. Existing instrumental techniques that promise to trace CaB and WaMB are provided with low detectability, as in case of DSC that can detect WaMB, but not promisingly in low-organic soils (Hurrass and Schaumann 2005). AFM-nTA, being capable of revealing nanoscale thermal properties, is expected to reveal low-intensity physicochemical processes that are normally not expressed in bulk methods like DSC or TMA. It was additionally tested to identify nanoregions with specific thermal properties.

Summarizing, in this thesis, it is attempted to test the following hypotheses:

1. SOM chemical characteristics, cations and the interaction conditions are decisive for CaB.
2. Cross-linking by multivalent cations depends on the suprastructure of SOM, defined by functional group density.

3. Aging-induced supramolecular conformational changes would result to form more and stronger CaB and/or WaMB.
4. Hydration water molecules enhance cross-linking via CaB-WaMB associations, but weaker than more direct CaB, and induce stronger WaMB-related aging effects.
5. Organo-mineral associations are held together by supramolecular interactions of SOM, which in turn is defined by the chemical characteristics of SOM.

and with AFM-nTA, we aimed to substantiate the following:

6. Localised thermal behavior is a valid tool to distinguish soil material characteristics and to reveal related microscale heterogeneity.
7. SOM-relevant properties in low organic soils can be detected by using nanothermal analysis, with a higher sensitivity than bulk methods.
8. Combination of nanomorphological and nanomechanical parameters with nanothermal properties allows identification of materials, when provided with test materials.

1.4 Structure of the thesis

Chapter 2 provides a critical review on cation-SOM interactions, with special focus on CaB and CaB-WaMB, describing the current state of the art of the topic.

In order to verify the hypotheses 1, 2, and 3, an experimental strategy was designed and validated using a peat OM. This is shown in chapter 3. The method involves removal of omnipresent cations, adjustment of pH to the initial value either before or after cations addition and cation addition. Effects of addition of different cations in varying amount on chemical and physicochemical properties of the peat were aimed to explore. Measures were taken to monitor the effects of pH at which cations come in contact with the OM, and to separate them from the effects due to final pH. The method was further expected to help in understanding the physicochemical restructuring, brought about by removal of original cations, change in pH and incorporation of cations. Cations with different valency were selected owing to their ubiquity in soils and to their known cross-linking potential.

Low cation exchange capacity of peat indicates larger separation of functional groups than in SOM. This allows to verify hypothesis 2. Treated samples were investigated after aging of several weeks to focus on hypothesis 3.

To get deeper insight into the hypotheses 1 and 2 and to validate the experimental strategy proposed in chapter 3, it was again tested in a soil sample, with a different set of cations. Result of that experiment is shown in chapter 4. Cations used to treat with soil sample (alkaline earth metals) were selected such a way that they differ mainly in characteristics of hydration. This would allow distinguishing outer sphere CaB and CaB-WaMB associations leading to the verification of hypothesis 4. Investigations on cation treated, but aged sample were done to explore hypothesis 3.

In order to get insight into the influence of inorganic, mineral materials on primary structural quality of SOM, a set of artificial soils were analysed for thermal stability and combustion energy using simultaneous thermogravimetry-differential scanning calorimetry (TGA-DSC). Development of pore structure with the formation of SOM was assessed using ^1H nuclear magnetic resonance (NMR) relaxometry to assess organo-mineral associations. This study is described in chapter 5.

Nanothermal analysis was conducted on a set of soils and organic and mineral standard samples and is shown in chapter 6. The results were compared with that from bulk differential scanning calorimetry (DSC) analysis which showed WaMB transitions in different SOM to different extents. This helps to assess the method, based on hypotheses 6 and 7. An erratum to this chapter was published (Schaumann and Kunhi Mouvenchery 2012), with missing values of table 2 inside, and is given at the end of the chapter. Further potentials of AFM were investigated on a set of young soils with different age, provided with two organic test materials, as described in chapter 7. Nanomorphological (surface roughness) and nanomechanical (adhesion force) parameters were combined with the observed nanothermal properties. This, together with the usage of test materials was expected to improve the quality of the result, with respect to hypothesis 8.

Chapter 8 summarizes the results with a synthesis of the whole thesis. Supporting information to the chapters 3 and 7 are given in the annex.

References

- Adhikari, M. and G. Chakrabarti (1976). Contribution of natural and microbial humic acids to water repellency in soil. *Journal of the Indian Society of Soil Science* 24(2): 217-219.
- Ahmed, N., C. Varadachari, et al. (2002). "oil clay-humus complexes. II. Bridging cations and DTA studies. *Australian Journal of Soil Research* 40(4): 705-713.
- Aochi, Y. O. and W. J. Farmer (1997). Role of Microstructural Properties in the Time Dependent Sorption/Desorption Behavior of 1,2-Dichloroethane on Humic Substances. *Envir Sci Technol* 31(9): 2520-2526.

- Aquino, A. J. A., D. Tunega, et al. (2011). The functionality of cation bridges for binding polar groups in soil aggregates. *International Journal of Quantum Chemistry* 111: 1531-1542.
- Baalousha, M., M. Motelica-Heino, et al. (2006). Conformation and size of humic substances: Effects of major cation concentration and type, pH, salinity, and residence time. *Colloids and Surfaces a-Physicochemical and Engineering Aspects* 272(1-2): 48-55.
- Brigante, M., G. Zanini and M. Avena (2009). Effect of pH, anions and cations on the dissolution kinetics of humic acid particles. *Colloids and Surfaces a-Physicochemical and Engineering Aspects* 347(1-3): 180-186.
- Burauel, P. and F. Fuhr (2000). Formation and long-term fate of non-extractable residues in outdoor lysimeter studies. *Environmental Pollution* 108(1): 45-52.
- Buurman, P., B. v. Lagen, et al. (2002). Increase in thermal stability of soil humic substances as a result of self-association. *Organic Geochemistry* 33(3): 367-381.
- Chien, Y.-Y., E.-G. Kim, et al. (1997). Paramagnetic Relaxation of Atrazine Solubilized by Humic Micellar Solutions. *Environmental Science and Technology* 31: 3204-3208.
- Chilom, G. and J. A. Rice (2005). Glass transition and crystallite melting in natural organic matter. *Organic Geochemistry* 36(10): 1339-1346.
- Chiou, C. H., S. J. Chang, et al. (2006). New fabrication process for monolithic probes with integrated heaters for nanothermal machining. *Japanese Journal of Applied Physics Part 1-Regular Papers Brief Communications & Review Papers* 45(1A): 208-214.
- Clapp, C. E. and M. H. B. Hayes (1999). Sizes and shapes of humic substances. *Soil Science* 164(11): 777-789.
- Conte, P. and A. Piccolo (1999). Conformational Arrangement of Dissolved Humic Substances. Influence of Solution Composition on Association of Humic Molecules. *Environmental Science and Technology* 33(10): 1682-1690.
- Conte, P., R. Spaccini, et al. (2007). Spectroscopic and conformational properties of size-fractions acid separated from a lignite humic. *Chemosphere* 69(7): 1032-1039.
- Cozzolino, A., P. Conte, et al. (2001). Conformational changes of humic substances induced by some hydroxy-, keto-, and sulfonic acids. *Soil Biology & Biochemistry* 33(4-5): 563-571.
- David, J., M. Weiter, et al. (2011). Stability and structural aspects of diketopyrrolopyrrole pigment and its N-alkyl derivatives. *Dyes and Pigments* 89(2): 137-143.
- Drastik, M., A. Ctvrtnickova, et al. (2009). Aggregation of humic and fulvic acids in diluted solutions. *Energy, Environment, Ecosystems, Development and Landscape Architecture*. N. Mastorakis, C. Helmis, C. D. Papageorgiou, C. A. Bulucea and T. Panagopoulos: 163-168.
- Duvigneau, J., H. Schonherr, et al. (2011). Nanoscale Thermal AFM of Polymers: Transient Heat Flow Effects. *Acs Nano* 4(11): 6932-6940.
- Egeberg, P. K. and J. J. Alberts (2002). Determination of hydrophobicity of NOM by RP-HPLC, and the effect of pH and ionic strength. *Water Research* 36: 4997-5004.
- Engebretson, R. R. and R. van Wandruszka (1994). Microorganization in dissolved Humic Acids. *Environmental Science and Technology* 28: 1934-1941.
- Essington, M. E. (2003). *Soil and water chemistry*, CRC Press.
- Fedotov, G., V. Putlyaev, et al. (2008). Nanostructural organization of peat glues and routes to improve soil structures. *Doklady Chemistry* 422(1): 208-211.
- Flaig, W. (1958). *Die Chemie der organischer Stoffe in Boden und deren physiologische Wirkung*. Verhandl., II u. IV Komm. int. Bodenk. Ges. 2.

- Gaiffe, M., B. Duquet, et al. (1984). Biological stability and physical behavior of an argillohumic complex placed under different conditions of saturation with calcium or potassium. *Plant and Soil* 77(2-3): 271-84.
- Ghosh, K. and M. Schnitzer (1980). Macromolecular structure of humic substances. *Soil Science* 129: 266-276.
- Haberhauer, G., A. J. A. Aquino, et al. (2001). Modeling of molecular interactions of soil components with organic compounds. *Special Publication - Royal Society of Chemistry* 273(Humic Substances): 209-219.
- Haider, K. and J. P. Martin (1967). Synthesis and Transformation of Phenolic Compounds by *Epicoccum nigrum* in Relation to Humic Acid Formation. *1. 31: 766-772.*
- Haider, K., M. Spiteller, et al. (2000). Silylation of soil organic matter. Extraction of humic compounds and soil-bound residues. *Soil Biochemistry*. J.-M. Bollang and G. Stotzky. New York, Dekker. X: 139-170.
- Harding, L., W. P. King, et al. (2007). Nanoscale characterisation and imaging of partially amorphous materials using local thermomechanical analysis and heated tip AFM. *Pharmaceutical Research* 24(11): 2048-2054.
- Hayase, K. and H. Tsubota (1983). Sedimentary humic acid and fulvic acid as surface active substances. *Geochimica et Cosmochimica Acta* 47(5): 947-952.
- Horii, F. (2001). Structure of cellulose: recent developments in its characterization. *Wood and Cellulosic Chemistry* (2nd Edition). New York, Dekker: 83-107.
- Hu, C., Y. Liu, et al. (2003). Extracellular carbohydrate polymers from five desert soil algae with different cohesion in the stabilization of fine sand grain. *Carbohydrate Polymers* 54(1): 33-42.
- Hurrass, J. and G. E. Schaumann (2005). Is glassiness a common characteristic of soil organic matter? *Environmental Science and Technology* 39(24): 9534-9540.
- Jenkinson, D. S. (1981). The fate of plant and animal residues in soil. . *The chemistry of soil processes* D. J. Greenland and M. S. B. Hayes. Chichester, John Wiley and Sons: 505-561.
- Kalinichev, A. G., E. Iskrenova-Tchoukova, W. Y. Ahn, M. M. Clark and R. J. Kirkpatrick (2011). Effects of Ca²⁺ on supramolecular aggregation of natural organic matter in aqueous solutions: A comparison of molecular modeling approaches. *Geoderma* 169: 27-32.
- Kim, J. E., E. Fernandes, et al. (1997). Enzymatic coupling of the herbicide bentazon with humus monomers and characterization of reaction products. *Environmental Science & Technology* 31(8): 2392-2398.
- Kleber, M. and M. G. Johnson (2010). *Advances in Understanding the Molecular Structure of Soil Organic Matter: Implications for Interactions in the Environment*. *Advances in Agronomy*, Vol 106. D. L. Sparks. San Diego, Elsevier Academic Press Inc. 106: 77-142.
- Kleber, M., P. Sollins, et al. (2007). A conceptual model of organo-mineral interactions in soils: self-assembly of organic molecular fragments into zonal structures on mineral surfaces. *Biogeochemistry* 85(1): 9-24.
- Kohl, S. D., P. J. Toscano, et al. (2000). Solid-state ¹⁹F NMR investigation of hexafluorobenzene sorption to soil organic matter. *Environmental Science and Technology* 34(2): 204-210.
- Kononova, M. M. and N. P. Belchikova (1961). Rapid methods of determination the humus composition of mineral soils. *Pochvovedenie* 10: 75.
- Kucerik, J., P. Bursakova, et al. (2012). Hydration of humic and fulvic acids studied by DSC. *Journal of Thermal Analysis and Calorimetry* 110: 451-459.

- Kucerik, J., H. Cechlovska, et al. (2009). Lignite humic acids aggregates studied by high resolution ultrasonic spectroscopy: Thermodynamic stability and molecular feature. *Journal of Thermal Analysis and Calorimetry* 96(2): 637-643.
- Langford, C. H. and J. R. Melton (2005). When should humic substances be treated as dynamic combinatorial systems? *Humic Substances: Molecular Details and Applications in Land and Water Conservation*. E. A. Ghabbour and G. Davies. New York, Taylor & Francis: 65-78.
- LeBoeuf, E. J. and W. J. Weber (1997). A distributed reactivity model for sorption by soils and sediments. 8. sorbent organic domains: discovery of a humic acid glass transition and an argument for a polymer-based model. *Environmental Science and Technology* 31(6): 1697-1702.
- Leinweber, P., G. Reuter, et al. (1993). Organo-mineral soil clay fractions in fertilization experiments: mineralogy, amounts and quality of organic matter and influence on soil properties. *Applied Clay Science* 8(4): 295-311.
- Lishtvan, I. I. (1977). Modern ideas on some physicochemical properties of peat. *Khim. Tverd. Topl.* 11(3): 43-48.
- Lou, X. W., Q. S. Zhu, et al. (2004). Simulation of size exclusion chromatography for characterization of supramolecular complex: a theoretical study. *Journal of Chromatography A* 1029(1-2): 67-75.
- Lu, Y. and J. J. Pignatello (2004). Sorption of apolar aromatic compounds to soil humic acid particles affected by aluminum(III) ion cross-linking. *Journal of Environmental Quality* 33(4): 1314-1321.
- Mazzei, P. and A. Piccolo (2012). Quantitative Evaluation of Noncovalent Interactions between Glyphosate and Dissolved Humic Substances by NMR Spectroscopy. *Environmental Science & Technology* 46(11): 5939-5946.
- Miano, T. M., A. Piccolo, et al. (1992). Infrared and Fluorescence Spectroscopy of Glyphosate-Humic Acid Complexes. *Science of the Total Environment* 123: 83-92.
- Mikutta, R., M. Kleber, et al. (2006). Stabilization of Soil Organic Matter: Association with Minerals or Chemical Recalcitrance? *Biogeochemistry* 77(1): 25-56.
- Namjesnik-Dejanovic, K. and P. A. Maurice (1997). Atomic force microscopy of soil and stream fulvic acids. *Colloids and Surfaces A: Physicochemical and Engineering Aspects* 120(1-3): 77-86.
- Nanny, M. A., J. M. Bortiatynski, et al. (1997). Noncovalent Interactions between Acenaphthenone and Dissolved Fulvic Acid As Determined by ¹³C NMR T1 Relaxation Measurements. *Environmental Science and Technology* 31(2): 530-534.
- Nardi, S., G. Concheri, et al. (1996). Biological activity of humus. *Humic substances in terrestrial ecosystems*. A. Piccolo. Amsterdam: 361-406.
- Nebbioso, A. and A. Piccolo (2012). Advances in humeomics: Enhanced structural identification of humic molecules after size fractionation of a soil humic acid. *Analytica Chimica Acta* 720(0): 77-90.
- Patrakov, Y. F., S. A. Semenova, N. I. Fedorova, D. P. Ivanov and K. A. Dubkov Modification of the organic matter of brown coals with nitrous oxide. *Solid Fuel Chemistry* 46(3): 159-163.
- Piccolo, A. (2001). The supramolecular structure of humic substances. *Soil Science* 166: 810-832.
- Piccolo, A. (2002). The supramolecular structure of humic substances: A novel understanding of humus chemistry and implications in soil science. *Advances in Agronomy* 75: 57-134.
- Piccolo, A. and P. Conte (1999). Molecular size of humic substances. *Supramolecular associations versus macromolecular polymers* (Reprinted from *Advances in*

- Environmental Research, vol 3, pg 508-521, 2000). *Advances in Environmental Research* 3(4).
- Piccolo, A. and P. Conte (2000). Molecular size of humic substances. Supramolecular associations versus macromolecular polymers. *Advances in Environmental Research* 3: 508-521.
- Piccolo, A., P. Conte, et al. (2003). Effects of some dicarboxylic acids on the association of dissolved humic substances. *Biology and Fertility of Soils* 37(4): 255-259.
- Piccolo, A., P. Conte, et al. (2005). Increased conformational rigidity of humic substances by oxidative biomimetic catalysis. *Biomacromolecules* 6(1): 351-358.
- Piccolo, A., A. Cozzolino, et al. (2000). Polymerization of Humic Substances by an Enzyme-catalyzed Oxidative Coupling. *Naturwissenschaften* 87: 391-394.
- Piccolo, A. and J. S. C. Mbagwu (1999). Role of Hydrophobic Components of Soil Organic Matter in Soil Aggregate Stability. *Soil Science Society of America Journal* 63(6): 1801-1810.
- Piccolo, A. and S. Nardi (1996). Macromolecular Changes of humic substances induced by interaction with organic acids. *European Journal of Soil Science* 47: 319-328.
- Piccolo, A., S. Nardi, et al. (1996). Micelle-like conformation of humic substances as revealed by size exclusion chromatography. *Chemosphere* 33(4): 595-602.
- Rossini, C. J., J. F. Arceo, et al. (2001). Use of in-situ atomic force microscopy to monitor the biodegradation of polyhydroxyalkanoates (PHAs). *Macromolecular Symposia* 167: 139-151.
- Rudolph, N. and G. E. Schaumann (2006). Effect of Lead and Calcium on glassiness in soil organic matter. *Humic Substances - Linking Structure to Functions. Proceedings of the 13th Meeting of the International Humic Substances Society in Karlsruhe*. F. H. Frimmel and G. Abbt-Braun. Karlsruhe, Universität Karlsruhe. 45-II: 833-836.
- Schaumann, G. E. (2006). Soil organic matter beyond molecular structure. 1. Macromolecular and supramolecular characteristics. *Journal of Plant Nutrition and Soil Science* 169(2): 145-156.
- Schaumann, G. E. (2006). Soil organic matter beyond molecular structure. 2. Amorphous nature and physical aging. *Journal of Plant Nutrition and Soil Science* 169(2): 157-167.
- Schaumann, G. E., D. Gildemeister, et al. (resubmitted 2013). Cation specific formation and aging of cross-links in soil organic matter (SOM). *Journal of Soils and Sediments*.
- Schaumann, G. E. and J. Hurraß (2003). Changes of porosity and soil physical chemistry due to drying and re-wetting cycles. *Mitteilungen der Deutschen Bodenkundlichen Gesellschaft* 101: 39-40.
- Schaumann, G. E., F. Lang, et al. (2006). Do multivalent cations induce cross-links in DOM precipitates? *Humic Substances - Linking Structure to Functions. Proceedings of the 13th Meeting of the International Humic Substances Society in Karlsruhe*. F. H. Frimmel and G. Abbt-Braun. Karlsruhe, Universität Karlsruhe. 45-II: 941-944.
- Schaumann, G. E. and S. Thiele-Bruhn (2011). Molecular modelling of soil organic matter: Squaring the circle? *Geoderma* 169: 55-68.
- Schaumann, G. E. and Y. Kunhi Mouvenchery (2012). Erratum to: Potential of AFM-NanoThermal Analysis to study the microscale thermal characteristics in soils and natural organic matter (NOM). *Journal of Soils and Sediments* 12(1): 115
- Schneckenburger, T., C. V. Lattao, et al. (2012). Preparation and characterization of humic acid cross-linked with organic bridging groups. *Organic Geochemistry* 47(2012): 132-138.
- Schneckenburger, T., G. E. Schaumann, et al. (2012). Short-term evolution of hydration effects on soil organic matter properties and resulting implications for sorption of naphthalene-2-ol. *Journal of Soils and Sediments* 12(8): 1269-1279.

- Schnitzer, M. and S. U. Khan (1972). *Humic Substances in the environment*. New York, Dekker.
- Schulten, H.-R. (1997). Molecular modeling of humic sorption processes of xenobiotic organic compounds in humic and soil particles.
- Schulten, H. R. and P. Leinweber (2000). New insights into organic-mineral particles: composition, properties and models of molecular structure. *Biology and Fertility of Soils* 30(5-6): 399-432.
- Schulten, H. R., P. Leinweber, et al. (1998). Analytical pyrolysis and computer modeling of humic and soil particles. *Structure and Surface Reactions of Soil Particles*. New York, John Wiley & Sons. 4: 281-324.
- Senesi, N., B. Xing, et al. (2009). *Biophysico-Chemical Processes Involving Natural Nonliving Organic Matter in Environmental Systems* Hoboken, NJ, John Wiley & Sons Inc.
- Simpson, A. J., W. L. Kingery, et al. (2002). Molecular structures and associations of humic substances in the terrestrial environment. *Naturwissenschaften* 89(2): 84-88.
- Six, J., R. T. Conant, et al. (2002). Stabilization mechanisms of soil organic matter: Implications for C-saturation of soils. *Plant and Soil* 241(2): 155-176.
- Smith, M. B. and J. March (2007). *March's Advanced Organic Chemistry: Reactions, Mechanisms, and Structure*, Wiley.
- Spaccini, R., A. Piccolo, et al. (2001). Decomposition of maize straw in three European soils as revealed by DRIFT spectra of soil particle fractions. *Geoderma* 99(3-4): 245-260.
- Sparks, D. L. (1995). *Environmental Soil Chemistry* 1 ed. San Diego, Academic Press, Inc.
- Steed, J. W. and J. L. Atwood (2000). *Supramolecular Chemistry: A concise introduction*. Chichester, John Wiley & Sons, Ltd.
- Stevenson, F. J. (1994). *Humus Chemistry: Genesis, Composition, Reactions*. New York, Wiley.
- Sutton, R. and G. Sposito (2005). Molecular structure in soil humic substances: The new view. *Environmental Science and Technology* 39(23): 9009-9015.
- Swift, R. S. (1989). Molecular weight, size, shape and charge characteristics of humic substances: Some basic considerations. *Humic substances II: In search of structure*. M. H. B. Hayes, P. MacCarthy, R. L. Malcolm and R. S. Swift. New York, John Wiley & Sons: 449-465.
- Tarasevich, Y. I., S. A. Dolenko, M. Y. Trifonova and E. Y. Alekseenko (2013). Association and colloid-chemical properties of humic acids in aqueous solutions. *Colloid Journal* 75(2): 207-213.
- ten Hulscher, T. E. M. and G. Cornelissen (1996). Effect of temperature on sorption equilibrium and sorption kinetics of organic micropollutants—a review. *Chemosphere* 32(4): 609-26.
- Tielemans, M., P. Roose, et al. (2012). Multiphase coatings from complex radiation curable polyurethane dispersions. *Progress in Organic Coatings* 75(4): 560-568.
- Tipping, E., Ed. (2004). *Cation Binding by Humic Substances*. Cambridge Environmental Chemistry Series. New York, Cambridge University Press.
- Vlckova, Z., L. Grasset, et al. (2009). Lignite pre-treatment and its effect on bio-stimulative properties of respective lignite humic acids. *Soil Biology & Biochemistry* 41(9): 1894-1901.
- von Wandruszka, R., M. Schimpf, et al. (1999). Characterization of humic acid size fractions by SEC and MALS. *Organic Geochemistry* 30(4): 229-235.
- Wang, Y. S., X. Q. Shan, M. H. Feng, G. C. Chen, Z. G. Pei, B. Wen, T. Liu, Y. N. Xie and G. Owens (2009). Effects of Copper, Lead, and Cadmium on the Sorption of 2,4,6-

- Trichlorophenol Onto and Desorption from Wheat Ash and Two Commercial Humic Acids. *Environmental Science & Technology* 43(15): 5726-5731.
- Wershaw, R. L. (1986). A new model for humic materials and their interactions with hydrophobic organic chemicals in soil-water or sediment-water systems. *Journal of Contaminant Hydrology* 1: 29-45.
- Wershaw, R. L. (2004). Evaluation of Conceptual Models of Natural Organic Matter (Humus) From a Consideration of the Chemical and Biochemical Processes of Humification Scientific Investigations Report 2004-5121. G. A. Norton and C. G. Groat. Reston, Virginia, U.S. Department of the Interior, U.S. Geological Survey 49.
- Wrobel, K., B. B. M. Sadi, et al. (2003). Effect of metal ions on the molecular weight distribution of humic substances derived from municipal compost: Ultrafiltration and size exclusion chromatography with spectrophotometric and inductively coupled plasma-MS detection. *Analytical Chemistry* 75(4): 761-767.
- Xia, G. and J. J. Pignatello (2001). Detailed Sorption Isotherms of Polar and Apolar Compounds in a High-Organic Soil. *Environmental Science and Technology* 35(1): 84-94.
- Xing, B. and J. J. Pignatello (1997). Dual-mode sorption of low-polarity compounds in glassy poly(vinyl chloride) and soil organic matter. *Environmental Science and Technology* 31(3):792-799.

Chapter 2

[Cation-mediated cross-linking in natural organic matter: a review](#)

Kunhi Mouvenchery, Y., Kucerik, J., Diehl, D., Schaumann, G.E. (2012)

Reviews in Environmental Science and Biotechnology 11: 41-54

Chapter 3

[Restructuring of a peat in interaction with multivalent cations:](#)

[Effect of cation type and aging time](#)

Kunhi Mouvenchery, Y., Jäger, A., Aquino, A.J.A., Tunega, D, Diehl, D.,

Bertmer, M., Schaumann, G.E. (2013) PLoS ONE 8(6): e65359.

doi:10.1371/journal.pone.0065359

Chapter 4

Cation mediated cross linking in soil organic matter: role of hydration shell

Kunhi Mouvenchery, Y., Schaumann, G.E.

publication in preparation

4.1 Introduction

The chapter 2 demonstrates three different types of CaB, possible within SOM, depending on the hydration status of cations; direct CaB, indirect CaB via hydration shell and CaB-WaMB associations including additional water molecules, apart from the hydration water. Among them, the latter two are assumed to be more relevant in SOM, since cations mostly occur in hydrated state, under natural conditions (see chapter 2). A recently published study by Schaumann et al. (2013) showed the relevance of CaB-WaMB associations, for the biogeochemical functioning of SOM. They assessed the mobility of differently confined water in cationic hydration shells and in CaB-WaMB associations using ^1H NMR, in relation with wettability characteristics. That study, thus points to the need of obtaining deeper insight into the interplay between cations and water molecules involved in these specific interactions. Even though a few studies, attempting to demonstrate CaB and WaMB in general, have come out (Schaumann et al. 2006; Aquino et al. 2011; Kunhi Mouvenchery et al. 2012; Schaumann et al. 2013; Kunhi Mouvenchery et al. 2013; Schaumann et al. submitted 2013), no focus was given to the role of hydration water in determining the type of CaB, yet. Recognising this lack of knowledge, study described in this chapter was dedicated to reveal the role of cation hydration water in CaB interactions.

Water molecules present in the cation hydration shell are hypothesised to enhance cross-linking, especially with the potential to bridge larger distances. Water molecules confined in CaB-WaMB associations may be more dynamic whereas hydration water molecules are rather fixed in its position due to stronger binding with cations. Thus the more hydrated cation is expected to bridge larger distances within the OM matrix. Higher dynamicity of its hydration water is expected to cause stronger aging effect to achieve the maximum rigidity state, faster. This study aims to verify these hypotheses via targeted experiment. Further, it has been seen in the previous chapter that the cation treatment procedure did not induce immediate effect on matrix rigidity in the peat OM and it implied that the physicochemical structure of OM is determinant for the formation of CaB and WaMB (Kunhi Mouvenchery et al. 2013). Therefore, this additional study using a different OM sample was supposed to help in evaluating the validity of the experimental strategy in inducing cross-links. This would also allow to find out variation in response of a different physicochemical system of OM to cation treatment.

To that end, a forest floor soil, rich in SOM was used. Since the cationic size and stability of hydration shell are decisive for inner- or outer sphere complexation, potentially cross-linking

cations were selected such a way that effects due to their other ionic properties could be separated. Alkaline earth metal cations (Mg^{2+} , Ca^{2+} , Ba^{2+} , etc.) were used, since the three are well known for their cross-linking potential (Zhang 1995).

4.2 Materials and Methods

Materials

The sample used for this study was obtained from an organic surface layer of a Haplic Podzol (pH 3.8, CEC_{eff} $303 \pm 23 \text{ mmol}_c\text{kg}^{-1}$) sampled in a forest stand dominated by 80 year old Norway spruces (*Picea abies* L. [Karst.]) in South Germany. The effective spatial distance between cation exchange sites based on CEC_{eff} , assuming that they are uniformly distributed, is $\sim 2.8 \text{ nm}$. The sample was air-dried, sieved ($< 2 \text{ mm}$) and equilibrated at $20 \text{ }^\circ\text{C}$ for at least 28 days prior to use. MgCl_2 , CaCl_2 , BaCl_2 , NaOH , HCl , HNO_3 , BaCl_2 and MgSO_4 were purchased from Sigma Aldrich. All chemicals used in this study were of analytical grade.

Methods

The experimental procedures are the same as in the study described in previous chapter (Kunhi Mouvenchery et al. 2013). Procedures adopted for cation treatment, analysis of treated samples to estimate total cation content, cation exchange capacity and step-transition temperature are briefly noted here in the following paragraphs.

Removal of cations originally present in the peat. 10 g soil was first shaken for 24 hours at a speed of 15 rpm in 225 ml of de-ionised water, with a non-selective Amberlite resin (IR 120, H^+ form with exchange capacity of $2.3 \text{ mmol}_c\text{g}^{-1}$ from Merck, Darmstadt; 12.5 g resin per 10 g peat) packed in plastic gauzes. This resulted in pH of 2.8. One resin-treated sample was isolated from the treatment solution without further treatment, to be able to distinguish the effects of cations from that of the resin treatment procedure.

Cation treatment. The resin packets were removed gently from the treatment solution and then the pH was adjusted to the original pH (3.8), based on the previous result (see chapter 3) that more cations were incorporated into peat OM higher pH. 1M NaOH solution (3.2 ml) was used. This makes the treated and untreated samples comparable, in terms of pH. Directly after pH adjustment, 25 ml of solutions of MgCl_2 , CaCl_2 and BaCl_2 (1.2, 6.1, 9.7 12.1 and $18.2 \text{ mmol}_c\text{L}^{-1}$), respectively, were added. Amount of cations to be applied was defined with the aim to occupy a fraction of its CEC_{eff} by the added ions. Degree of saturation of 10, 50,

80, 100 and 150 % of CEC_{eff} were anticipated. This corresponds to cation concentrations of 30.3, 151.5, 242.4, 303.0 and 454.5 $mmol_c kg^{-1}$, respectively.

Additionally, 10 g of the soil was treated merely with water, without involving resin-treatment and pH adjustment, in order to assess the swelling effect and other structural changes caused by mechanical agitation during the treatment process. This sample is named as 'water-treated' sample.

Isolation and storage of cation treated peat. Each soil-solution mixture was filtered through 0.45 micrometer filters under suction pressure. The filtrates were later analysed for cation content. The collected solid materials were dried at 25 °C in a thermostat for three days and then equilibrated for at least two weeks in an atmosphere with 76 % relative humidity, maintained using saturated NaCl solution, prior to any analysis. One untreated soil sample was stored in the same way and subjected to similar analysis as done for the treated samples.

Analysis of sample properties

Total metal analysis. Total cation content was determined by a microwave-assisted acid digestion in a microwave digestion chamber (Microwave MarsXpress (CEM GmbH)) using reverse aqua regia ($10 ml g^{-1}$). All extracts were analysed using an ICP-OES instrument (Thermo Fisher Scientific, Germany) to quantitatively determine the major cations – Al^{3+} , Ca^{2+} , Mg^{2+} , Na^+ and Fe^{3+} . The emission wavelengths used were, 588.955 nm, 279.078 nm, 183.944 nm, 233.527 nm, 167.019 nm, 238.204 nm for Na^+ , Mg^{2+} , Ca^{2+} , Ba^{2+} , Al^{3+} , Fe^{3+} , respectively.

Effective Cation Exchange Capacity (CEC_{eff}). The exchangeable cations were first exchanged against 0.1 M $BaCl_2$ solution (25 ml) and the barium ions were then exchanged against 0.05 M Mg^{2+} using $MgSO_4$ solution (25 ml). The amount of unexchanged magnesium ions was determined by ICP-OES (Thermo Fisher Scientific, Germany).

Differential Scanning Calorimetry (DSC). Thermal analysis to determine step transition temperature was done using a DSC Q1000 (TA Instruments, Germany) with refrigerated cooling system and nitrogen as purge gas. Measurements were conducted in the temperature range between -50 °C and 110 °C. Baseline was corrected with the TZero Technology® by

TA Instruments. Data were analysed using Universal Analysis software, version 4.1 (TA Instruments).

Samples were analysed again after four months and eight months in order to investigate the effect of aging. In order to be able to observe the rate of change in T^* , the result will be discussed, considering the whole 8 weeks as two slots of 4 week duration.

4.3 Results and Discussion

Cation content after treatment. Figure 1 shows the cation content of cation-treated (1A,1B and 1C), resin-treated, water-treated and untreated soil samples (1D). The untreated SOM contained mainly Na^+ ($2.85 \pm 1.3 \text{ mmol}_c\text{kg}^{-1}$), Mg^{2+} ($42.53 \pm 0.36 \text{ mmol}_c\text{kg}^{-1}$), Ca^{2+} ($118.47 \pm 1.9 \text{ mmol}_c\text{kg}^{-1}$), Al^{3+} ($60.21 \pm 3.6 \text{ mmol}_c\text{kg}^{-1}$) and Fe^{3+} ($79.98 \pm 0.66 \text{ mmol}_c\text{kg}^{-1}$). Water treated sample has the same cation composition (figure 1). The resin-treated sample contained much lower amount of all cations ($3.77 \pm 2.7 \text{ mmol}_c\text{kg}^{-1}$ of Mg^{2+} , $5.53 \pm 1.7 \text{ mmol}_c\text{kg}^{-1}$ of Ca^{2+} , $14.82 \pm 0.21 \text{ mmol}_c\text{kg}^{-1}$ of Al^{3+} and $12.89 \pm 0.24 \text{ mmol}_c\text{kg}^{-1}$ of Fe^{3+}). Resin-treatment resulted in removal of 88 % of initially present total cations, which corresponds to 91 % of Mg^{2+} , 95 % of Ca^{2+} , 75 % of Al^{3+} and 83 % of Fe^{3+} , relative to their initial amount. Comparably lower removal of Al^{3+} and Fe^{3+} could possibly be due to the formation of inorganic colloids by the two cations, as suggested in previous chapter (Kunhi Mouvenchery et al. 2012).

Cation-treated samples contain 32-76 % of the initial cation content, varying with the added amount and cation type. It is notable that the highest uptake of Mg^{2+} , Ca^{2+} and Ba^{2+} reached only up to 76 % of the amount of total cations that were initially present in the SOM, even if the added amount of cations ranged above the initial cation content. This is indicative for that cation removal, conducted by exchange resin induces irreversible changes within the SOM, partly, which prevent the uptake of further cations. Structural hindrance might have been induced, at least at some parts of the OM structure. It could be that protonation of the system induced by resin-treatment brings functional groups together to form H-bonds and thus make them inaccessible for added cations, as already suggested in the previous chapter.

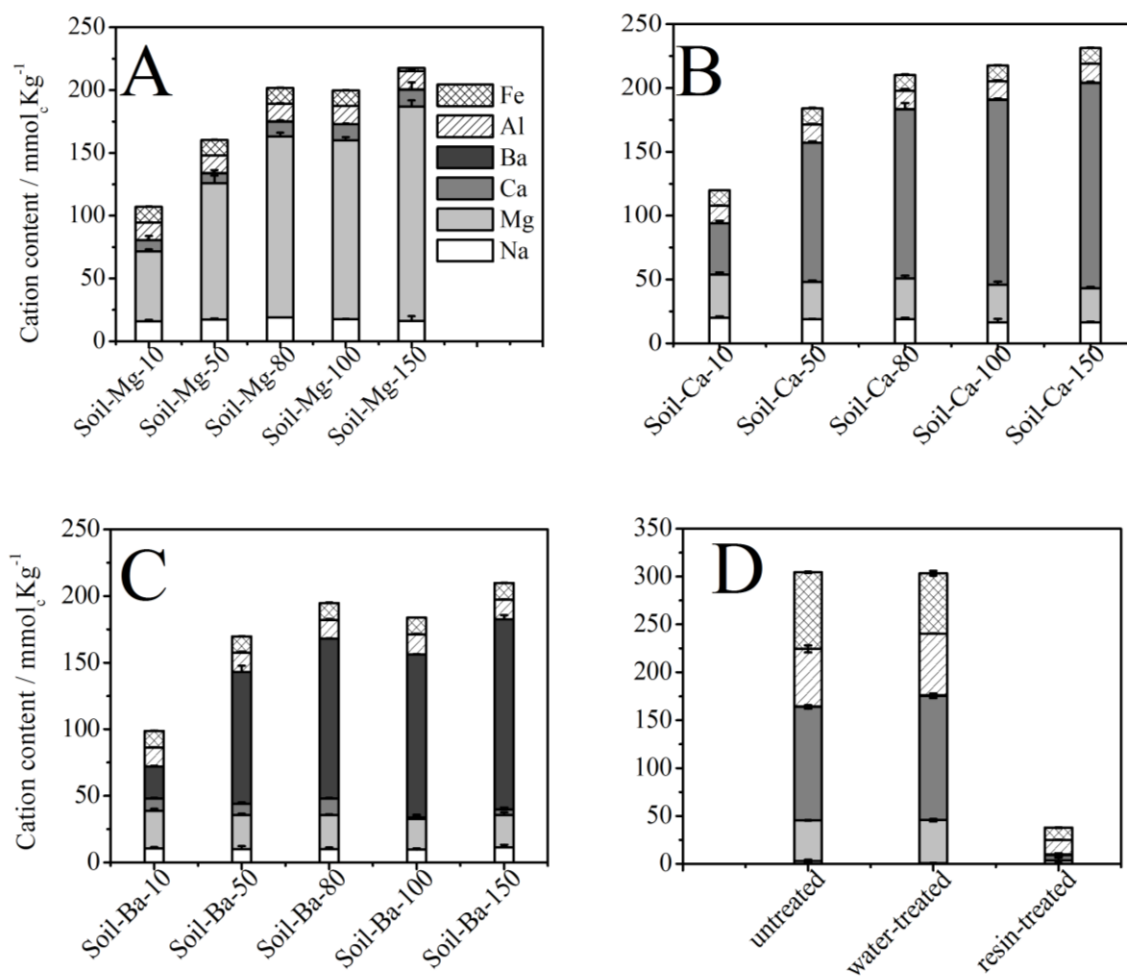


Figure 1. Cation content of untreated and all treated soil samples. A) Soil-Mg, B) Soil-Ca C) and Soil-Ba. Numbers in x-axis label show the added concentration in terms of percentage of CEC_{eff} of original soil. D shows the data of untreated, water-treated and resin-treated samples.

Cation sorption. Cation sorption was well-described by Langmuir isotherm (Kunhi Mouvenchery et al. 2013) ($R^2 = 0.79, 0.85$ and 0.93 for Mg, Ca and Ba sorption, respectively), as shown in figure 2. The sorption parameters – Langmuir coefficient (k) and maximum sorbable concentration (Q_{max}) – are shown in figure 3. k , which indicates the affinity of SOM to individual cation increases in the order: $Mg < Ca < Ba$. Q_{max} values revealed inverse relation, showing that Ba sorption is more restricted than Ca sorption which is even more restricted than sorption of Mg.

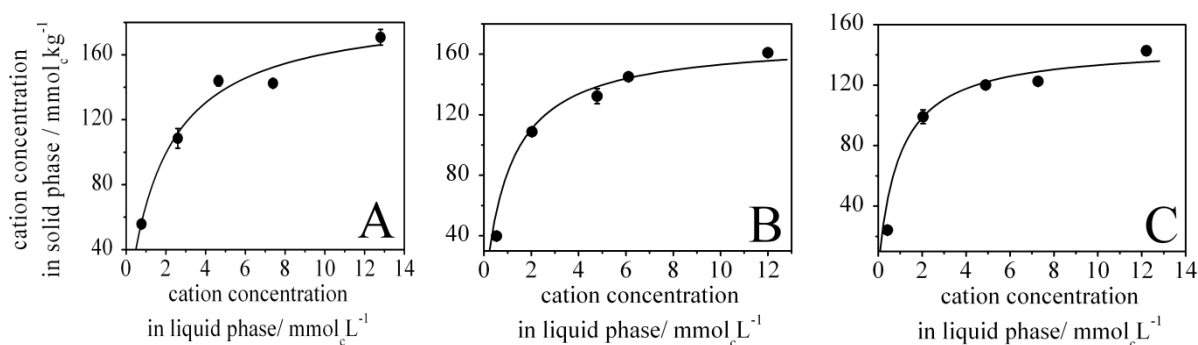


Figure 2. Cation Sorption isotherms for A) Mg²⁺, B) Ca²⁺ and C) Ba²⁺ sorption. The lines show Langmuir fit (equation 1 in chapter 3) of the data.

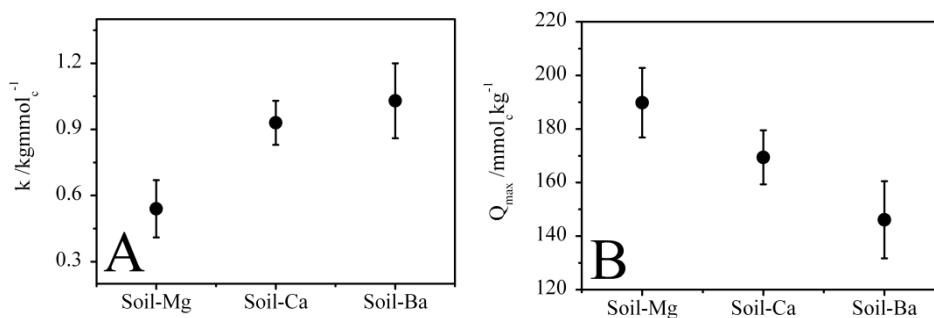


Figure 3. Langmuir sorption parameters. A) Langmuir coefficient (k) and B) Maximum sorbable concentration (Q_{max}).

The Langmuir mode of sorption suggests that sorption increases strongly with increase in sorbent concentration at its lower values and, at higher amount of sorbents, intensity of sorption becomes lower and reaches a maximum concentration, beyond which no sorption takes place. Such a development is expectable in SOM samples, as cation sorption depends up on the number of deprotonated functional groups and cation exchanging sites, which is very low in the OM under discussion, relative to other SOM samples.

Dependency of k on cation type can be explained, based on higher charge to size ratio of Ba²⁺ than Ca²⁺ and Mg²⁺, in the hydrated state. Thus, stronger Ba²⁺ can bind with more functional groups than the other two cations would do. On the other hand, it can be seen that Q_{max} is directly proportional to the cationic size in hydrated state. Radii of Mg²⁺, Ca²⁺ and Ba²⁺ in hydrated state are 400 pm, 300 pm and 250 pm, respectively. This could be explained by the large effective distance (~2.8 nm) between adjacent OM functionalities, as follows. Such large distance may not be easily bridged by small cations. It might be that larger Mg²⁺ in

hydrated state bridge larger voids between functional groups, in association with more water molecules, whereas smaller ions such as Ca^{2+} and Ba^{2+} can bridge only smaller voids. The notion that the effective distance between functional groups are relatively larger, thus explains the uptake of more Mg^{2+} than the smaller cations. Thus it can be seen that the uptake of cations is determined by interplay of cationic strength and size in hydrated state.

Further, it can be seen that Q_{max} values ($189 \pm 13 \text{ mmol}_c\text{kg}^{-1}$, $169 \pm 10 \text{ mmol}_c\text{kg}^{-1}$ and $146 \pm 14 \text{ mmol}_c\text{kg}^{-1}$ for sorption of Mg^{2+} , Ca^{2+} and Ba^{2+} , respectively) were much lower than the amount of total cations in the original soil ($305 \pm 12 \text{ mmol}_c\text{kg}^{-1}$). This is in line with the observation that only partial uptake was undertaken, even if the total added amount exceeded CEC_{eff} (see the previous section), but needs further explanation.

Effect of cation treatment on general soil parameters

Cation exchange capacity (CEC_{eff}). Effective cation exchange capacity of treated samples is shown in figure 4. Untreated ($303 \pm 23 \text{ mmol}_c\text{kg}^{-1}$) and water treated soils ($311 \pm 18 \text{ mmol}_c\text{kg}^{-1}$) possessed comparably similar CEC_{eff} , whereas the resin-treated sample revealed higher exchange capacity ($414 \pm 12 \text{ mmol}_c\text{kg}^{-1}$). Cation-treated samples revealed exchange capacity ranging from 310-560 $\text{mmol}_c\text{kg}^{-1}$, depending on type and amount of incorporated cation. Mg-Soil samples showed gradually increasing CEC_{eff} with increase in amount of Mg^{2+} . Ca-Soil and Ba-Soil showed stronger increase with cation concentration (slopes: 0.93 and 1.45, respectively). But at very higher concentrations, the CEC_{eff} values become comparable.

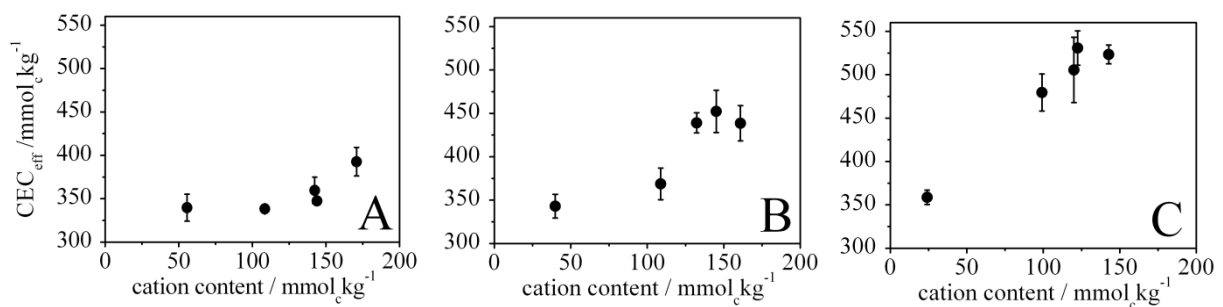


Figure 4. Cation exchange capacity of cation-treated samples. A) Soil-Mg, B) Soil-Ca and C) Soil-Ba. Values of untreated and resin-treated samples were $303 \pm 23 \text{ mmol}_c\text{kg}^{-1}$ and $414 \pm 12 \text{ mmol}_c\text{kg}^{-1}$, respectively.

Similar CEC_{eff} for untreated and water-treated samples indicates that treatment procedure that included thorough shaking of the sample with water did not affect the binding status of cations and no significant amount of exchangeable cations were mobilised as water-soluble salts. Significantly higher CEC_{eff} of resin-treated samples shows that removal of exchangeable cations opened more sites for exchange against Ba^{2+} in CEC experiment. On contrary, an equivalent amount of Ba^{2+} was not sorbed to the SOM during addition of Ba^{2+} in cation treatment procedure. A much higher concentration of $BaCl_2$ used during the experiment to estimate CEC_{eff} would explain these contradicting observations.

Similar CEC_{eff} at higher loading of cations in case of Soil-Ca and Soil-Ba indicates that additional cations, added beyond a limit value occupy non-exchange sites and are not available for exchange.

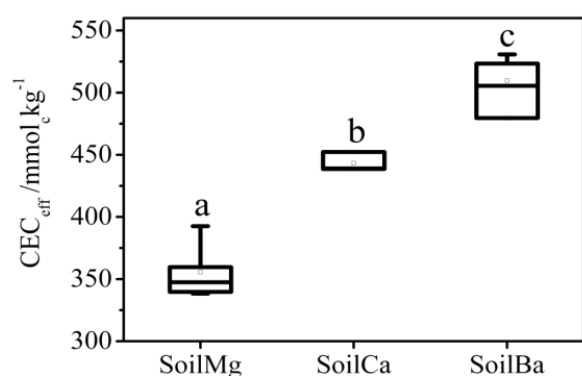


Figure 5. Cation exchange capacity of samples with high cation loading, distinguished by the type of added cation. Letters on top of the box distinguishes statistically significant groups.

At higher cation content, CEC_{eff} vary in the order: Soil-Mg < Soil-Ca < Soil-Ba (figure 5). This is in contradiction to the expectation that stronger cations would form stronger binding and are less exchangeable than the weaker cations. No reasonable argument can be assigned for this unexpected dependence, currently.

WaMB-transition temperature (T^*). T^* of the untreated and water-treated samples were found to be 62.5 ± 0.7 °C and 62.1 ± 1.2 °C, respectively. Resin-treated sample has lower T^* (58.3 ± 0.8 °C). Cation-treated samples revealed T^* values ranging from 56.1 ± 1.1 °C to 60.4 ± 1.0 °C, depending on the type and amount of added cations (figure 6).

The observation that untreated and water-treated samples revealed similar T^* values suggests that treatment procedure did not affect OM matrix rigidity significantly, in this soil. But the resin-treated soil had lower T^* , indicating that replacement of exchangeable cations by protons had lowered the matrix rigidity. A relatively higher matrix rigidity of the untreated soil suggests that it contained already existing CaB and/or WaMB which were disrupted

during resin-treatment. The hydrophobic interactions between protonated functional groups in resin-treated sample are weaker than polar interactions involved in CaB and WaMB and thus they can be easily disrupted at lower temperatures, resulting in lower T^* .

It can be seen from figure 6 that Ca^{2+} - and Ba^{2+} - treatment increased the matrix rigidity after resin-treatment, but the system did not reach the state of untreated soil ($T^* = 62.3 \text{ }^\circ\text{C}$), even at highest loading of cations ($T^*_{\text{max}} = 61.5 \text{ }^\circ\text{C}$). This could be understood when considering that treated samples, even the one with highest cation loading, possess lower cation content than the untreated soil. This confirms the notion that untreated soil itself possesses CaB or CaB-WaMB associations within its OM matrix.

Figure 6 shows that T^* of Soil-Mg samples did not show significant dependence on the amount of Mg^{2+} ($P=0.8$). On contrary, T^* increased linearly with increase in cation content for Soil-Ca and Soil-Ba samples ($P=0.01$ and 0.01 , respectively). Further, box plot in figure 7 shows T^* values for each cation-treatment, over all the cation concentrations. Such a graph is expected to reveal effect of cation type, as each set contained samples with comparable cation content.

Soil-Mg samples did not show concentration-dependant matrix rigidity (figure 6), revealing that newly added cations form similar, weak interactions that are vulnerable to disruption, easily. However, concentration-dependence of T^* in Ca^{2+} - and Ba^{2+} -treated samples (figure 6) shows that the two cations increase OM matrix rigidity by forming CaB.

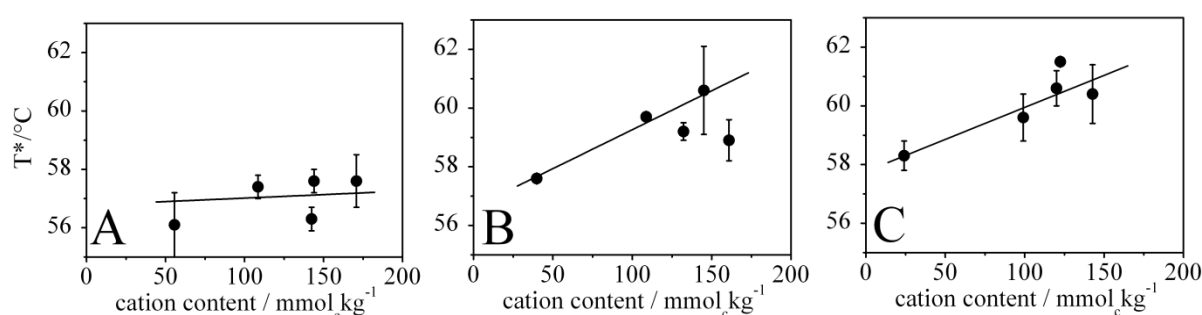


Figure 6. WaMB-transition temperature of treated samples. A) Soil-Mg, B) Soil-Ca and C) Soil-Ba. The lines show linear fit of the data. The values of untreated and resin-treated samples were $62.5 \pm 0.7 \text{ }^\circ\text{C}$ and $58.3 \pm 0.8 \text{ }^\circ\text{C}$, respectively.

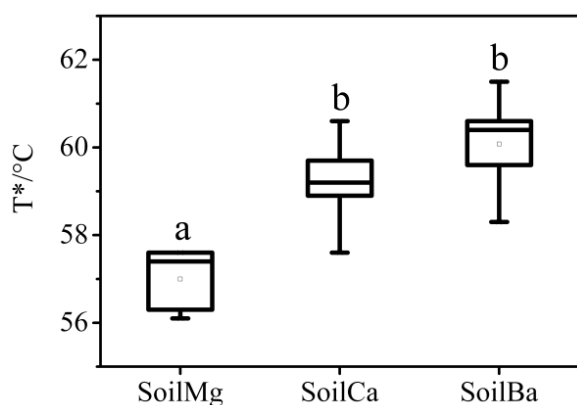


Figure 7. WaMB-transition temperatures distinguished by cation type. Each box contains data for all values of cation content, including replicates. Letters on top of the box distinguishes statistically significant groups.

Soil-Mg samples revealed lower T^* than Soil-Ca and Soil-Ba samples (figure 7). The lower T^* value revealed by Soil-Mg than the resin-treated soil and the Soil-Ca and Soil-Ba samples suggests that Mg^{2+} either reduces the OM matrix rigidity by disrupting the existing cross-links or it forms weaker cross-links within the SOM. Interference by Mg^{2+} within the existing cross-links, without forming stronger interactions are less favoured. Also the notion that the stronger Ca^{2+} and Ba^{2+} did not cause such bond disruptions contradicts the suggestion. But formation of weaker cross-links by Mg^{2+} is possible, considering that Mg^{2+} fits only in larger voids, due to the larger size of hydrated Mg^{2+} ; as already discussed based on higher Q_{max} of Mg^{2+} sorption (see discussion of figure 3). Therefore, it binds with more binding partners than required by Ca^{2+} and Ba^{2+} . Thus the cationic charge density is distributed among many functional groups, forming weaker individual bond and thus vulnerable to disruption at low temperature. This also explains lower T^* shown by Soil-Mg than the other two sets of cation treated samples.

Aging effect on T^* . Figure 8 shows T^* values measured after 4 and 8 weeks. T^* of all the samples increased significantly during both the time intervals. Untreated and resin-treated samples reached T^* of 66.2 ± 0.4 °C and 67.2 ± 0.9 °C, respectively, after 8 weeks of storage. Values shown by cation treated samples varied between 60.6 °C and 65.0 °C, depending on cation type. T^* of Soil-Mg samples remained independent on cation concentration even after 8 weeks of aging. Parallel to this, T^* of Soil-Ca and Soil-Ba samples become less dependent on cation content, as the aging time increases. Further, aging effect on matrix rigidity (change in T^* , ΔT^*) during the first 4 weeks after treatment and during the following 4 weeks are shown as box plots in figure 9A and 9B, respectively. The 8 week duration was splitted into two 4 week periods, in order to visualise the change in the speed of development in ΔT^* . It shows that in the first 4 weeks, T^* of Soil-Mg samples increased by 2.9 ± 0.3 °C and that of Soil-Ca and Soil-Ba increased by 1.7 ± 0.6 °C and by 1.7 ± 0.7 °C, respectively. Aging

during the next 4 weeks showed more influence on matrix rigidity, with resultant ΔT^* values of 5.2 ± 0.6 °C, 2.1 ± 1.0 °C and 1.8 ± 0.9 °C, respectively for Soil-Mg, Soil-Ca and Soil-Ba samples. This shows that structural reorganisation/aging get faster in time. Untreated and resin-treated samples increased their T^* values by 3.9 ± 1.2 °C and 8.0 ± 0.3 °C, respectively, during the 8 weeks of aging.

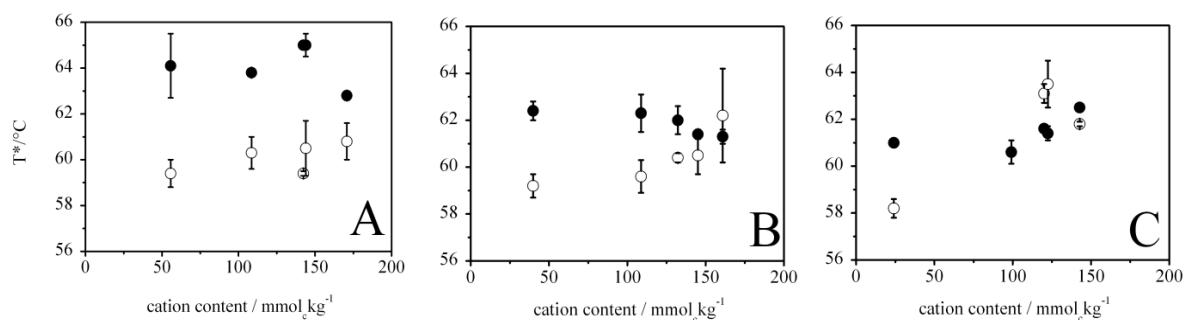


Figure 8. WaMB-transition temperature after sample aging for 4 weeks (○) and 8 weeks (●). A) Soil-Mg, B) Soil-Ca and C) Soil-Ba.

Higher T^* after first 4 weeks and even higher values after next 4 weeks indicate that the SOM undergoes structural reorientation to form more and more rigid matrix. It can be that during the storage time, intrinsic mobility of supramolecular OM segments, water molecules and cations occur such a way that more and more CaB, WaMB and/or CaB-WaMB are formed. It can also be that existing CaB-WaMB associations slowly loose water molecules from their sites, owing to structural changes to form stronger CaB interactions. Physicochemical structural alterations can displace weakly bound water molecules in CaB-WaMB associations, when the spatial distribution of OM functionalities is in favour. However, this process will occur slowly, as no external energy was applied. This explains considerably higher matrix rigidity after 8 weeks than after 4 weeks. Further, fading of concentration dependence in Soil-Ca and Soil-Ba samples with time is indicative for homogenisation of OM matrix with respect to matrix rigidity, in each sample group.

Moreover, Soil-Mg samples attained significantly higher matrix rigidity (figure 8) than Soil-Ca and Soil-Ba samples, after 8 weeks of storage. This shows that structural dynamicity to reach the potential CaB and /or WaMB state is much higher in Mg-Soil samples. It can be that either the exiting CaB or CaB-WaMB associations loose the excess water molecules to form stronger bridges or pure WaMB interactions are newly developed. In either case, water molecules play determinant role. On the other hand, Soil-Ca and Soil-Ba samples are

dominated by effects of cations and degree of restructuring is lower. As Ca and Ba possess stronger hydration shell, the degree of water molecule-related dynamicity is lower in those two sets of samples.

Box plots in figure 9A and 9B shows that Soil-Mg samples undergo stronger structural changes, as the increase in T^* is significantly higher than the other samples, in both aging time intervals. This shows that Soil-Mg samples are more mobile. This is in accordance with that Soil-Mg samples showed lower rigidity immediately after treatment. A less rigid system is more mobile and undergoes more intensive changes in time. It could be that the weakly bound water molecules around Mg^{2+} are redistributed and misplaced from the vicinity of the cation to form longer (and hence weaker) bridges, owing to the structural mobility of SOM. Less hydrated Mg^{2+} can form stronger bridges to result in much higher T^* . The structural requirement that the voids to be bridged by bare/less hydrated cations is possibly met, after significant restricting of SOM. This then provides a hint that storage time itself can strengthen CaB by loss of water molecules from CaB-WaMB associations or from cation hydration shell. Similar is the case for resin-treated sample which underwent a higher net increase in matrix rigidity in 8 weeks, than the untreated, Soil-Ca and Soil-Ba samples. But the changes are lower than that occurred in Soil-Mg, by the same duration, in accordance with the lower T^* for Soil-Mg directly after treatment. Lower degree of changes occurred in untreated samples than most of the treated samples again shows that the soil, in the original form, possessed significant cross-linking which was altered by various steps of treatment procedure.

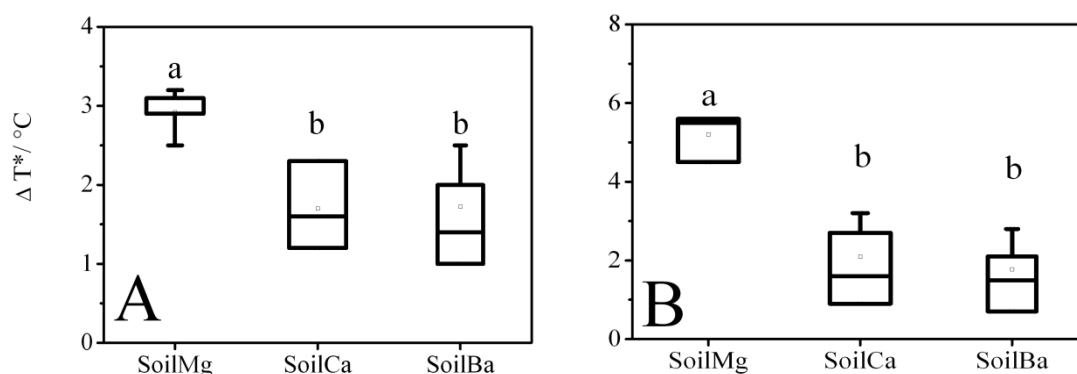


Figure 9. Change in WaMB-transition temperature after sample aging during A) the first 4 weeks and B) 4-8 weeks (B). Letters on top of the box distinguishes statistically significant groups.

4.4 Conclusions

Irrespective of having low exchange capacity than general SOM materials, OM in this soil sample exhibited potential to be cross-linked by bivalent cations. Uptake of Mg^{2+} was much higher than Ca^{2+} and Ba^{2+} , possibly due to its larger size in hydrated state, which may fit well in large voids within the OM. Contradicting, Soil-Mg samples were found to have lower CEC_{eff} . Mg^{2+} is a weaker cross-linker, based on matrix rigidity. It even disrupted the existing interactions to get lower rigidity, as reflected by lower T^* than the resin-treated sample. However, aging induced significant structural reorientation in Soil-Mg samples whereas the Soil-Ca and Soil-Ba samples showed lower increment in matrix rigidity. Aging in Soil-Mg samples is indicated to be controlled by WaMB than by CaB. It suggests that cross-linking by Ca^{2+} and Ba^{2+} imparted restriction to the OM segment mobility. The current study adds to the general understanding on CaB interaction, by showing the relevance of hydration water. However, to understand the exact role and dynamics of water molecules in various types of CaB, it is planned to extend the study by stressing the treated samples with repeated drying-wetting events. Such a procedure is supposed to induce stronger, more direct CaB, by gradual release of water molecules from cation hydration shell.

References

- Aquino, A. J. A., D. Tunega, G. E. Schaumann, G. Haberhauer, M. H. Gerzabek and H. Lischka (2011). The functionality of cation bridges for binding polar groups in soil aggregates. *International Journal of Quantum Chemistry* 111: 1531-1542.
- Kunhi Mouvenchery, Y., A. J. A. Aquino, A. Jaeger, D. Diehl, M. Bertmer and G. E. Schaumann (accepted, 2013). Restructuring of a peat in interaction with multivalent cations: Effect of cation type and aging time. *Plos One*.
- Kunhi Mouvenchery, Y., J. Kučerík, D. Diehl and G. E. Schaumann (2012). Cation-mediated cross-linking in natural organic matter - a review. *Reviews in Environmental Science and Bio/technology* 11(1): 41-54.
- Schaumann, G. E., D. Diehl, M. Bertmer, A. Jaeger, P. Conte, G. Alonzo and J. Bachmann (2013). Combined Proton NMR wideline and NMR Relaxometry to study SOM-water interactions of cation-treated soils. *Journal of Hydrology and Hydromechanics* 61(1): 50-63.
- Schaumann, G. E., D. Gildemeister, D. Diehl, Y. Kunhi Mouvenchery and S. Spielvogel (submitted 2013). Cation specific formation and aging of cross-links in soil organic matter (SOM). *Journal of Soils and Sediments*.
- Schaumann, G. E., F. Lang and J. Frank (2006). Do multivalent cations induce cross-links in DOM precipitates? *Humic Substances - Linking Structure to Functions. Proceedings of the 13th Meeting of the International Humic Substances Society in Karlsruhe*. F. H. Frimmel and G. Abbt-Braun. Karlsruhe, Universität Karlsruhe. 45-II: 941-944.
- Zhang, D. (1995). TG and DSC study of the properties of coked molecular sieve catalyst. *Journal of Thermal Analysis* 45(1-2): 141-150.

Chapter 5

Organo-mineral associations in artificial soil samples: chemical quality of
organic matter and development of physicochemical structure

Kunhi Mouvenchery, Y., Schaumann, G.E.

publication in preparation

5.1 Introduction

Primary and secondary structures of OM are equally important for its biogeochemical functioning, as demonstrated in the introduction of this thesis. The two levels of structural organisation are interrelated and are mutually in relations with SOM functioning. Apart from chemical composition of individual molecular segment, its stability, reactions with neighbouring molecules and with biotic and abiotic external agents, etc. are responsible for the higher level structural organisation (see chapter 1). Microbially mediated organo-mineral associations were found to impart physical structure to the soil aggregates (Pronk et al. 2012).

However, the interrelation between the SOM chemical properties and physical structure of organo-mineral associations has not been directly demonstrated yet. This chapter aims to assess the role of chemical properties of SOM in defining soil aggregates. It is hypothesised that the mineral materials are important for chemical properties of OM and hence the secondary level interactions within SOM and between SOM and mineral surfaces. A highly simplified system of artificial soils was used, in order to have simple systems with small number of variables. The OM structural quality was assessed using a thermoanalytical method in which thermogravimetry (TGA) is coupled with DSC (TGA-DSC) to produce mass loss and energetic information, simultaneously. Here, quality of OM is defined in terms of thermal stability. ^1H NMR relaxometry was employed to observe the development of porosity with the development of OM in the samples. Development in pore structure could produce hints on the interaction between mineral and organic domains.

5.2 Materials and methods

Materials

The artificial soil samples used in this study have been provided by Dr. Geertje Pronk and have been described by Pronk et al (2012). The mixtures consisted of illite, montmorillonite, ferrihydrite, boehmite and/or charcoal, of similar texture. Eight samples (A-H) were used, constituents of which are given in table 1. For detailed description of sample preparation, composition of each soil and properties of individual material, please see Pronk et al (2012). The artificial soils were incubated in the dark in an incubation chamber at 20 °C and with constant water content of 60 % of maximum water holding capacity. The soils were incubated with sterilised manure material and with a microbial community extracted from natural soil. The experiment involved 4 sampling time: $t_1=3$ months, $t_2=6$ months, $t_3=12$ months and $t_4=18$ months. The start of incubation was considered as t_0 . Sample H incubated

for 12 months (H3) was not analysed due to its unavailability. To make the discussion easier, the samples were grouped into four, depending on composition (table 1).

Table 1. Composition of the artificial soil materials and their classification, accordingly.

Sample name	Composition	Grouped in to
A	Quartz Montmorillonite	Clay-containing
B	Quartz Illite	Clay-containing
D	Quartz Montmorillonite Illite	Clay-containing
C	Quartz Ferrihydrite	Ferrihydrite-containing
F	Quartz Illite Ferrihydrite	Ferrihydrite-containing
E	Quartz Montmorillonite Charcoal	Charcoal-containing
H	Quartz Illite Ferrihydrite Charcoal	Charcoal-containing
G	Quartz Illite Boehmite	Boehmite-containing

Methods

^1H NMR transverse relaxation time (T_2). Samples were moistened to water content of 20 % (w/w on dry mass basis). With this method, the mobility of water molecules confined in porous structures can be assessed (Jaeger, 2005). ^1H transverse relaxation decay were recorded on a Bruker Minispec 7.5 NMR Relaxometer (Bruker, Germany) at a magnetic field strength of 0.176 T applying CPMG (Carr-Purcell-Meiboom-Gill) pulse sequence using the following acquisition parameters: echo time (TE) = 0.15 ms, recycle delay (RD) = 12 s, number of echoes (NE) = 1000 and number of scans (NS) = 64. Decay curves were fitted on bi-exponential equation, using the software origin 7.5, from OriginLab.

Thermal analysis. Thermal analysis of the samples was performed on a NETZSCH Proteus TGA-DSC-MS instrument (NETZSCH, Selb, Germany) where mass loss and heat flow accompanied by heating and mass spectra of products of combustion can be acquired at once. Samples were heated from 30-1000 °C in open pans at a rate of 10 K min⁻¹ under synthetic air atmosphere (flow rate 50 mL min⁻¹).

5.3 Results and discussion

^1H NMR transverse relaxation time (T_2). Two water populations were revealed by the bi-exponential fit with T_2 in the ranges of 8-10 ms and 20-73 ms. The component with fastest relaxation ($T_2 < 10$ ms) was discarded from discussion because the differences are too small to be discussed. Figure 1 shows the development in T_2 of each soil mixture during the time of incubation. The coloured lines drawn along the figures highlight the observed tendential development. The values varied between samples, depending on the composition and incubation time. Relatively higher T_2 values were observed for sample H (62.97 ± 0.9 ms), than other samples, at time t_0 . All the samples, except C and F showed similar patterns of time-development, with initial increase in T_2 and then decrease. Among them, sample D attained its highest T_2 after 6 months of incubation whereas the rest achieved highest T_2 after 3 months. Samples C and F showed decrease-increase-decrease pattern. All samples have comparable T_2 after 18 months (23 ± 5 ms).

Relatively small T_2 values reflect water molecules that are confined within small pores (Jaeger, 2005). Higher T_2 of sample H could be due to the presence of charcoal, which is highly porous in nature (Schaumann and Kunhi Mouvenchery 2012). However, the third charcoal-containing soil (E) showed T_2 in the range of other samples. This might be due to

the presence of clayey ($< 2 \mu\text{m}$, Pronk et al. 2012) montmorillonite in that sample. The small clay particle might fill the porous structure of quartz and hence only even smaller pores are filled with water, resulting in smaller T_2 .

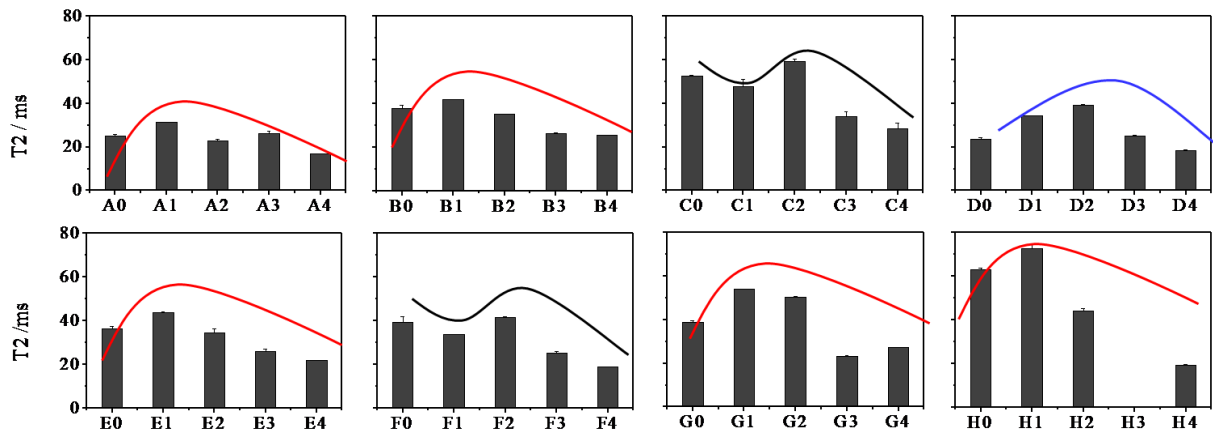


Figure 1. ^1H T_2 relaxation time of the artificial soils showing development with incubation time. Labels on x-axis show the sample name and the incubation time. The lines in each graph show tendencies of development of T_2 , distinguished by colour. They are artificially drawn, not based on any calculation or fitting.

Concerning the temporal development, the generally observed increase-decrease pattern suggests that during the incubation, effective pore size increases and then decreases. Two phases of pore size development can be observed. The first phase where T_2 increases could be because inter-aggregate pores develop. The following decrease of effective pore size could be due to the microbial build up, which cause the pores to be filled by microbial products such as extra-cellular polymeric substances (EPS). Such materials may fill up the pores and acts as gluing agent between mineral particles to hold the aggregate structure. The idea need to be verified in future. Within this group of soils, all other samples passed the phase of inter-aggregate pore development faster (3 months) than sample D (6 months). It suggests that illite and montmorillonite together retards the first phase, even though they did not impart such effects, when present individually. Based on the current results, no clear explanation can be drawn, and the suggestion need to be verified.

The initial lowering in T_2 of ferrihydrite-containing samples (C and H) may suggest that in the initial 3 months, paramagnetic iron (Fe III) interfere magnetisation decay of water protons. Paramagnetic species induce rapid signal decay, resulting in small T_2 values (Foley et al. 1996). It could be that Fe III of ferrihydrite undergoes dissolution to reach the water that is confined in pores. Then, the increased T_2 after next three months may be indicative for more prominent effect of pore size development than the effect of dissolved Fe III. As in other

samples, after achieving the state of largest pore structure, the second phase of evolution starts, with increased contribution of microbial activity.

The notion that all samples attained similar T_2 values and hence pore structure, after 18 months of incubation, indicates that they have similar physicochemical structure, reflected in pore size distribution, irrespective of the constituent mineral. It may suggest that their pore structure become dominated by microbial exudates such as EPS and biofilm. Thus it could be stated that effect of mineral component dominates in the early stage of SOM formation only, and at some point of time (18 months in these artificial soils) the OM dominates the structure. This is against the expectation that mineral materials undertake crucial role in the characteristics properties and functioning of organo-mineral associations.

Thermal analysis. All the thermograms revealed two temperature ranges (30-400 °C and 400-550 °C) of intensive mass loss, accompanied by strong exothermal energetic changes, as represented by figure 3. The temperature ranges varied slightly between samples. A small endothermic peak, owing to the inversion of quartz (Plante et al. 2009) was observed around 570 °C, in all the samples. The OM fraction that is thermally degraded below 400 °C is termed as thermolabile fraction whereas the more stable fraction is called as thermostable fraction. The term lability used here, cannot be understood as thermodynamic lability, but describes the thermally less stable materials. The exothermic peak in DSC record shows that heat was evolved during the heating, reflecting combustion of OM.

Thermostable fraction. The amount of thermostable fraction was calculated from mass loss above 400 °C, as percentage of the total burned material. This could give information on the stability of OM material within each soil sample. None of the samples showed significant development in OM stability, during the time of incubation (data not shown). Figure 3A shows box plots of amount of thermostable fraction of each group of samples, distinguished by their composition, over all the data (including incubated samples).

It can be seen that each sample group differ significantly from each other, at a level of 0.05. The amount of thermostable fraction increases in the order: ferrihydrite < boehmite < clay minerals < charcoal. The high amount of thermostable fraction in charcoal-containing samples could be due to the high thermal stability of charcoal (Plante et al. 2009). Boehmite and ferrihydrite are found to labilise the OM. In other words, the OM formed in presence of

these two minerals is less stable. Altogether, it can be seen that stability of SOM depends up on the type of mineral material involved.

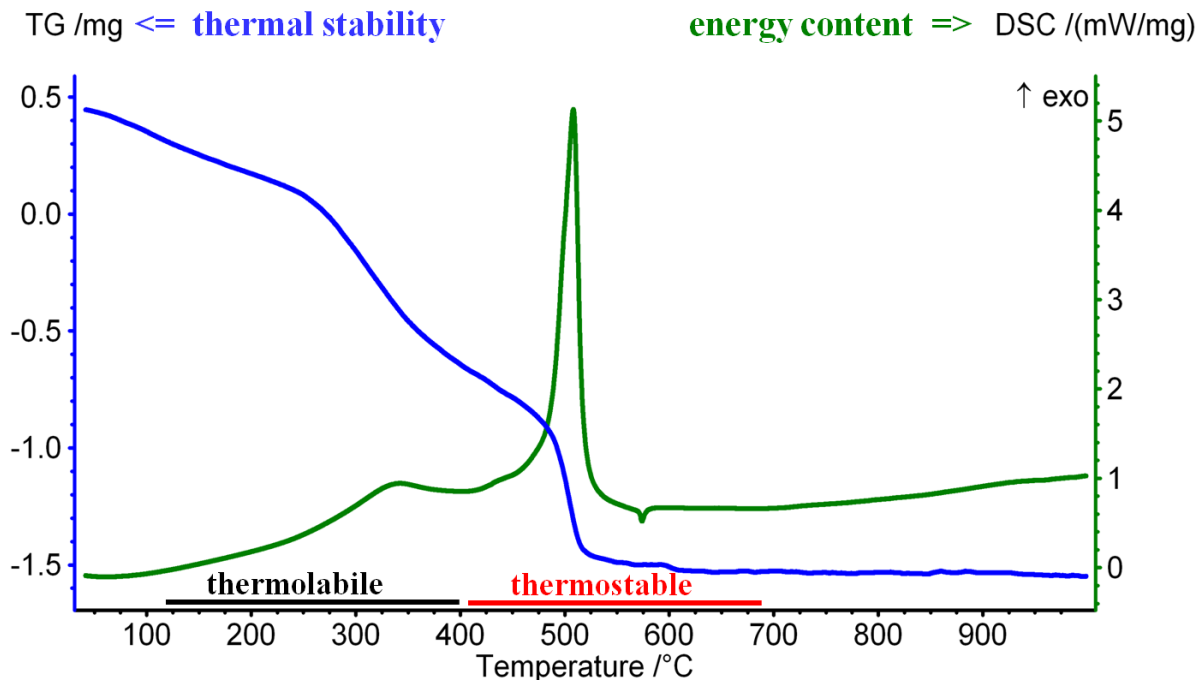


Figure 2. Representative TGA (blue) and DSC (green) thermograms showing mass loss and heat flow in TGA-DSC experiment, and the classification of two OM fractions depending on the temperature range of combustion.

Calorific value of the OM. Calorific value, calculated as the energy released by burning of 1g of organic matter, over the whole range of temperature is shown in box plots in figure 3B. Clayey and boehmite samples were found to have similar calorific values. The values were lower for ferrihydrite soils whereas charcoal soils revealed the highest values.

The high energy content of charcoal soils reflects the thermal properties of charcoal. In those samples, mass loss and associated heat evolution of SOM might be masked by those of charcoal. Ferrihydrite reduced the energy content of the OM showing that it induces SOM stability.

Calorific values of thermolabile and thermostable fractions are shown in figures 3C and 3D, respectively, in order to assess the energy content of the stable and labile OM. Thermolabile fraction was affected by minerals, in the same way as the total calorific value: ferrihydrite < clay minerals = boehmite < charcoal (figure 3C). But the thermostable fraction was affected only by ferrihydrite (figure 3D), with a reduction in calorific value.

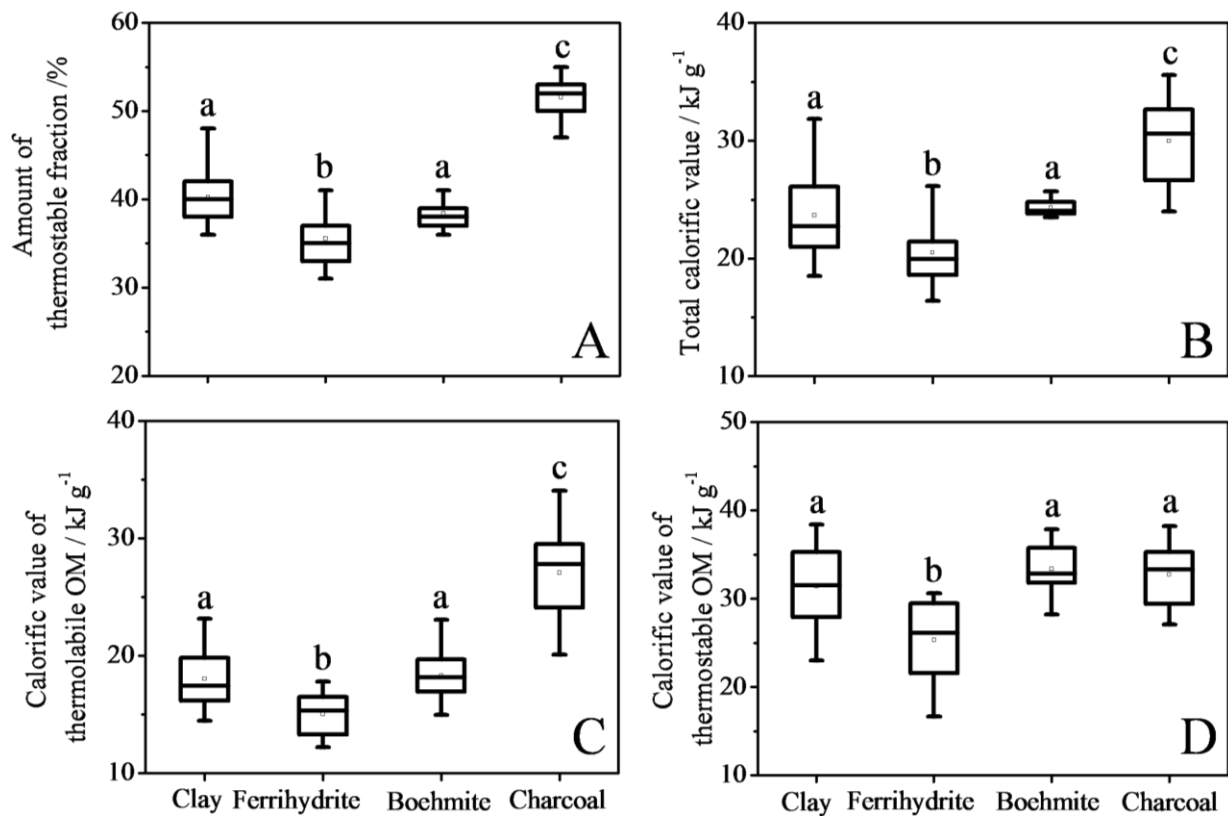


Figure 3. thermal stability parameters of SOM in each group of artificial soil, as assessed by TGA-DSC; the amount of thermostable fraction of SOM relative to the total burned OM A), calorific values of the total burned OM B), thermolabile fraction of SOM C) and thermostable organic matter D).

It shows that ferrihydrite stabilizes OM in both fractions. Thus, SOM in soils C and F can be considered to contain molecules with strong chemical bonds. It can be that the microbial activity was affected by the presence of ferrihydrite and the mineral-microbial associations in that soil produce a different type of OM than in the absence of ferrihydrite. ^1H T_2 observation that ferrihydrite undergo dissolution from the two artificial soils suggests that it was made available for the microbes.

But the effect of charcoal was not visible for the thermostable fraction, but for thermolabile fraction and for the total calorific value of OM. This suggests that in charcoal soils, thermolabile fraction predominates in the total energy content of SOM. As charcoal is very stable and burns only above 400 °C (Plante et al. 2009), it is expected to contribute to the thermostable fraction. Under this consideration, the thermolabile fraction represents the SOM. Figure 3C, then suggests that thermolabile fraction of the OM formed in presence of

charcoal contain relatively weak chemical bonds and hence they are disruptable by applying low amount of heat energy, resulting in high amount of exothermic energy.

5.4 Conclusions

Different mineral-microbial associations were found to produce OM with different chemical quality, in terms of thermal stability and calorific value. Ferrihydrite induced stabilization effect in organic matter, while SOM produced in presence of charcoal burned with usage of lower amount of energy. However, charcoal contributed to the thermostable OM. ^1H T_2 shows solubilisation of ferrihydrite in the beginning of incubation, which might have affected microbial activity to produce differently characterised OM. The ^1H NMR relaxometry suggests that formation of organo-mineral associations involve mainly two phases: development of inter-aggregate pore structures followed by microbial build-up within the pores. The duration of the phases varied from 3 months to 6 months, depending on the soil composition. The results show that mineral materials are crucial for the quality of organic matter (primary structure). Formation and development of OM during the 18 months of incubation make all the soils to attain similar physicochemical structure, as defined by pore size distribution. The results obtained from the two independent methods (^1H NMR relaxometry and thermal analysis) were not in accordance with the expectation that organo-mineral associations are maintained by supramolecular structure of SOM which is defined by SOM chemical characteristics, at least in a visible manner by the applied methodologies.

Acknowledgements

We would like to thank Dr. Geertje. J. Pronk (Technical University of Munich, Germany) for sharing the artificial soil samples.

References

- Foley, I., S. A. Farooqui, et al. (1996). Effect of paramagnetic ions on NMR relaxation of fluids at solid surfaces. *Journal of Magnetic Resonance, Series A* 123(1): 95-104.
- Jaeger, F., E. Grohmann and G. E. Schaumann (2005). Do swelling and microbial activity affect pore size distribution in humous soil samples? *Geophysical Research Abstracts* 7(SSS9: Quantification of soil structure and soil porosity changes caused by natural and anthropogenic affects): EGU05-A-02313; SSS9-1MO3P-0262.
- Plante, A. F., J. M. Fernández, et al. (2009). Application of thermal analysis techniques in soil science. *Geoderma* 153(1-2): 1-10.

- Pronk, G. J., K. Heister, et al. (2012). Development of biogeochemical interfaces in an artificial soil incubation experiment; aggregation and formation of organo-mineral associations. *Geoderma* 190(0): 585-594.
- Schaumann, G. E. and Y. Kunhi Mouvenchery (2012). Potential of AFM-Nanothermal Analysis to study the microscale thermal characteristics in soils and natural organic matter (NOM). *Journal of Soils and Sediments* 12(1): 48-62.

Chapter 6

[Potential of AFM–nanothermal analysis to study the microscale thermal characteristics in soils and natural organic matter \(NOM\)](#)

Schaumann, G.E., Kunhi Mouvenchery, Y. (2012) Journal of Soils and Sediments 12 (1): 48-62

Chapter 7

Linking Atomic Force Microscopy with nanothermal analysis to assess
microspatial distribution of materials in young soils

Kunhi Mouvenchery, Y., Miltner, A., Schurig, C., Kästner, M,
Schaumann, G.E. (submitted, 2013) *Geochimica et Cosmochimica Acta*

Abstract

Atomic force microscopy (AFM) coupled with nanothermal analysis (nTA) was implemented to qualitatively assess micro- and nanoscale spatial distribution of various materials in soils of a chronosequence from the Damma Glacier forefield, Switzerland. Selected micro-regions in the samples were investigated via AFM for spatial distribution of topography and adhesive forces and via nanothermal analysis for local thermal properties. These were compared with those of bacterial cells and plant material as organic test materials representing different soil organic matter sources.

Based solely on thermal characteristics, only three types of materials were distinguished, which could not be unambiguously assigned to particular materials. By combining adhesion size information and local thermal characteristics, discrimination of material types was further refined. Significant parts of the investigated microregions contain materials with characteristics similar to the test materials of either plant or bacteria. Coverage of inorganic surfaces by organic materials increased with increasing soil-glacier distance. Structures of size 200-500 nm showing adhesion and thermal characteristics similar to those of test bacteria could represent microbial cell envelopes. In the investigated microregions, the abundance of these structures increased with increasing soil age. Results demonstrated that AFM, combining topographic information, force mapping and thermal analysis allow qualitative discrimination of materials and their spatial distribution even if their chemistry or adhesion forces are similar.

Key words

Nanothermal analysis, Atomic Force Microscopy (AFM), adhesion force, soil organic matter, cell envelope fragments, Glacier forefield

1. Introduction

Structural heterogeneity and complexity are intrinsic features of soils (Odum, 1969). Soil characteristics vary with respect to a number of factors such as water content, nutrients, occurrence of inorganic surfaces for adherence, organic carbon sources such as plant and animal debris etc. All these types of heterogeneity are important for the occurrence, growth and development of microbes within soils as well as for several soil physical and chemical properties. Thus heterogeneity in soils will, in turn, affect the formation and development of soil organic matter (SOM), because SOM originates from degradation products of plant materials (Kogel-Knabner, 2002) and from microbial cell residues (Miltner, et al., 2009, Miltner, et al., 2012). Gradients in spatial distribution of microbial species thus results in a heterogeneous distribution of organic matter (OM) in soils with respect to the source, structure, stability and functioning. Therefore, heterogeneity in soil physical and chemical structure and heterogeneity in distribution of various microbial species are synergistically interdependent.

Microorganisms form non-uniform patchy communities or hot-spots selectively in different structural compartments in soil (Franklin & Mills, 2003, Becker, et al., 2006, Lehmann, et al., 2008). Although a huge number of bacteria (about 10^{12} /g soil) live in soil, far less than 1% of the soil particle surfaces are covered by bacterial cells (Young & Crawford, 2004). Soil particle size and aggregate fractions, along with other factors, cause such selectivity (Gupta & Germida, 1988, Chenu, et al., 2001), making them vulnerable to environmental factors to different extents (Ranjard, et al., 2000). For example, bacteria residing on aggregate surfaces were found to be affected stronger by mercury contamination than those living in pore structures (Ranjard, et al., 2000). Similarly, the different habitats where bacteria occur can control their survival, activity and ecological functions (Mummey & Stahl, 2004, Styrishave, et al., 2012). Spatial distribution of degrader microbial organisms with respect to organic contaminants (Styrishave, *et al.*, 2012) and soil structural features (Nunan, *et al.*, 2001) determine bioavailability and were even proposed as a reason for persistence of organic pollutants (Styrishave, *et al.*, 2012). Spatial heterogeneity in soils has also been reported to be a key factor for coexistence of different microbial species (Dechesne, *et al.*, 2008).

Spatial organization of SOM within mineral assemblage has far reaching consequences, leading to a control of the quantity and the physical and chemical quality of SOM and thus soil properties as a whole (Nunan, *et al.*, 2001, Young & Crawford, 2004). Variation in soil structures such as pore network could result in varying degrees of spatial and temporal

distribution of flow pathways for solutes and substrates (Young & Ritz, 1998). Similar effects may also happen with respect to water availability, dissolution of gases etc., leading to preferential colonization of certain soil structures by microbes. Physical entrapment of substrates and nutrients within soil morphological structures can restrict their accessibility for microbes which can also cause such community structures to distribute non-uniformly (Powelson, 1980). Chemical structural variations will also result in heterogeneous distribution of nutrients (Hildebrand, 1990), pollutants and water molecules. Chemical heterogeneity mainly arises from distribution of OM functional groups and supramolecular rearrangements (Schaumann, 2006, Schaumann & Thiele-Bruhn, 2011), but also from distribution of different materials having similar chemical characteristics. This heterogeneity will affect the development of microbial patches at various soil regimes, indirectly, owing to restricted or enhanced accessibility for water and nutrients.

For example, closely neighboured functional groups can be bridged by water molecules or multivalent cations forming water molecule bridges (WaMB) and cation bridges (CaB), respectively (Aquino, *et al.*, 2011, Schaumann & Thiele-Bruhn, 2011, Kunhi Mouvenchery, *et al.*, 2012). This can lead to a more rigid OM matrix where small nutrient, substrate or contaminant molecules can be physically entrapped (Schaumann & Thiele-Bruhn, 2011) and thus their availability to microbes will be restricted. This could trigger the colonization of microbes away from the surroundings of such units of rigid networks. Hence, spatial distribution of chemical environments is a decisive factor controlling formation and functioning of biogeochemical interfaces (BGI). However, not only chemical environments are heterogeneously distributed, but also materials with similar chemical composition, but with different material properties (e.g., thermal stability, mechanical stability, morphology).

Heterogeneity is a function of scale (Li & Reynolds, 1995, Nunan, *et al.*, 2001, Ettema & Wardle, 2002, Nunan, *et al.*, 2002, Lehmann, *et al.*, 2008, Totsche, *et al.*, 2009) and therefore needs to be assessed at each scale with scale-specific questions and methods. The biggest challenge for microscale and nanoscale techniques lies in finding suitable methods to determine chemical and material properties with high spatial resolution and without disturbing the sample structure (Herrmann, *et al.*, 2007, Totsche, *et al.*, 2009) and to analyze representative parts of the sample. Currently available microscopic and spectroscopic methods with resolution up to sub-micrometer to nanometer scales include X-ray photoelectron spectroscopy (XPS) (Allen, *et al.*, 1999, Barr, *et al.*, 1999, Arnarson & Keil, 2001, Amelung, *et al.*, 2002), scanning transmission X-ray microscopy (STXM) (Kinyangi,

et al., 2006, Lehmann, *et al.*, 2008), scanning electron microscopy (SEM) (Chenu&Plante, 2006, Areekijserree M, *et al.*, 2009, Miltner, *et al.*, 2012), scanning laser microscopy using fluorescence and luminescence markers (Jansson, 2003), atomic force microscopy (AFM) (Maurice, *et al.*, 1996), Nano secondary ion mass spectrometry (NanoSIMS) (Li & Reynolds, 1995, Herrmann, *et al.*, 2007), matrix assisted laser desorption ionization-time of flight mass spectrometry (MALDI-TOF-MS) (Engelke, *et al.*, 2003, Tsirogianni, *et al.*, 2005, Siricord& O'Brien, 2008, Uhlik, *et al.*, 2011) and X-ray and nuclear magnetic resonance (NMR) computer tomography (CT) (Young, *et al.*, 2001).

Among them, AFM is capable to achieve the highest resolution of several nanometres, revealing material properties such as interaction forces with the tip material, operating in very small quantities (up to several hundred piconewtons) (Cheng, *et al.*, 2009). Atomic force spectroscopy (AFS), acquiring sample-tip interaction force when they approach each other, is able to provide material specific information on intermolecular interactions at nanometer scale (Leite& Herrmann, 2005). Its applicability in soil science has been proved in studies on surface hydrophobicity (Cheng, *et al.*, 2009), interaction between microbial species and natural organic matter (NOM) (Abu-Lail, *et al.*, 2007), characterization of various mineral surfaces (Eastman & Zhu, 1996, Leite, *et al.*, 2003) etc. Introduction of peak force quantitative nanomechanical mapping (PFQNM) allows for extraction of more detailed information on mechanical force distributions on surfaces. This mode of AFM is meanwhile commonly applied in material science (e.g. Tieleman*et al.*, 2012) and in microbiology (e.g. Heu*et al.* 2012), but not yet in soil science, to the best of our knowledge. Although nanomechanical and physicochemical characteristics already give some information on surface chemistry, materials with similar chemical composition cannot easily be distinguished without investigation of additional material characteristics.

Localised thermal analysis in nanoscale (nanothermal analysis; AFM-nTA) is another promising AFM application, which was only recently applied to soils to reveal thermomechanical properties at the nanometer and micrometer scales (Schaumann & Kunhi Mouvenchery, 2012). In this pilot study, various inorganic and organic regimes separated by nanometer and sub-micrometer distances were distinguished and their spatial distribution was explored.

The objective of this study was to explore the potential of complementing AFM force mapping by AFM-nTA to distinguish spatial moieties in soils in the micrometer and upper

nanometer scale additionally by their thermal characteristics. For this explorative study, we selected young soils from a glacier forefield along a 150 year chronosequence, where heterogeneity was expected to be low compared to mature soils. The soils were already chemically characterized for total C, total N, lipids and plant derived biomass (Smittenberg, *et al.*, 2012), soil physicochemical properties such as pH, cation exchange capacity and base saturation, chemical composition, biochemical gradients such as microbial C, N and P, phospholipid fatty acids (PLFA), SOM properties (Bernasconi, *et al.*, 2011, Duemig, *et al.*, 2011), vegetation succession (Miniaci, *et al.*, 2007, Toewe, *et al.*, 2010, Bernasconi, *et al.*, 2011), microbiological diversity (Sigler, *et al.*, 2002, Sigler & Zeyer, 2002, Bernasconi, *et al.*, 2011), etc. Recently, gradients in total fatty acid, water contact angle and microhydrophobicity with soil age were assessed in addition to PLFA, by Schurig *et al.* (2013). 200 nm to 500 nm sized flat organic fragments were detected in SEM micrographs, the abundance of which increased with increasing soil age. They were hypothesized as microbial cell envelope fragments contributing to SOM genesis (Miltner, *et al.*, 2012, Schurig, *et al.*, 2013). This, however, requires further verification.

In our previous publication (Schaumann & Kunhi Mouvenchery, 2012), AFM-nTA was performed on different soils and standard materials such as quartz, charcoal and manure to represent various inorganic and organic moieties. In this study, we further explored the methodology and tested the potential of PFQNM-nano thermal combination to distinguish different material characteristics in soil samples. Nanoscale distribution of various types of materials in the young Damma glacier soils and changes in distribution of those materials and material properties with time were examined using a combination of PFQNM and AFM-nTA. Furthermore, we investigated to which extent materials with characteristics of two organic test materials (plant and microbial materials) could be identified in selected regions of interest (ROI) in the soil. The objective was to find out to which extent the combination of the selected characteristics helps identifying certain materials in soil, despite its complexity.

Materials and Methods

Materials. The sampled chronosequence is located in the Damma glacier forefield in Switzerland (46°38' N, 8°27' E; ~ 2000 m above sea level). Details on the Damma glacier forefield have been described previously by Bernasconi *et al.* (2008; 2011).

Historical records report a recession of the Damma glacier since 1850, with an average retreat rate of about 10 m a⁻¹. This recession was interrupted by two re-advances (1920-1928 and

(1970-1992), resulting in two small end moraines in the forefield and a division of the forefield into three areas of different soil age (Bernasconi, *et al.*, 2011). The bedrock material of the forefield is granite without significant change along the chronosequence (Bernasconi, *et al.*, 2011).

Soil sampling. Soil samples were taken in August 2009 at 8 sampling sites as described by Schurig *et al.* (2012). Approximate soil ages range from 0 to 120 years. Briefly, at each sampling site ten subsamples were taken from below the root layer of the surface vegetation (< 5 cm) in a 5 m circumference around the sampling sites DG0-DG18. Subsamples were pooled and sieved immediately by passing through a 2 mm sieve. All samples were kept on ice during transport to the laboratory.

As representatives for plant derived and microbial derived materials that form major contributors to SOM, we selected two test materials. One is a pure culture of *Bacillus subtilis ssp. spizizenii* (DSM 347) cells grown on mineral medium with glucose. This test material was chosen to be able to search for materials in soils similar to those of intact cells of a typical soil bacterium. This Gram-positive bacterium may differ slightly in thermomechanical characteristics from Gram-negative bacteria and fungi that may occur in soil, due to different cell envelope structures and constituents. However, they may reflect cell envelope characteristics of common soil microbes, which differ from those for materials originating from higher organisms such as plants. The second one is a long fibrous piece of plant root material, of 0.5 mm thickness and 3 mm length, picked manually with a pair of forceps from soil DG 0. This material was selected because it better represent partially degraded plant material entering the soil than fresh plant parts. The surface structure on the plant material shown by the SEM image suggests occurrence of very small mineral particles and fungi (figure S1 in supporting information, SI). Care was taken to select an ROI (region of interest) without any fungal hyphae and with as few mineral particles as possible.

AFM - force mapping and nTA. Air-dried soil samples and the plant material were fixed on glass slides using double-sided adhesive tape. The particles were gently spread on the tape with a spatula in order to fix them sufficiently to withstand the AFM analysis without movement, and loosely-fitting particles were removed by a stream of pressurized air. This procedure for AFM sample preparation is reliable in case of particles of large grain size like soils (Schaumann & Kunhi Mouvenchery, 2012). The bacterial culture was centrifuged, and a small amount of the pellet was spread on a glass slide and air-dried overnight before analysis under AFM.

ROI on each sample were selected using an environmental scanning electron microscope (ESEM Quanta 250 from FEI Company, Frankfurt, Germany) in low vacuum mode. Image acquisition parameters (acceleration voltage 5-8 kV, pressure 90 Pa) were adapted so that non-destructive imaging was ensured (Stokes, 2008). EDX was not performed in order to avoid beam damage. ROI were randomly selected among relatively even regions, assessed by optical appearance, considering that an uneven surface is not suitable for AFM analysis. For that, regions on 100-200 μm large soil grains were considered in order to be able to relocate the ROI under AFM and to engage the probe without damage. For each sample, at least four ROI were selected for AFM analysis. The low number of ROI and the arbitrary selection of ROI will, therefore, allow to explore the material distribution in the ROI, but this distribution is not necessarily representative with respect to quantification in whole soil, which was not in the focus of this study. We therefore restricted quantification within the selected ROI.

The selected ROI were re-located in the AFM (Dimension ICON, Veeco, New York/USA) which was coupled to a thermal analytical unit (VITA, Veeco, New York,/USA). PFQNM and nanothermal analysis were performed using a thermal probe (VITA-DM-NANOTA-200) made of doped Si, provided by Bruker (Germany). Deflection sensitivity of the tip was estimated to be 108 nm/V and the tip radius was 31 nm. Temperature calibration over a range of 30 °C to 300 °C of the probe was done using polycaprolactone, polyethylene terephthalate, high density polyethylene and metallic gallium. All AFM measurements were performed at room temperature and at a relative humidity between 28 and 32%. To ensure tip quality and to be sure that no sample material was attached to the tip during analysis, the drive frequency of the tip was checked before and after every imaging, which always stayed constant (66 ± 1 kHz).

Images were acquired over an area of 2 μm x 2 μm at a scan rate of 0.5 Hz. Data were captured along 512 lines with 512 points on each line. Height, dissipation, adhesion and peak force images were recorded in each channel. Currently available nanothermal probes have spring constants below 3 Nm^{-1} . With this, they are too soft to obtain reliable DMT modulus and deformation data on hard soil surfaces (Veeco Instruments, 2010). Height images were analysed using the Nanoscope analysis software (Veeco, New York,/USA). Average surface roughness (Ra) was calculated as the mean of height deviations from the mean plane, which could provide primary information on surface morphology and regarding spatial heterogeneity. Adhesion histograms were generated on each image with a bin size of 5 nN.

After imaging in PFQNM mode, 16 points on each image were selected along a 4x4 grid and thermal analysis was performed, heating the tip from 30 °C to 300 °C at a rate of 1 K s⁻¹. Cantilever deflection, which reflects the dimensional change (expansion or compression) at the sample surface by heating, was recorded in units of voltage (V) as a function of temperature in the thermogram. The grid of size 4x4 with 16 data acquisition points was selected after ensuring that these points are far enough from each other to avoid analysing areas which may have been affected by heat during prior analysis of points in the next neighbourhood. This was done by comparing images before and after heating, based on alterations in morphological features.

In a complementary analysis, we analyzed the size distribution of structural elements in each AFM height image. The analysis software (Nanoscope analysis software from Veeco, New York, USA) counts units of conjoined pixels recording similar heights as individual particles. Size distribution of such well isolated structural features with a threshold height of 20 nm over the ROI was obtained. Histograms were constructed with a bin size of 25 nm. We furthermore identified 8 to 10 structural features of 200-500 nm size in each image which were suggested to represent potential candidates for cell envelope fragments according to Schurig *et al.* (2012) and Miltner *et al.* (2012). Their selection was made after verifying that they lie far enough from previously heated regions and from each other to avoid artefacts. Nanothermal analysis was performed also on such features and their average adhesion force values were extracted from the adhesive force images. In this strategy, particle size will form the basic criterion to which information on thermal and mechanical properties are added in further steps, in order to achieve better resolution for results.

Nanothermograms were analyzed using the software Origin 7.5 from OriginLab. Thermograms were grouped with respect to thermogram shape as follows: Each thermogram was divided into sub-regions indicating thermal expansion or compression. Their slopes on basis of linear regression characterize the apparent linear expansion coefficient (α) or the apparent linear compression coefficient (κ) in units of 1 mV °C⁻¹, depending on whether it is positive or negative. The points of intersection of two linear components correspond to the respective inflection temperatures. Grouping was performed based on the intersection temperature and/or on the direction and magnitude of slopes. This procedure was unique and unambiguous and did not require any statistical analysis.

2. Results and Discussion

2.1 Surface heterogeneity

ESEM images showing ROI as well as AFM height and adhesion force images of one representative image for each soil sample are shown in figure 1. AFM height and adhesion images of $2\ \mu\text{m} \times 2\ \mu\text{m}$ subsections of the test materials are shown in figure 2 (panels B and C) in addition to a $10 \times 10\ \mu\text{m}$ AFM image of bacteria showing a group of cells and an ESEM micrograph of the plant material (panel A).

The plant material and soils revealed smooth, layered or fluffy surfaces (see images of samples DG 0, DG 2, and DG 10, respectively). Differences in frequency of occurrence, size and shape of morphological structures were observed between the soil samples, but also between replicates (data not shown). Spherical structures of dimensions varying between 20 nm and 500 nm were detected on each soil sample in varying size distribution.

Figure 3 shows R_a for each investigated site together with the standard deviation calculated from the four replicates of each sample site. R_a increases from sample DG 0 ($2 \pm 1\ \text{nm}$) to DG 18 ($45 \pm 13\ \text{nm}$). Also, the standard deviation between ROI increases with increasing soil age. R_a of each $2\ \mu\text{m} \times 2\ \mu\text{m}$ region and the standard deviation of R_a between such individual micro-regions correspond to nanoscale and microscale heterogeneity, respectively. Thus, heterogeneity with respect to surface morphology in both spatial scales increase with increasing distance from the glacier tip.

The averaged frequency histograms of sizes of structural features in the ROI (figure S2 in SI) suggested that with increasing distance to the glacier, the abundance of structures smaller than 100 nm decreased. In contrast, the abundance of structures of 200-500 nm size increased with increasing distance, from 5% to 57% of the total number of identified particles (figure S3 in SI). The qualitative increase of 200-500 nm large structures in the ROIs is in line with Schurig et al. (2013) for soil samples of the same chronosequence. It may indicate increasing abundance of organic materials with increase in soil age. On contrary, it can also be that roughness of the surface increases by time due to mechanical stresses or mineral weathering, possible during soil genesis, giving rise to morphological variations.

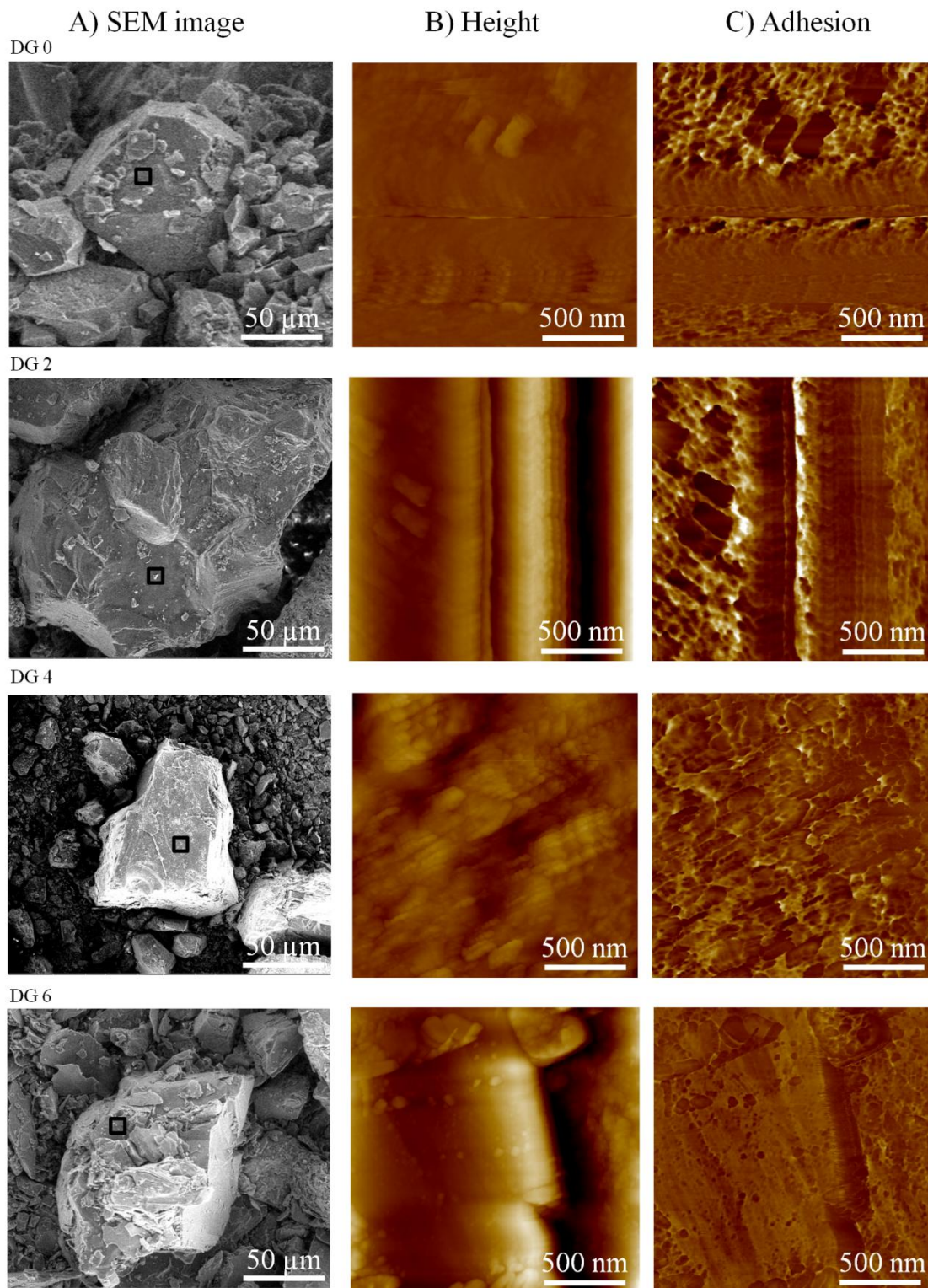


Figure 1, part 1. Micrographs showing ROI of Damma Glacier soil samples identified under ESEM (Panel A) and AFM height (panel B) and adhesion images (panel C). Height images reveal smooth, fluffy and layered surfaces. Color scale: In height images, darkest and lightest points correspond to a depth of 80 nm and a height of 80 nm, respectively, from the mean plane. For adhesion images, darkest and lightest points correspond to forces of 0 nN and 50 nN, respectively.

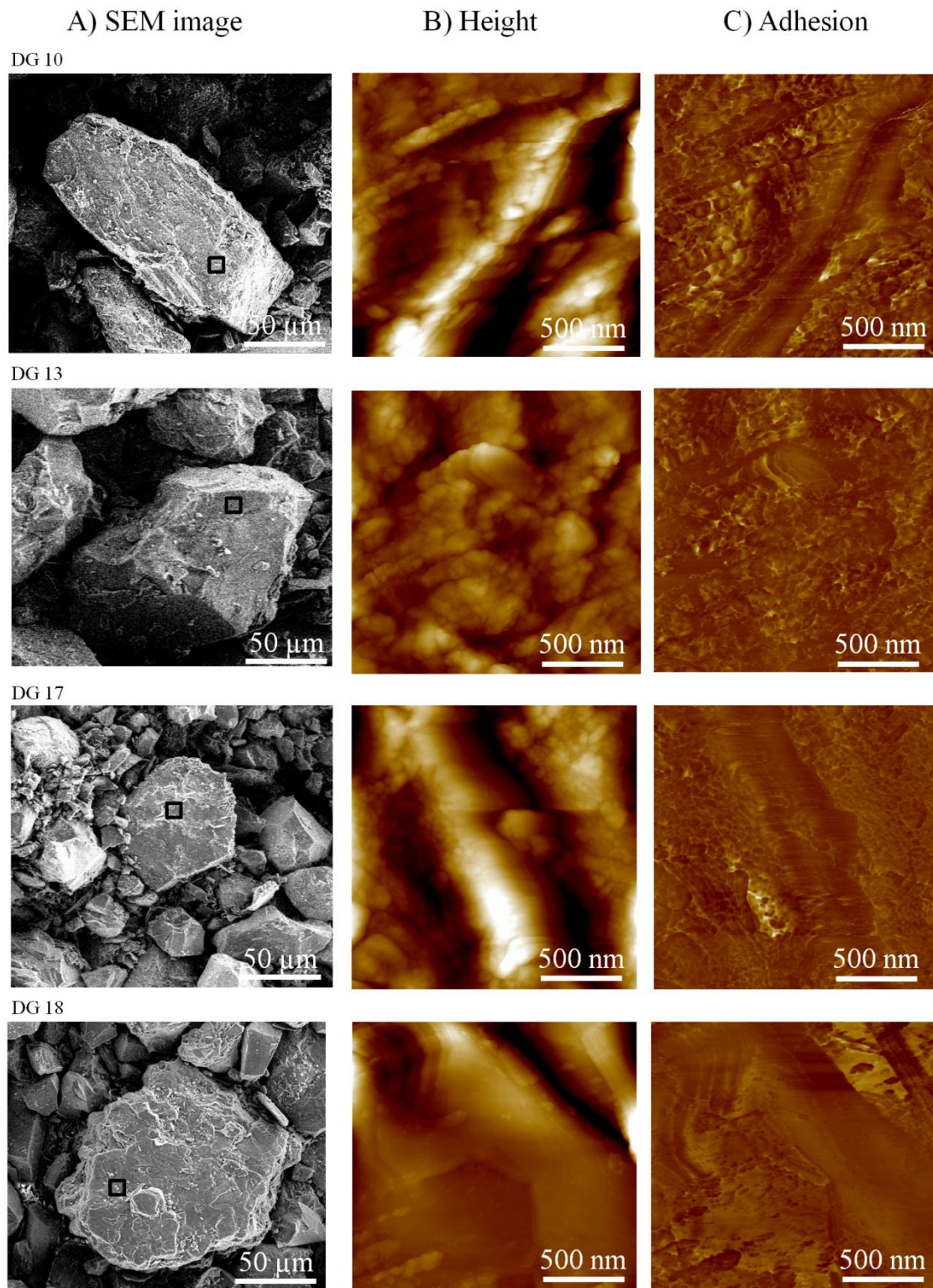


Figure 1, part 2. Micrographs showing ROI of Damma Glacier soil samples identified under ESEM (Panel A) and AFM height (panel B) and adhesion images (panel C). Height images reveal smooth, fluffy and layered surfaces. Color scale: In height images, darkest and lightest points correspond to a depth of 80 nm and a height of 80 nm, respectively, from the mean plane. For adhesion images, darkest and lightest points correspond to forces of 0 nN and 50 nN, respectively.

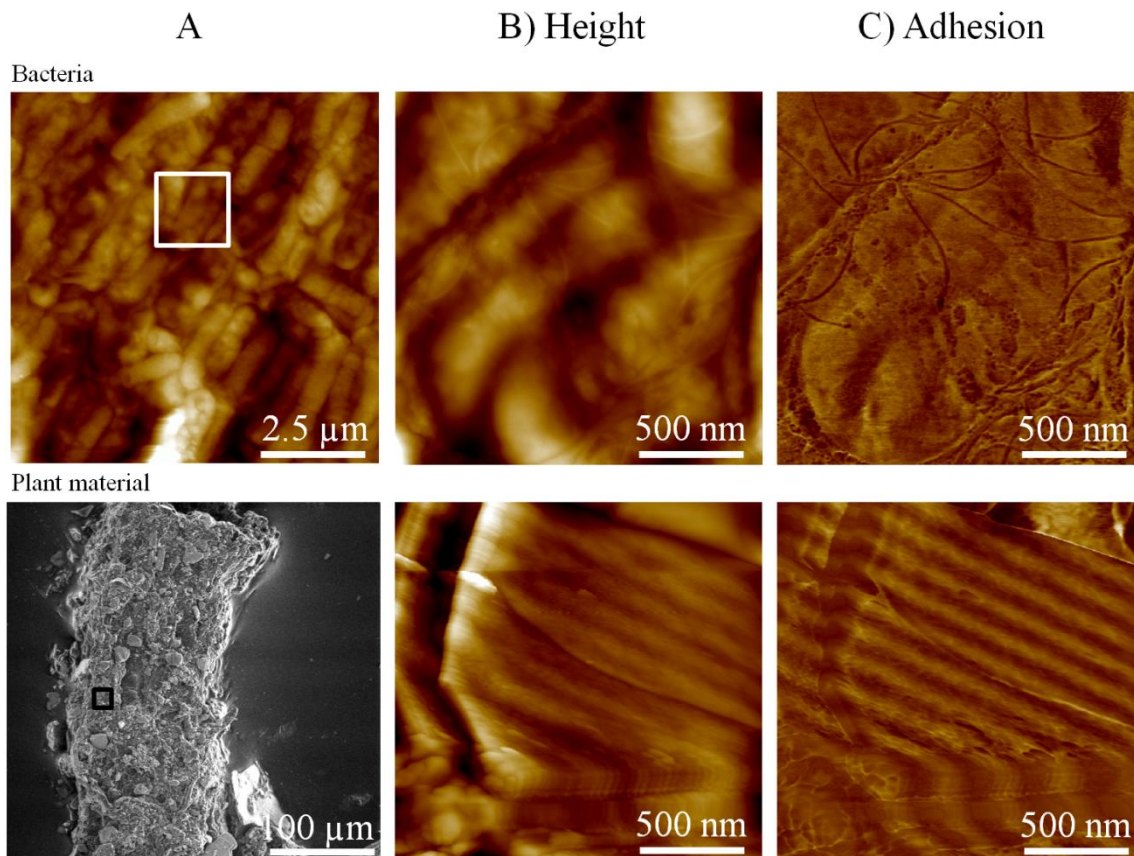


Figure 2. AFM height (panel B) and adhesion (panel C) images of bacterial and plant test materials. The larger height image of bacteria in panel A shows a cloud of several cells, the marked area of which was scanned for a closer view, as shown in the other two panels. Panel A shows the ESEM image for plant material. Color scale: In height images, darkest and lightest points correspond to a depth of 80 nm and a height of 80 nm, respectively, from the mean plane. For adhesion images, darkest and lightest points respectively correspond to forces of 20 nN and 40 nN for bacteria and 0 nN and 50 nN for plant material. Reproducibility of the linear pattern on the surface of plant material was confirmed by testing in a different scan angle (45°).

Bernasconiet al. (2011) reported an increase in several physicochemical parameters such as total organic carbon, total nitrogen, cation exchange capacity, microbial C, bacterial and fungal biomass etc. with soil development, along the same chronosequence. Our AFM results suggest that also nanoscale morphological heterogeneity increases with increasing soil age and support the idea that soil formation is a process increasing spatial heterogeneity on all spatial scales; from the nm sale to the μm scale and to larger scales at least up to 50 cm (Bernasconi, et al., 2011).

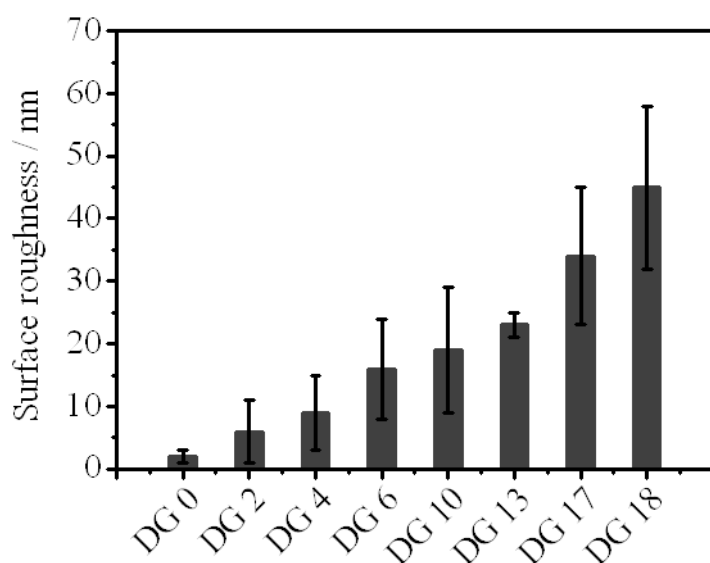


Figure 3. Development of surface roughness (Ra) in soils as average of four images, as given by the absolute values. The error bars show the standard deviations between ROI within each sample.

Bernasconi *et al.* (2011) reported an increase in several physicochemical parameters such as total organic carbon, total nitrogen, cation exchange capacity, microbial C, bacterial and fungal biomass etc. with soil development, along the same chronosequence. Our AFM results suggest that also nanoscale morphological heterogeneity increases with increasing soil age and support the idea that soil formation is a process increasing spatial heterogeneity on all spatial scales; from the nm scale to the μm scale and to larger scales at least up to 50 cm (Bernasconi, *et al.*, 2011).

2.2 Adhesive force distribution

Adhesive interactions between the tip and sample are characteristics of surface morphology as well as the material of which both the tip and sample are made (Eastman & Zhu, 1996). In our experiment, we used the same tip to image all the samples. Therefore the effect of the tip properties is the same for all measurements and thus can be neglected for the comparison of the samples. Large adhesion forces indicate larger stickiness between tip and surface (Pelin, *et al.*, 2012). Tip-surface adhesive interactions were profiled in adhesion images (figures 1 and 2, C panels).

Adhesive forces range between 0 nN and 50 nN in all images (figures 1, 2 and 4). Figure 4 shows histograms of adhesion forces on each soil, as an average of four imaged regions, with the error bars showing standard deviation between imaged micro-regions within each sample.

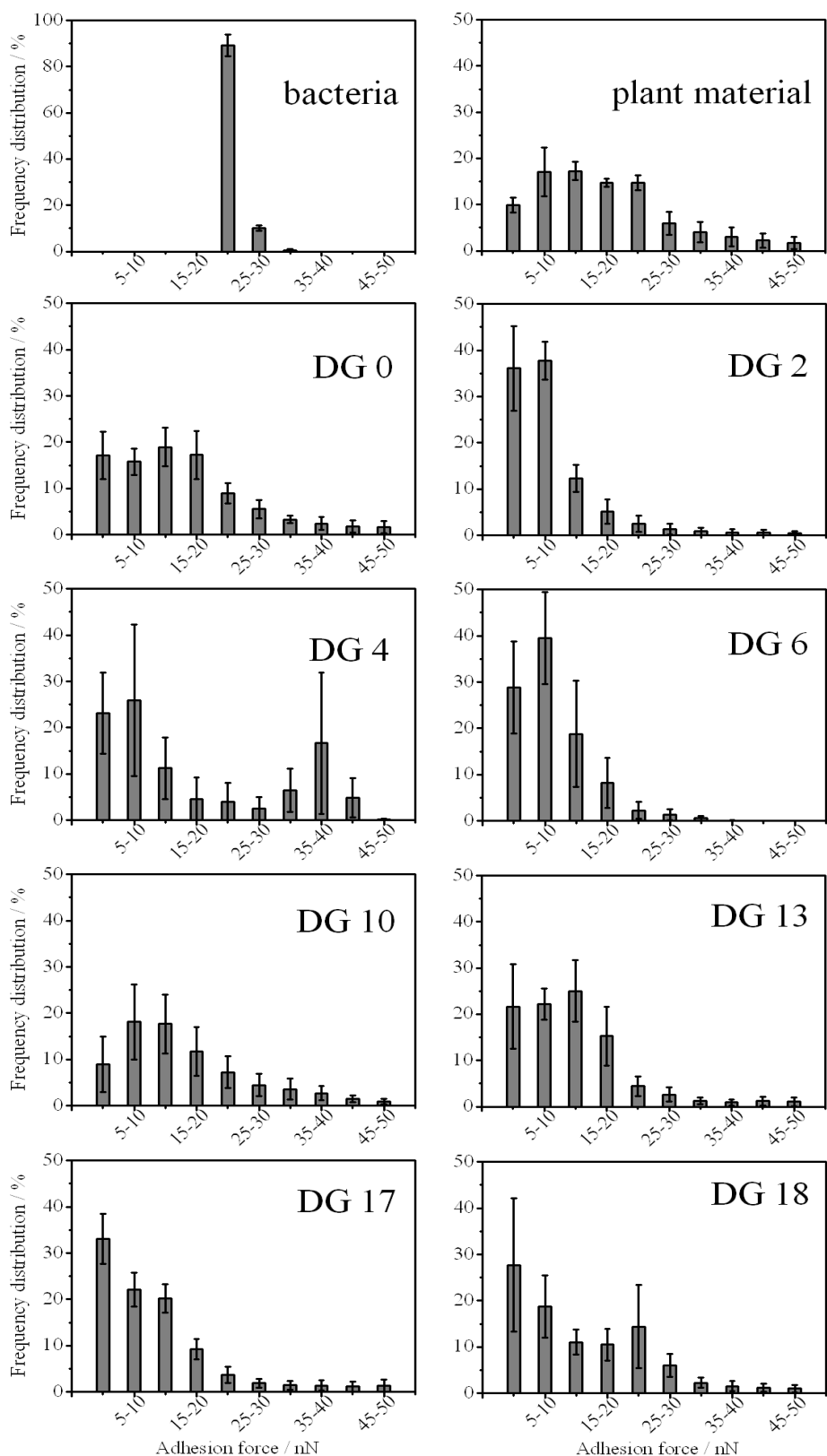


Figure 4. Sample-tip adhesion force histogram, showing similar distribution in plant materials and soils. The narrower distribution in bacteria shows higher homogeneity of the surface. The adhesion force range with maximum abundance varies between samples (total number of force curves per each histogram is 262144).

The bacterial cells used as test material in this study showed a comparably narrow range of adhesive force distribution ranging between 20 nN to 30 nN with the highest abundance of forces between 20 and 25 nN (90% of the total number of data points). For the plant material, 74% of the data points revealed forces of 0-25 nN. A broader distribution with most forces ranging from 20 nN to 50 nN was observed in the soil samples, where the highest abundant adhesive force values also differed between the individual samples. The broader force distribution shown by the plant-originated material than that of the bacterial surfaces may be due to wider range of different cell structures and constituents in the plant material. The soil samples may contain organic matter with different degrees of degradation, organic matter coatings, root exudates, EPS or other organic compounds. This could have caused a broader distribution of adhesive forces within the ROI in soils. Furthermore, it cannot be excluded that part of the regions contains very small clay particles and iron oxides which contribute to the width of the distribution. Particulate organic matter is also expected to consist of more than one material, therefore we expect a wide range of adhesion forces also for particulate organic matter. Force distribution histograms alone will, therefore, not help to differentiate between various materials with similar chemical composition, and additional characteristics are required for more detailed and unambiguous analysis. Nevertheless, each individual AFM adhesion image shows clear domains and structural units exhibiting adhesion forces from 0 to 50 nN (see figure 1, panel C and figure 4) indicating nanoscale material heterogeneity. Variation in occurrence of peak positions in histograms between samples is indicative for the sample-to-sample variability and thus development of μm -scale heterogeneity. Also the size of error bars in the histograms reflects the degree of microscale chemical heterogeneity, i.e. the ROI-to-ROI variability. The degree of heterogeneity varies between ROI, within and between samples, but does not show a clear development with the soil age.

2.3 Nanothermal analysis

Thermograms revealed by the test materials and soil samples are shown in figure 5.

Test material 1: bacterial cells. The thermogram of the bacterial cells consists of three phases - an initial steep expansion up to 120 °C followed by a slight compression until 220 °C and a steeper compression phase afterwards (figure 5, bacterial cells). Therefore, three temperature ranges with different thermal characteristics were distinguished in the thermogram. The positive slope in the temperature region A (between 30 °C and 100 °C) with an expansion coefficient of $\alpha = 0.046 \text{ V } ^\circ\text{C}^{-1}$, while the other two had negative slopes with compression coefficients of $\kappa_I = 0.0030 \text{ V } ^\circ\text{C}^{-1}$ (temperature range B: 120 °C to 220 °C)

and $\kappa_2 = 0.046 \text{ V } ^\circ\text{C}^{-1}$ (temperature range C: 220 °C to 300 °C). This corresponds to an expansion - slight compression - strong compression sequence. The expansion A can be due to thermal expansion of cell envelope material at relatively low temperatures. The compression phases B and C are most probably due to heat-induced softening and thermal degradation of the cells, respectively.

Test material 2: plant material. The thermogram revealed by the fibrous plant root material (figure 5, plant material) is entirely different from the one of the bacteria, probably due to chemically more complex supporting tissue in plants than in bacterial cell envelopes. It consists of an initial steep compression phase from 30 °C to 170 °C ($\kappa = 0.011 \text{ V } ^\circ\text{C}^{-1}$) followed by an expansion phase ($\alpha = 0.029 \text{ V } ^\circ\text{C}^{-1}$). The initial compression can be due to temperature-induced softening of the material, which may be overlaid by thermal expansion of cells underneath that becomes effective after completion of the compression phase of the top layer.

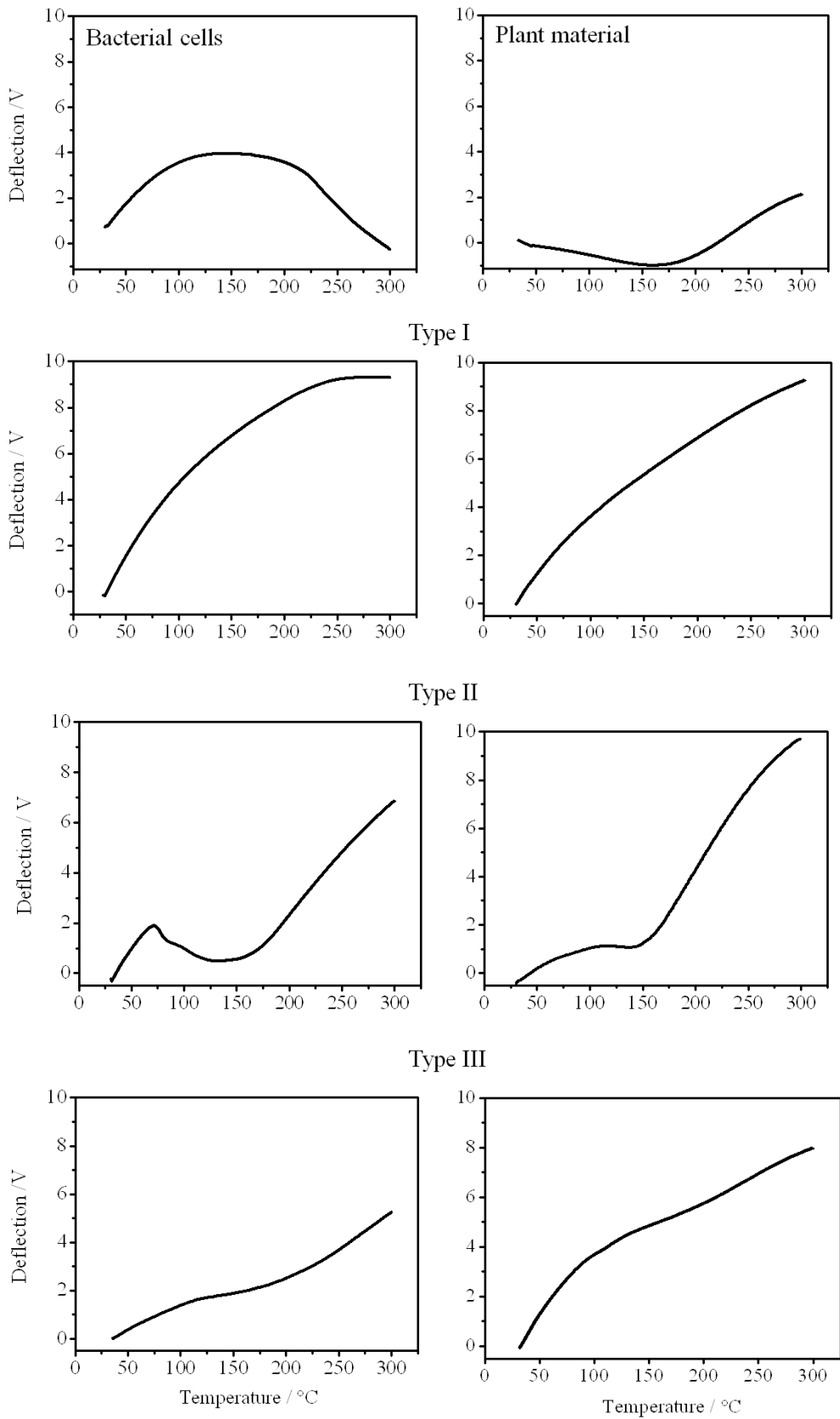


Figure 5. Different types of thermograms revealed by test materials (top panels) and soil samples. Thermograms detected in soil samples are grouped into three individual types with respect to the temperatures of occurrence of various thermal events (for details see text).

Occurrence of only one, organic type thermogram contradicts the suggestion raised by adhesion data that the plant material might be covered by mineral particles, although it still cannot be excluded that they occur in very low amounts and were not detected by the thermal analysis. Presence of fungi on partly degraded plant material cannot fully be excluded for our test material. However, according to SEM images, there were no intact fungal hyphae close to our ROI. Smaller fragments of fungal hyphae, which might be present but are not visible in the SEM images, were considered part of this test material. Difference in thermal behavior of the two test materials could be due to difference in their cell structure. For example, plants have more complex and hard materials such as lignin, cellulose and suberin; the former two are characterized by glass transitions at 72 °C (LeBoeuf, 1998) and 225 °C (Akim, 1978), respectively, and the latter one shows melting around 40 °C (Cordeiro, *et al.*, 1998). The bacterial cells mainly contain peptidoglycans, lipids and proteins in their cell envelopes. Proteins (Welzel, 2002) and bacterial polysaccharide (Villain-Simonnet, *et al.*, 2000) undergo conformational changes above 50°C, and 65 °C, respectively. Nanothermograms of neither plant material nor bacteria show any of these thermal events identified in defined chemicals. This might be due to overlap of more than one process in the two test materials, due to the complexity in their cell structures and chemical composition. Identification of the defined thermal characteristics observed in the nanothermograms of the test materials cannot be done in the current state as this requires targeted experiments with a huge set of samples with well known thermal properties. This will be done in future, to explore further utilities of AFM-nTA.

When interpreting nTA thermograms, it is important to consider that the effective thermal expansion or compression will always be a result of all materials reached by the heat of the tip. According to the manufacturer, the resolution of the tip is 1 μm^3 . Therefore, it has to be assumed that the immersion depth of the heat is in the range of 1 μm . Within this range, it can be expected that more than one material is layered in the soil sample. Each individual layer will contribute to the overall thermal expansion or compression. Therefore, a compression on the very top layer can be masked by a parallel expansion of the layer beneath. The second layer expands later than the top most one because it is only indirectly heated by heat transfer. The extent of contribution will depend on the thermal conductivity of the material along the vertical dimension. Similar effects have been demonstrated for polymeric materials (Duvigneau, *et al.*, 2008).

Soil samples. Our soil samples revealed different types of thermal profiles, varying in number and slopes of components and their intersection temperatures. They can be grouped into three thermogram types based on the general features (expansion or compression) present and the temperature regions at which individual sub-regions switch to the next phase. Representative thermograms of type I, II and III are shown in figure 5.

Type I thermograms revealed one steep expansion phase throughout the investigated temperature range. Only in few thermograms of this type, expansion stopped around 250 °C. This thermogram type resembles type E in the previous study (Schaumann and Kunhi Mouvenchery 2012) and, accordingly, we preliminarily attributed it to inorganic materials. This is in line with the fact that for inorganic surfaces most thermal events occur above 300 °C (see Plante *et al.* 2009), although a compression phase starting at 120 °C was observed for ground quartz (Schaumann & Kunhi Mouvenchery, 2012). Final verification of this assignment will require a larger dataset including a variety of mineral materials.

Type II. In this type, two expansion phases are clearly separated by a compression phase starting from range of 70-90 °C and lasting up to 150-170 °C. The majority of these thermograms was characterized by steep compression ($\kappa =$ of 0.023 V °C⁻¹) whereas few others expressed only slight compression ($\kappa =$ 0.0031 V °C⁻¹) in the second sub-region. This difference could be due to a fast-expanding layer present underneath in the latter case, which masks the intrinsic compression phase of the layer which is under direct influence of the heated tip. This pattern of thermal events was not observed before, but the presence of the compression phase suggests that it could be representative for organic material. Differences in the extent of compression and expansion might indicate different thicknesses of organic layers on mineral material.

Type III thermograms consist of two steep expansion phases interrupted by a compression phase or a mild expansion regime, depending on the location. The transitions between the phases occur in the ranges of 100-120 °C and 200-225 °C. Similar thermal profiles, but with different slopes, were observed previously in samples of charcoal, manure and a peat and were attributed to organic regimes, especially due to the presence of a compression phase (Schaumann & Kunhi Mouvenchery, 2012). The current thermograms differ in intensity of the compression phase in the second sub-region (between 100-120 °C and 210-225 °C) which could either be due to several various types of organic regimes or to the effect of underneath layers or both.

This grouping was generally clear and unambiguous; thermograms within each group varied only with respect to total expansion, degree of expression of maxima, minima and inflections and their exact positions, which indicate further sub-types of materials. In the samples investigated in this study, the thermograms of type II and III could stand for fresh or degraded biological materials, either from microbes or from plants. Type II and plant material thermograms are characterized mainly by the compression phase with their coefficients of compression lying within same range ($\kappa = 0.023\text{-}0.0031 \text{ V } ^\circ\text{C}^{-1}$ for type II and $\kappa = 0.0011 \text{ V } ^\circ\text{C}^{-1}$ for plant material). Also, the temperature range up to which compression proceeds is the same for both thermograms (160-180 °C for type II and 170 °C for plant material). Therefore, regions with type II thermograms could be candidates for degraded plant material in soils. But the presence of an initial expansion phase in type II was not observed in the plant material. The plant residues in the soils have passed more intensive degradation processes than the test plant material which had a size of some mm. Our regions of interest in the soil samples did not contain such large materials. Biological degradation results in a decreasing size of individual particles and thus layer thickness of the organic material. Therefore, the thermogram will be an overlay resulting from thermal behavior of a thin organic layer on inorganic material. If verified in future studies, this will imply that the initial thermal expansion is due to the inorganic surfaces beneath the organic structure, when compression of the organic material is not yet significant (see figure 5, type II). Only at temperatures above 70°, compression of the organic layer becomes the dominating process.

In a comparable way, type III thermograms reveal certain similarities with the thermogram of the bacteria. Comparing the temperature ranges of occurrence of characteristic compression phases in the second sub-region (100-120 °C to 200-225 °C for type III and 120 °C to 220 °C for bacterial thermograms), type III thermograms can be claimed to be akin to bacterial thermograms. However, the two classes of thermograms differ from each other in the slope of the compression phase and in development of the third phase. The third phase proceeds as expansion in type III and as compression in case of the bacteria, which is even steeper than the preceding one. This could be, as suspected before, due to the effect of material present in layers beneath the surface. This is particularly important in this case because the test material consisted of a thick layer of bacteria whereas we expect only thin layers of bacterial-derived organic material on the mineral surfaces in soil. Other potential factors are the difference in degradation state of the test bacterial cells (intact biomass) versus partly degraded cell envelope fragments (necromass) in soils.

In the same way, any organic matter in soil including particulate OM, organic coatings, swellable substances or carbohydrates may also contribute to the thermal behavior of a ROI. Organic coatings are, for example, expected to show an overlay of thermograms related to organic and inorganic materials.

2.4 *Distribution of thermograms within the soils*

To estimate the distribution of thermogram types within the ROI of the AFM images, thermal data collected along a 4x4 grid over the surface of each 2 μm x 2 μm AFM image were evaluated. The distribution shown on adhesion images is given in the SI (figure S4). The highest number (more than 50%) of the points revealed type I thermograms in all samples. Differences were noted in thermal behavior at individual nanodomains within each 2 μm x 2 μm image (figure S4), and in the pattern of distribution between replicate images for each individual site (data not shown). The former is representative for nanoscale heterogeneity and the latter for microscale heterogeneity. The distribution pattern varied between samples, revealing development in the two types of heterogeneity with soil development. The degree of heterogeneity in the different spatial scales is lower than observed in a peat and sandy soil investigated in a previous study (Schaumann & Kunhi Mouvenchery, 2012), owing to the lower complexity of the very young soils in the glacier forefield.

The abundance of each thermogram type changed with increasing distance to the glacier forefield (figure 6). Abundance of type I thermograms, which were attributed to inorganic materials, decreased with increasing distance ($P < 0.0002$), and abundance of type III thermograms (attributed to organic materials of microbial origin) increased with increasing distance ($P < 0.0001$). The trend is less significant for type II (hypothesized plant materials, $P < 0.7$). Thus, the data from the selected ROIs suggest that the area of bare inorganic surfaces decreases with soil development, probably due to increasing coverage by organic moieties. This is supported by the increasing TOC and fatty acid contents of the soil samples with increasing distance from the glacier (Bernasconi, *et al.*, 2011, Schurig, *et al.*, 2013). However, for a general verification of the provided hypotheses, additional evidence from other properties and materials with significantly more AFM images, in particular for quantification, are needed.

2.5 Combining adhesive force information and thermal characteristics

As discussed in sections 2.2 and 2.4, individual adhesive force and thermal analysis could not assign the material types unambiguously. Aiming to attain more concrete discrimination of the three types of materials revealed by nTA alone, the thermal characteristics were combined with force characteristics. We analyzed individual nanodomains along the 4x4 grid combining the two sets of information gained independently of each other. For this, adhesion forces at the 16 locations on all images, of all soils, falling on the grid were extracted and related to the respective thermogram type (figure S5A). Thus nanomechanical properties of each material type distinguished by thermal behavior was assessed using the whole set of soils, provided that they share similar structural features, and similar thermomechanical behavior, but to different extents. To make the discussion easier, different domains are arbitrarily named after their thermal behavior, further in the text (i.e. domains with type I, II and III thermograms will be called type I, type II and type III materials, respectively), despite the fact that they were discussed in a preceding chapter with potential attributions to soil constituents.

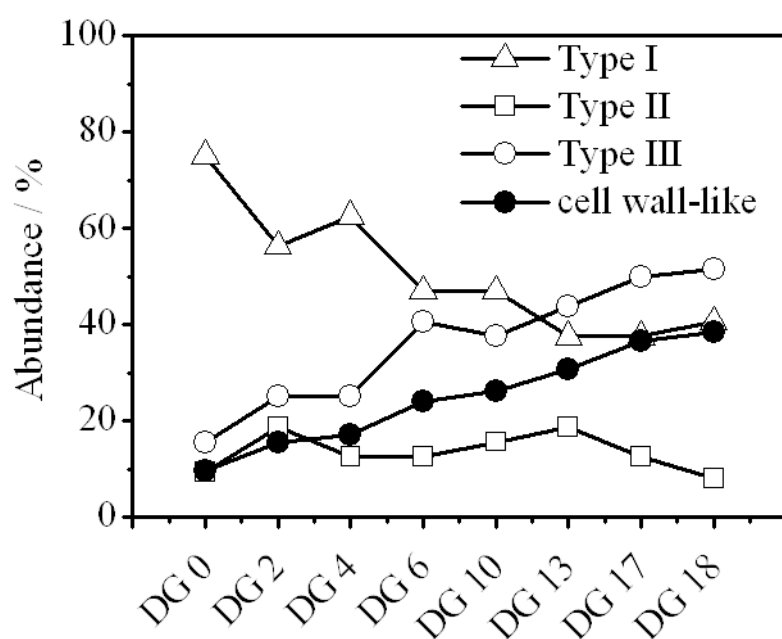


Figure 6. Distribution of different thermogram types in soil samples, collected along a 4x4 grid on each AFM image. The closed circles represent the cell envelope-like materials characterized by thermal behavior and adhesion forces comparable to the test bacterial cells and with size anticipated for the microbial cell envelope materials.

Adhesion force values for each soil obtained from this partial analysis showed that almost all samples had forces ranging from 0 nN to 40 nN, except DG 0, DG 2 and DG 17 which showed an additional range of 40-50 nN. Samples at intermediate distance from glacier forefield revealed a narrower range of 0-40 nN (data not shown). The range is slightly narrower in comparison with the complete image analysis (0-50 nN shown in figure 4), since in the partial analysis we targeted only some selected nanodomains on the 4x4 grid. Relating the adhesion force values at each region to the corresponding thermogram type, distinguished

the thermograms with respect to their distribution within each adhesion force range (figure S5A). Abundance of type I and type II materials tended to decrease with increasing adhesion force. The development is significant (significance level= 0.05) only in the intermediate force range (20 - 40 nN) for type I and in the very low (0-20 nN) and intermediate force ranges for type II. Type III materials showed highest abundance (47%) in the intermediate force range-between 20 nN and 30 nN (difference from other force ranges is significant on a 5 % level). The latter thus indicates that 47% of the type III materials may be of microbial origin since both the adhesion and thermal data match those of the test bacterial cells. However, 53% of type III materials revealed other adhesion force values, indicating that also other material types belong to type III materials, e.g. different types of microbial residues with different degrees of degradation or other materials with similar thermal characteristics. Also material underlying the surface material might contribute to differences in thermogram characteristics. 65% of the type II materials reveal adhesion forces similar to those of the test plant material (0-20 nN) and could, therefore, be of the same origin and/or degree of degradation as the test plant material, while 35% of type II materials reveal larger forces, indicating other degrees of degradation and/or different origin. The majority of the type I materials (~90 %) revealed a wide range of adhesion forces (0-30 nN), which suggests a large variety of inorganic materials, potentially with differing degree of weathering and/or organic coatings - as it is typical for soils. This analysis underlines the supportive value of combining different properties to distinguish different material characteristics.

2.6 Nanothermograms and adhesion forces of 200 nm to 500 nm large structures

In order to investigate the hypothesis that features of 200-500 nm represent microbial cell envelope fragments and that they increase in number with soil age (Schurig, *et al.*, 2013), we conducted an additional analysis on the same AFM images, in which 8 to 10 potential candidates per image were chosen based on their size and nanothermal analysis was conducted on each of these candidates.

Figure S6 shows the selected potential candidates and expressed thermogram type. As expected, not all 200-500 nm large features reveal thermograms of type III. Instead, more than 50% of them exhibited characteristics assigned to inorganic materials (type I). This clearly indicates that morphology and the size range of structural features cannot be the only criteria to identify certain material characteristics. This is underlined by an AFM study of clay minerals by Liu *et al.* (Liu, *et al.*, 2003), which revealed fluffy features larger than 200 nm on organic-free clay minerals.

Hence, thermogram types were related to adhesion force exhibited by respective localities (figure S7). Tip-surface adhesive forces of the selected features of 200-500 nm ranged between 0 and 30 nN (see also figure S8). In tendency, the percentage of structures having forces of 0-10 nN decreased with increasing soil-glacier distance, whereas the abundance of structures with forces of 20-30 nN increased with increasing soil-glacier distance.

Similar to the grid analysis described in the previous section, the distribution of different types of materials into various force ranges was assessed considering structural units in the size range of 200-500 nm, characteristic of microbial cell envelope fragments (figure S5B). 53% of these structures with type I thermograms revealed forces between 0 nN and 10 nN, while 38% revealed 10-20 nN. In contrast, 18% and 48% of type II materials showed forces between 0-10 nN and 10-20 nN, respectively. Therefore, 66% of the type II materials in this size range resemble the test plant material (type II thermogram and adhesion forces 0-20 nN). Similarly, 73% of type III materials with sizes 200-500 nm revealed adhesion forces between 20-30 nN and thus resemble the test bacterial material. The non-overlapping error bars in figure S5B shows that the development is significant (accounting for variance within 5 % significance level, between the force ranges). Thus, combination of adhesion and thermal properties with morphology allows to recognize structures resembling test materials with respect to the combined interaction force and thermomechanical properties, out of the larger set of candidates selected solely by size.

The observation that a large part of the selected 200-500 nm large structures do not match with the test materials of this study indicates the presence of a higher variety of material types showing similar size and thermal behavior, but different adhesion forces. It is worth to remember at this point that individual thermograms falling under type III differ in coefficients of expansion or compression and the exact temperature at which each phase becomes dominant (which resulted in a characteristic range of temperatures in the definition of type III). Thus not all type III materials are identical. SEM-EDX studies of the soil samples from the Damma glacier indicated that bacterial residues may be encrusted with Si or Fe (Miltner, *et al.*, 2012). Even these small changes can affect the surface properties of the residues significantly. Further attribution of the 200-500 nm large structures to additional material types is promising and requires significant expansion of the material database.

In the light of these considerations, it can be assumed that material type III with adhesion forces in the range of 20-30 nN represents microbial derived materials. Type I materials can

be distinguished further into various kinds of inorganic surfaces, based on adhesion data. Likewise, type II materials could be consisting of three or more types of plant-derived degradation products of different tissues.

As discussed above, 73% of the material type III structures sized 200-500 nm have the same combination of characteristics as the test bacterial material and have therefore been attributed to cell envelope-like material. The other fraction may consist of another type of microbial biomass (e.g. Gram negative bacteria or fungi) due to different adhesion forces and thermal behavior in comparison to the test bacteria. Closed circles in figure 6 show the abundance of cell envelope-like moieties in the ROI of investigated soil samples. It increased significantly from 10% in soil DG 0 to 39% in DG 18 ($P < 0.0001$). Although for final quantification a larger number of ROI is required, this development is qualitatively in accordance with a previous study (Schurig, *et al.*, 2013), but suggests that the high coverage of the soil particle surfaces estimated by means of SEM image analysis solely based on morphology (Schurig, *et al.*, 2013) may be an overestimation. Further constrains were not possible in that study, but have been provided in this study by combining size and morphological information with thermal characteristics and adhesion force information.

3. Conclusions

The current study demonstrates that the combination of the two independent AFM tools (force mapping and thermal analysis) allows to locate and distinguish structural features in soils on a BGI-relevant scale. The investigated ROI indicated materials similar to bacterial and plant test materials with regard to the combination of morphological, physicochemical, mechanical and thermal characteristics.

Combination of nanothermal analysis with adhesion force data allows to discriminate different materials in nanoscale regions with a higher degree of certainty than obtained either by PFQNM or by nTA alone. The clarity of discrimination is further increased by combination with morphological characteristics, e.g., the size as done in our study. By this approach, the bias resulting from overlapping of adhesion force ranges between several materials is overcome. Also, the challenges that thermal behaviour at certain points is always the overlay of responses of several layers, can be overcome by the suggested combination of material properties and physicochemical properties. The increase of abundance of the bacterial-like material type and the decrease of bare inorganic surfaces in the investigated

ROI with age of soil, qualitatively supports the cell envelope hypothesis (Miltner, *et al.*, 2012, Schurig, *et al.*, 2013).

The current study focused on the distribution of material properties and material types on the selected ROI. To be able to describe the whole soil based on material properties more reference samples including both organic and inorganic materials and a significantly larger set of ROI will be needed. To explore the further potential of AFM-nTA, as suggested in this study, more complex and developed soil systems should be investigated, and the currently existing database needs to be extended by more representative organic and inorganic test materials. If quantification of composition is required, a sufficiently large set of representative ROI has to be chosen. However, the qualitative characteristics alone will already help to identify and distinguish various soil constituents on material basis and may help to understand the significance of the contribution of soil microbiology to SOM development. The current approach could be further improved by additional use of chemical force microscopy (Alsteens, *et al.*, 2007), allowing for an even clearer discrimination between materials.

Acknowledgement

We acknowledge Ms. Priya Mary Abraham and Dr. Walter Schreiber for fruitful discussions. We thank Rienk Smittenberg for granting access to the BigLink sites in the Damma glacier forefield. This study has been supported by the Deutsche Forschungsgemeinschaft, Project SCHA849/8 and MI 598/2 within the priority program SPP 1315 Biogeochemical Interfaces in Soil and by the European Commission in the framework of the IP ModelPROBE (contract number 213161).

References

- Abu-Lail LI, Liu Y, Atabek A & Camesano TA (2007) Quantifying the adhesion and interaction forces between *Pseudomonas aeruginosa* and natural organic matter. *Environmental Science & Technology* **41**: 8031-8037.
- Akim EL (1978) Cellulose - Bellwether or Old Hat. *Chemtech* **8**: 676-682.
- Allen GC, Eastman JR, Hallam KR, Graveling GJ, Ragnarsdottir KV & Skuse DR (1999) Mineral/reagent interactions: an X-ray photoelectron spectroscopic study of adsorption of reagents onto mixtures of minerals. *Clay Minerals* **34**: 51-56.
- Alsteens D, Dague E, Rouxhet PG, Baulard AR & Dufrene YF (2007) Direct Measurement of Hydrophobic Forces on Cell Surfaces Using AFM. *Langmuir* **23**: 11977-11979.
- Amelung W, Kaiser K, Kammerer G & Sauer G (2002) Organic carbon at soil particle surfaces - Evidence from X-ray photoelectron spectroscopy and surface abrasion. *Soil Science Society of America Journal* **66**: 1526-1530.

- Aquino AJA, Tunega D, Schaumann GE, Haberhauer G, Gerzabek MH & Lischka H (2011) The Functionality of Cation Bridges for Binding Polar Groups in Soil Aggregates. *International Journal of Quantum Chemistry* **111**: 1531-1542.
- Areekijseeree M, Panishkan K, Sanmanee N & K S (2009) Microanalysis by SEM-EDX on Structure and Elemental Composition of Soils from Different Agriculture Areas in the Western Region of Thailand. *Journal of Microscopy Society of Thailand* **23**: 152-156.
- Arnarson TS & Keil RG (2001) Organic-mineral interactions in marine sediments studied using density fractionation and X-ray photoelectron spectroscopy. *Organic Geochemistry* **32**: 1401-1415.
- Barr TL, Hoppe EE, Hardcastle S & Seal S (1999) X-ray photoelectron spectroscopy investigations of the chemistries of soils. *Journal of Vacuum Science & Technology A* **17**: 1079-1085.
- Becker JM, Parkin T, Nakatsu CH, Wilbur JD & Konopka A (2006) Bacterial activity, community structure, and centimeter-scale spatial heterogeneity in contaminated soil. *Microbial Ecology* **51**: 220-231.
- Bernasconi SM, Bauder A, Bourdon B, *et al.* (2011) Chemical and biological gradients along the Damma glacier soil chronosequence, Switzerland. Vol. 10 ed.ed.s.), p.pp. 867-883.
- Cheng SY, Bryant R, Doerr SH, Wright CJ & Williams PR (2009) Investigation of Surface Properties of Soil Particles and Model Materials with Contrasting Hydrophobicity Using Atomic Force Microscopy. *Environmental Science & Technology* **43**: 6500-6506.
- Chenu C & Plante AF (2006) Clay-sized organo-mineral complexes in a cultivation chronosequence: revisiting the concept of the 'primary organo-mineral complex'. *European Journal of Soil Science* **57**: 596-607.
- Chenu C, Hassink J & Bloem J (2001) Short-term changes in the spatial distribution of microorganisms in soil aggregates as affected by glucose addition. *Biology and Fertility of Soils* **34**: 349-356.
- Cordeiro N, Belgacem NM, Gandini A & Neto CP (1998) Cork suberin as a new source of chemicals: 2. Crystallinity, thermal and rheological properties. *Bioresource Technology* **63**: 153-158.
- Dechesne A, Or D & Smets BF (2008) Limited diffusive fluxes of substrate facilitate coexistence of two competing bacterial strains. *Fems Microbiology Ecology* **64**: 1-8.
- Duemig A, Smittenberg R & Koegel-Knabner I (2011) Concurrent evolution of organic and mineral components during initial soil development after retreat of the Damma glacier, Switzerland. *Geoderma* **163**: 83-94.
- Duvigneau J, Schonherr H & Vancso GJ (2008) Atomic force microscopy based thermal lithography of poly(tert-butyl acrylate) block copolymer films for bioconjugation. *Langmuir* **24**: 10825-10832.
- Eastman T & Zhu DM (1996) Adhesion forces between surface-modified AFM tips and a mica surface. *Langmuir* **12**: 2859-2862.
- Engelke CJ, Knicker H & Kogel-Knabner I (2003) MALDI-TOF MS as a new means of characterising condensed tannins in soil. *Abstracts of Papers of the American Chemical Society* **225**: U919-U919.
- Ettema CH & Wardle DA (2002) Spatial soil ecology. *Trends in Ecology & Evolution* **17**: 177-183.
- Fang HHP, Chan K-Y & Xu L-C (2000) Quantification of bacterial adhesion forces using atomic force microscopy (AFM). *Journal of Microbiological Methods* **40**: 89-97.
- Franklin RB & Mills AL (2003) Multi-scale variation in spatial heterogeneity for microbial community structure in an eastern Virginia agricultural field. *Fems Microbiology Ecology* **44**: 335-346.

- Gupta VVSR & Germida JJ (1988) Distribution of microbial biomass and its activity in different soil aggregate size classes as affected by cultivation. *Soil Biology and Biochemistry* **20**: 777-786.
- Herrmann AM, Ritz K, Nunan N, *et al.* (2007) Nano-scale secondary ion mass spectrometry - A new analytical tool in biogeochemistry and soil ecology: A review article. *Soil Biology & Biochemistry* **39**: 1835-1850.
- Heu CA, Berquand C, Elie-Caille & Nicod L (2012) Glyphosate-induced stiffening of HaCaT keratinocytes, a Peak Force Tapping study on living cells. *Journal of Structural Biology* **178**: 1-7.
- Hildebrand EE (1990) The Spatial Heterogeneity of Chemical-Properties in Acid Forest Soils and Its Importance for Tree Nutrition. *Water Air and Soil Pollution* **54**: 183-191.
- Jansson JK (2003) Marker and reporter genes: illuminating tools for environmental microbiologists. *Current Opinion in Microbiology* **6**: 310-316.
- Kinyangi J, Solomon D, Liang B, Lerotic M, Wirick S & Lehmann J (2006) Nanoscale Biogeochemical Complexity of the Organomineral Assemblage in Soil. *Soil Science Society of America Journal* **70**: 1708-1718.
- Kogel-Knabner I (2002) The macromolecular organic composition of plant and microbial residues as inputs to soil organic matter. *Soil Biology & Biochemistry* **34**: 139-162.
- Kunhi Mouvenchery Y, Kučerík J, Diehl D & Schaumann GE (2012) Cation-mediated cross-linking in natural organic matter - a review. *Reviews in Environmental Science and Bio/technology* **11**: 41-54.
- LeBoeuf EJ (1998) Macromolecular characteristics of natural organic matter and their influence on sorption and desorption behavior of organic chemicals. PhD Dissertation Thesis, The University of Michigan, Michigan, USA.
- Lehmann J, Solomon D, Kinyangi J, Dathe L, Wirick S & Jacobsen C (2008) Spatial complexity of soil organic matter forms at nanometre scales. *Nature Geoscience* **1**: 238-242.
- Leite FL & Herrmann PSP (2005) Application of atomic force spectroscopy (AFS) to studies of adhesion phenomena: a review. *Journal of Adhesion Science and Technology* **19**: 365-405.
- Leite FL, Riul A & Herrmann PSP (2003) Mapping of adhesion forces on soil minerals in air and water by atomic force spectroscopy (AFS). *Journal of Adhesion Science and Technology* **17**: 2141-2156.
- Li H & Reynolds JF (1995) On Definition and Quantification of Heterogeneity. *Oikos* **73**: 280-284.
- Liu C, Li XY, Xu FL & Huang PM (2003) Atomic force microscopy of soil inorganic colloids. *Soil Science and Plant Nutrition* **49**: 17-23.
- Maurice P, Forsythe J, Hersman L & Sposito G (1996) Application of atomic-force microscopy to studies of microbial interactions with hydrous Fe(III)-oxides. *Chemical Geology* **132**: 33-43.
- Miltner A, Bombach P, Schmidt-Brücken B & Kästner M (2012) SOM genesis: microbial biomass as a significant source. *Biogeochemistry* 1-15.
- Miltner A, Kindler R, Knicker H, Richnow H-H & Kaestner M (2009) Fate of microbial biomass-derived amino acids in soil and their contribution to soil organic matter. *Organic Geochemistry* **40**: 978-985.
- Miniaci C, Bunge M, Duc L, Edwards I, Buergermann H & Zeyer J (2007) Effects of pioneering plants on microbial structures and functions in a glacier forefield. *Biology and Fertility of Soils* **44**: 289-297.
- Mummey DL & Stahl PD (2004) Analysis of soil whole- and inner-microaggregate bacterial communities. *Microbial Ecology* **48**: 41-50.

- Nunan N, Wu K, Young IM, Crawford JW & Ritz K (2002) In situ spatial patterns of soil bacterial populations, mapped at multiple scales, in an arable soil. *Microbial Ecology* **44**: 296-305.
- Nunan N, Ritz K, Crabb D, Harris K, Wu KJ, Crawford JW & Young IM (2001) Quantification of the in situ distribution of soil bacteria by large-scale imaging of thin sections of undisturbed soil. *Fems Microbiology Ecology* **37**: 67-77.
- Odum EP (1969) *The Strategy of Ecosystem Development*. Vol. 164 ed.), pp. 262-270.
- Pelin IM, Piednoir A, Machon D, Farge P, Pirat C & Ramos SMM (2012) Adhesion forces between AFM tips and superficial dentin surfaces. *Journal of Colloid and Interface Science* **376**: 262-268.
- Plante A, Magrini-Bair K, Vigil M & Paul E (2009) Pyrolysis-molecular beam mass spectrometry to characterize soil organic matter composition in chemically isolated fractions from differing land uses. *Biogeochemistry* **92**: 145-161.
- Powlson DS (1980) The Effects of grinding on microbial and non-microbial organic matter in soil. *Journal of Soil Science* **31**: 77-85.
- Ranjard L, Nazaret S, Gourbiere F, Thioulouse J, Linet P & Richaume A (2000) A soil microscale study to reveal the heterogeneity of Hg(II) impact on indigenous bacteria by quantification of adapted phenotypes and analysis of community DNA fingerprints. *Fems Microbiology Ecology* **31**: 107-115.
- Schaumann GE (2006) Soil organic matter beyond molecular structure. 1. Macromolecular and supramolecular characteristics. *Journal of Plant Nutrition and Soil Science* **169**: 145-156.
- Schaumann GE & Thiele-Bruhn S (2011) Molecular Modelling of Soil Organic Matter: Squaring the Circle? *Geoderma* **169**: 55-68.
- Schaumann GE & Kunhi Mouvenchery Y (2012) Potential of AFM-Nanothermal Analysis to study the microscale thermal characteristics in soils and natural organic matter (NOM). *Journal of Soils and Sediments* **12**: 48-62.
- Schurig C, Smittenberg RH, Berger J, *et al.* (2012) Microbial cell-envelope fragments and the formation of soil organic matter: a case study from a glacier forefield. *Biogeochemistry* **in press**. DOI 10.1007/s10533-012-9791-3
- Sigler WV & Zeyer J (2002) Microbial diversity and activity along the forefields of two receding glaciers. *Microbial Ecology* **43**: 397-407.
- Sigler WV, Crivii S & Zeyer J (2002) Bacterial succession in glacial forefield soils characterized by community structure, activity and opportunistic growth dynamics. *Microbial Ecology* **44**: 306-316.
- Siricord C & O'Brien PA (2008) MALDI-TOF mass spectrometry can be used for detection of pathogenic microorganisms in soil. *Australasian Plant Pathology* **37**: 543-545.
- Smittenberg RH, Gierga M, Göransson H, Christl I, Farinotti D & Bernasconi SM (2012) Climate-sensitive ecosystem carbon dynamics along the soil chronosequence of the Damma glacier forefield, Switzerland. *Global Change Biology* **18**: 1941-1955.
- Stokes DJ (2008) *Principles and Practice of Variable Pressure/Environmental Scanning Electron Microscopy (VP-ESEM)*. John Wiley & Sons, Ltd.
- Styrishave B, Bjorklund E, Johnsen A & Halling-Sorensen B (2012) The Spatial Heterogeneity of Polycyclic Aromatic Hydrocarbons in Soil Depends on Their Physico-chemical Properties. *Water Air and Soil Pollution* **223**: 969-977.
- Tielemans MP, Roose C, Ngo R, Lazzaroni & Leclère P (2012) Multiphase coatings from complex radiation curable polyurethane dispersions. *Progress in Organic Coatings* **75**: 560-568
- Toewe S, Albert A, Kleineidam K, *et al.* (2010) Abundance of Microbes Involved in Nitrogen Transformation in the Rhizosphere of *Leucanthemopsis alpina* (L.) Heywood

- Grown in Soils from Different Sites of the Damma Glacier Forefield. *Microbial Ecology* **60**: 762-770.
- Totsche KU, Rennert T, Gerzabek MH, Kögel-Knabner I, Smalla K, Spiteller M & Vogel H-J (2009) Biogeochemical interfaces in soil: The interdisciplinary challenge for soil science. *Journal of Plant Nutrition and Soil Science* **173**: 88-99.
- Tsirogianni E, Aivaliotis M, Karas M & Tsiotis G (2005) Detection and characterisation of catechol 2,3-dioxygenase in an indigenous soil Pseudomonad by MALDI-TOF MS using a column separation. *Biodegradation* **16**: 181-186.
- Uhlik O, Strejcek M, Junkova P, *et al.* (2011) Matrix-Assisted Laser Desorption Ionization (MALDI)-Time of Flight Mass Spectrometry- and MALDI Biotyper-Based Identification of Cultured Biphenyl-Metabolizing Bacteria from Contaminated Horseradish Rhizosphere Soil. *Applied and Environmental Microbiology* **77**: 6858-6866.
- VeecoInstruments (2010) *Peak Force QNM user guide B-004-1036-000*. Veeco Instruments Inc., New York.
- Villain-Simonnet A, Milas M & Rinaudo M (2000) A new bacterial exopolysaccharide (YAS34). II. Influence of thermal treatments on the conformation and structure. Relation with gelation ability. *Int J Biol Macromol* **27**: 77-87.
- Welzel PB (2002) Investigation of adsorption-induced structural changes of proteins at solid/liquid interfaces by differential scanning calorimetry. *Thermochimica Acta* **382**: 175-188.
- Young IM & Ritz K (1998) Can there be a contemporary ecological dimension to soil biology without a habitat? Discussion. *Soil Biology & Biochemistry* **30**: 1229-1232.
- Young IM & Crawford JW (2004) Interactions and self-organization in the soil-microbe complex. *Science* **304**: 1634-1637.
- Young IM, Crawford JW & Rappoldt C (2001) New methods and models for characterising structural heterogeneity of soil. *Soil & Tillage Research* **61**: 33-45.

Chapter 8

Conclusions and Synthesis

7.1 Cation-mediated cross-linking in SOM: further implications

The critical review in chapter 2 brings out the discussion that characteristics of both cations (e.g. cationic charge density, size) and OM functionalities (e.g. acidity, negative charge density and chemical structure) are determinant for the formation and functional features of CaB. Among the three types of CaB (inner sphere and outer sphere CaB, CaB-WaMB association), only the inner sphere CaB involves direct interaction between cations and OM molecules. The other two types of CaB involve interaction via water molecules. Thus direct CaB is expected to be more stable than the indirect CaB, since it involves electrostatic interaction whereas the others operate through H-bonds. However, the formation of inner sphere CaB would demand energy input, since bare cations do not occur in aqueous solutions, under normal conditions. But its possibility cannot be completely denied, at least in cases where bare cationic size suits well in the voids between the active functional groups and when additional input of dehydration energy is possible.

The outer spheres of CaB and CaB-WaMB involve water molecules as mediators between the cross-linking cation and the organic functional group. Relative abundance of these indirect interactions would be determined by the distance between functional groups and the availability of water molecules at appropriate positions. Molecular modelling described in chapter 3 (see figure 1) indicates that as the distance between functional groups increases, the water molecules in the cation hydration shell become mobile and beyond a threshold distance (25.8 Å for hydrated Al^{3+}), bridging is not possible due to the disruption of hydration shell and the WaMB water cluster. Therefore, spatial distribution of OM molecular segments should be such a way that the functional groups occur in sufficient spatial proximity to each other, to be linked by CaB. Such an arrangement can be referred as potential CaB site. Absence of CaB in the peat OM after treatment with cations, described in chapter 3, suggested the importance of existence of such potential CaB sites within SOM.

However, it is very unlikely that NOM consists of uniformly distributed potential sites throughout the matrix. Therefore, functional groups should occur in bunches (still randomly distributed) to achieve the potential state for CaB. This indicates the possible occurrence of CaB-relevant hotspots. Further, under certain conditions, not all the OM functionalities can be expected to occur in deprotonated state, as the degree of deprotonation is determined by the acidic character of chemical functional groups and pH. For example, complete dissociation of carboxylic groups and phenolic groups occur at pH 8 and 11, respectively

(Bloom and Skjellberg 2011). Such high pH is not relevant for environmental systems and hence the amount and type of deprotonated functional groups depend on pH. Hence existence of CaB-relevant hotspots depends on the external conditions and chemical characteristics apart from spatial distribution of functional groups. Intramolecular cross-linking (CaB and WaMB) affect the motional freedom of molecular segments. As discussed in chapter 1, SOM is provided with intrinsic mobility both in the primary and secondary levels. Cross-linking immobilises the mobile segments, reducing their mobility, as seen in case of Soil-Ca and Soil-Ba, described in chapter 4. Thus cross-linked OM matrix appear more rigid and show fewer tendencies to undergo structural reorganisation, than a counterpart having no cross-links. The term 'matrix rigidity' should be understood here as a measure of physicochemical structural mobility. Thus matrix rigidity does not necessarily indicate mechanical brittleness (glassiness) (see (Schaumann 2006)).

A cross-linked OM system would then exhibit alterations in its functions that depend on matrix rigidity, e.g. sorption of organic contaminants. Apart from chemical binding, sorption can additionally follow via physical entrapment within the cross-linked network (Schaumann and Thiele-Bruhn 2011). Further, diffusion of molecules within the OM matrix to the optimal binding site (voids, as described by polymer model of sorption; see chapter 1) would be decelerated in a more rigid state. The same will be the case of nutrient binding and their availability.

Disruption of direct CaB may not be as easy as disruption of indirect CaB and WaMB, because ionic bonds (several hundred kJmol^{-1} , depending on the involved atoms) are stronger interactions than H-bonds ($5\text{-}30 \text{ kJmol}^{-1}$) (Atkins and De Paula 2006). Indirect CaB can be broken by the disruption of H-bonds between water molecules (of hydration shell in case of outer sphere CaB and bridging water in case of CaB-WaMB) and active functional groups. Entropy-driven intrinsic structural reorganisation causing the cross-linked segments to move apart from each other, energy input in terms of heat or change in chemical potential due to the presence of extraneous molecules can disrupt cross-links. The former is the case shown in modelling results of chapter 3. However, such strong structural reorganisation opposing the structural stabilisation due to cross-linking demands input of energy, which could be sufficed by chemical and microbial influences to which SOM is exposed. Drying of soils in summer may cause disruption of water bridges, as in a DSC experiment, by temperature increase. WaMB transition is observed under DSC in the temperature range of $40\text{-}80 \text{ }^\circ\text{C}$, at heating

rate of 10 Kmin^{-1} (Schaumann and Antelmann 2000; Hurrass and Schaumann 2005; Schaumann 2005; Schaumann and LeBoeuf 2005; Schaumann and Bertmer 2008). Even though this temperature range is non-realistic in environment, the possibility of disruption of WaMB cannot be denied, since a slow heating can shift the process to lower, environmentally relevant temperatures (Thomas 2001). In a recent study, Kucerik et. al (Kucerik et al. in preparation) demonstrated this by applying different heating rate in DSC. Extrapolation of the observed shift of WaMB transition temperature to quasi-isothermal condition indicated that WaMB disruption and formation can take place simultaneously, at ambient temperature.

As the sample is being heated up, more and more energy is imparted to the molecular segments, increasing their mobility with increased contribution of translational and rotational modes of motion. At certain temperature, the mobility becomes too high to hold the structure and the relatively weak cross-links disrupt. The resultant structure will be more mobile and have higher heat capacity as measured by DSC (Hurrass and Schaumann 2005). It is important to note that WaMB transition is observed only in hermetically sealed pans, and in open pans continuous transition due to evaporation of water occurs (Schaumann 2006). The most striking feature of WaMB is its slow reversibility. Once the bridges are broken and water molecules (and probably cations) are released from their positions, they will not easily find the potential CaB sites back. The increased mobility of the system would form new suprastructure in which the hotspots are redistributed. However, disruption of WaMB under environmental conditions may not be as strongly irreversible as probed under DSC. The applied high temperature ($110 \text{ }^\circ\text{C}$) in DSC investigations would facilitate diffusion of water molecules away from the WaMB or CaB sites. But the environmental temperature may not be sufficient for both breakage of H-bonds and diffusion of water molecules. Hence water molecules stay in the voids between OM molecules, with a higher possibility to re-bridge the segments. On contrary, in DSC one may also expect incomplete, but faster reformation of WaMB and indirect CaB due to the pressure agitation within the sealed pans. Up to now, no comparative study on redevelopment of WaMB within and outside the pans, to understand the role of pressure agitation, is reported.

7.2 AFM-nTA to trace thermal properties relevant to OM in low-organic soils

Thermal events observed under AFM-nTA were compared to those of bulk, DSC measurement. A second heating run at the same nanoregime was found to reveal reversibility of transitions. Prolonging the heating to higher temperature only in the second heating cycle

ensured no thermal degradation or similar alterations in the first cycle, which could further affect low temperature processes.

Formation and relevance of CaB depends on the abundance and structural quality of OM within soils. The sandy soil containing 3.4 % organic carbon exhibited change in endothermic heat flow in DSC, indicating an overlay of WaMB-transition and endotherm due to poly(methylene) crystallite melting, in sealed pans. However, this was detected in DSC with very low intensity, whereas similar thermal event was detected in peat sample (SP), having 52 % organic carbon, with six times higher intensity. The two hypothetical reasons are lower detectability of the low-abundant process in soil by DSC and lower relevance of the process in the whole soil, both due to low OM content. But by exploring nanoscale thermal properties with high spatial resolution, thermal events potentially representing disruption of WaMB and melting of poly(methylene) crystallites were identified. Abundance of such processes, calculated as percentage of all thermal characteristics throughout the analysed sample size, was much higher than noticed by DSC. Abundance of this particular type of thermal behaviour in soil was only 1.2 times lower than in peat. Thus AFM-nTA proves to be able to detect thermal properties that are expressed in low magnitude and abundant in low amount.

Table 2 summarises comparable bulk DSC and nTA observations, which helped to obtain hints on nanothermal processes behind the thermal events. Similar nanothermal events in quartz and charcoal were attributed to different processes: water evaporation from structured surface in case of quartz (related to endothermic process in DSC) and glass transition in charcoal. These attributions were given depending on the nature of samples and based on literature reports. It suggests that in the preliminary state of application, AFM-nTA alone is not able to provide clear-cut information on processes. Further, mere comparison of nanothermograms with DSC data can raise overestimations. For example, WaMB is observed only in hermetically sealed pans in DSC (Schaumann 2006). But AFM-nTA was performed under open conditions, and with much (six times) faster heating which can shift thermal events of kinetic origin to higher temperatures. One argument is that the two methods differ very much in principle; DSC follows energetic changes whereas nTA follows mechanical changes with respect to heating. Hindrance on observation of WaMB in open pans in DSC due to evaporation of water may not appear in AFM-nTA. In nanothermal analysis, water evaporation would appear as a strong compression, as seen for quartz. WaMB transition might occur as interruption to the compression phase formed by the co-occurring

evaporation. Complementarity of the two methods under various conditions should be verified for concrete attribution of nanothermal events in comparison to DSC observations. However, hints on processes were already obtained and to fully understand them, a huge set of samples with defined thermal characteristics should be considered.

Table 2. Comparison of DSC and AFM-nTA features on the soils and standards, described in chapter 6

Sample	nTA observation	DSC observation
Quartz flour	150-170 °C; overlay of at least two compression phases	180-220 °C; endotherm
Charcoal	150-170 °C; interruption on compression	150-170 °C; glass transition
Sandy soil (LW)	50-80 °C; interruption on expansion	60-80 °C; WaMB transition, polymethylene crystal melting
Peat (SP)	50-80 °C; interruption on expansion	50-90 °C; WaMB transition, polymethylene crystal melting

The very first application of AFM-nTA described in chapter 6 brings out microscale heterogeneity in soils with respect to material characteristics and microspatial distribution of various types of materials. This would make a big leap in research on natural systems, especially SOM, since heterogeneity is an intrinsic soil property and problem in many investigations (Odum 1969). Further, proved potential of AFM-nTA to reveal the relevance of WaMB in a low-organic soil promises to be advantageous in structural investigations of such soil materials. The proposal of CaB and WaMB relevant hotspots within SOM suggests that formation and disruption of these cross-links are microscale processes, with their distribution determined by the spatial distribution of hotspots and heterogeneity of SOM. Thus AFM-nTA could be used for CaB and WaMB studies, after further methodical developments. Practical difficulties exist in relocating nano regions, once the sample was removed from the AFM stage. This makes a second analysis of nanoregions (for example, to visualise reformation of WaMB after several weeks) difficult.

However, extrapolation of the data acquired on a number of microregions to the whole soils cannot be blindly accepted, owing to the inherent soil heterogeneity. Representativeness is a

general problem in all AFM analysis, relevance of which become higher when considering that even the model quartz material showed significant nano- and micro scale heterogeneity.

7.3 The ‘cation experimental strategy’

The cation experimental strategy adopted in this thesis addresses the problem in experimental design.

- By inducing cation-SOM interaction at two different values of pH, it was made possible to evaluate pH effects separately.
- Importance of cation addition pH and final sample pH were discriminated.
- The selected cations represented mono-, bi- and trivalent cations of varying cationic charge density and size.
- The parameters used to evaluate changes caused by the experimental procedure included both physicochemical (proton mobility with ^1H relaxation time and ^1H wideline spectra, matrix rigidity as T^*) and chemical (CEC, DOC) SOM characteristics that reflect binding state of cations.

This set of experimental and methodical parameters represents the first set of characteristics that provide hints on existence and degree of cross-linking. This is reinforced by the study shown in chapter 4, which implemented the same experimental strategy on a different OM, partly, by which bivalent cations were able to induce cross-linking in that OM.

7.4 Implications of structural reorganisation in OM during cation treatment

Cation-peat interaction at controlled pH, described in chapter 3, did not reveal cross-linking, contradicting the expectations based on recent results (Lu and Pignatello 2004; Aquino et al. 2011; Schaumann and Thiele-Bruhn 2011; Schaumann et al. 2013; Schaumann et al. submitted 2013). However, this apparently negative result gives strong implications of structural requirement for CaB. Additionally, it is seen that the main structural requirement, that the deprotonated functional groups should be in sufficient proximity to each other, was met in case of SOM described in chapter 4.

The soil sample possessed slightly higher CEC_{eff} than the peat OM, still much lower than generally observed values for SOM samples. Exchangeable capacity is a measure of the number of functional sites, which is crucial for interaction with cations. Thus from the comparable exchange capacity, one would expect that both the samples respond to cation removal and cation addition similarly, with similar mode of interactions within their matrixes.

Contrarily, the slight difference in exchange capacity was pronouncedly reflected in their response to cation treatment, as the two samples show big differences in results. The peat was not significantly cross-linked by bi- or trivalent cations, immediately after treatment and underwent significant structural changes during aging. On contrary, the soil sample underwent significant cross-linking directly by cation treatment and was still vulnerable to further restructuring during aging time.

Apart from satisfying the physicochemical structural needs for CaB, the soil sample might also have higher mobility of organic molecular segments. This may help to overcome the structural barrier, to be cross-linked, easily during cation treatment. Also the peat OM exhibited strong restructuring during aging, indicating that the material also possessed restructuring potentials but significant only under certain conditions. The magnitude of such inherent potential to undergo structural reorientation is determined by physicochemical organisation of molecules (secondary structure) and the chemical composition (primary structure) of the material (Piccolo 2002). Therefore, a complete chemical characterisation of the two OM systems would help understanding the differences better.

Nevertheless, the main consequences of structural reorganisation in the frame of currently discussed cation experiment are,

- I. Protonation of functional groups via resin-treatment induced irreversible changes, partly, with respect to further exchangeability of protons.
- II. Selective occupancy of cations occurs, depending on their valency and size in hydrated state.
- III. Aging induces structural changes, with more pronounced effect on cation-treated sample than for the untreated sample in case of the peat OM and vice versa for the SOM sample. The effect is strongest for Na^+ than for Al^{3+} and for Mg^{2+} than for Ba^{2+} .

I. Resin-induced irreversibility. The reduced exchange capacity (stronger effect in peat than in the soil sample) of protons against cations after resin-treatment is indicative for physicochemical structural changes brought about by resin-treatment. This lead to a more rigid network where some of the exchange sites become un-/less accessible for the cations added later. A tendentially higher (even if in small magnitudes) WaMB transition temperature (T^*) and a significantly lower Lorentzian line fraction in ^1H wideline spectrum (see figure 1 of chapter 3) of resin-treated peat than the untreated one is in accordance with this explanation. But this is not the case with the SOM sample, as T^* was significantly lower

after resin-treatment than the untreated sample (chapter 4). As it contained cross-links already in the untreated state, the lowering of matrix rigidity might have been caused due to disruption of CaB and/or WaMB by pH reduction. Still it shows structural changes that inhibit binding of cations to certain extent. Conte and Piccolo (1999) previously observed structural rearrangement in dissolved HA samples induced by acid addition and attributed to higher degree of H-bond formation owing to pH reduction. Even though that study differ much in conception, type (HA vs whole peat OM) and physical state (dissolved vs solid state OM) of samples, the result points to the same direction that reduction in pH of OM cause structural reorientation.

Physicochemical structure could also be altered by resin-treatment procedure which involved thorough mixing of sample with water and resin for 24h. Mechanical agitation could be the driving force to have higher dynamicity of OM structure and thus to create a state in which most of the protonated functional groups become less accessible due to physical impedance. The more rigid OM matrix after cation removal (as for the peat OM, chapter 3), would represent energetically more stable state. Input of energy is necessary to undergo structural reformation to get back to the initial state in which protons are exchangeable. If this is true, it would imply that the mechanically induced structural modification (by shaking) in the following step was not sufficient for such thermodynamically less favoured reformation, as reflected by low uptake of cations, thereafter. Based on the observed structural irreversibility, it can be recommended to avoid physical modification of soil samples (for example, by milling) as a pre-treatment directly after sampling, as it would create a different physicochemical structure. Temperature (of drying) can also have similar effect, as discussed in a preceding section.

Swelling effects caused by mixing with water during treatment procedure is expected to open nanopores within the OM structure (Jaeger et al. 2005) and hence facilitate cation exchange. This is in contrary to the current observation, as cation uptake after treatment, during which the sample was in contact with water at least for 2 days, did not even reach the initial cation content of the peat. Further, for the soil sample described in chapter 4, it was seen that neither CEC_{eff} nor T^* was affected in water-treated sample. However, it can be suggested that all these effects -structural changes due to pH reduction, due to mechanical agitation and due to swelling- operate simultaneously, affecting cation exchange, and the effects of first two predominate over the other.

The kinetic restriction to cation binding to the peat OM for cation addition at pH 1.9, even if the pH was later raised to 4.1, (see section 3.2, chapter 3) indicates that the potential structural state is achieved only slowly, since additional driving force was absent and the allowed 2h was probably not enough. On contrary, for cation addition at pH 4.1, the OM had enough time to reach this potential binding state, since 24h was allowed in between pH adjustment and cation addition. The structural reorganization may have also continued during 24h time span after cation addition. Please refer figure 1 for a scheme showing structural reorganisation in the peat sample described by results of chapter 3, during the course of the adopted cations treatment strategy.

II. Selective occupancy of cations. The cation selectivity is seen to be controlled by cation valency and size. The OM structural organisation was found to be decisive also for the type of cations, apart from the mode of binding, as indicated by the noted inverse relation of uptake on cation valency in peat and by molecular modelling. The selective occupancy of cations of same valency within the SOM sample, seen in chapter 4, was explained based on cationic sizes. The relatively large voids, constituting the physicochemical organisation of SOM, could be occupied only by larger cations.

III. Aging-induced structural changes. In an ideal case of SOM sample, potential CaB sites might not be formed very easily in the beginning. Thus it requires considerable structural reorganisation to form indirect CaB, in a time scale of more than several weeks to months. The soil sample described in chapter 4 showed considerable restructuring during 4 weeks and it continued till 8 weeks, at least. In order to be able to reach the maximum rigidity state, the sample has to be stored longer and measured again in intervals of several weeks. Such a strategy is planned and T^* measurements of the soil samples will be continued at least up to six months. The aging-induced strengthening and reformations of CaB is in line with a previous study by Engebreston and von Wandruszka (1998), which demonstrated that binding of Mg^{2+} to aqueous humic acid involves a fast, initial binding step followed by a slow rearrangement phase in which bridging reactions lead to form inner sphere complexes of Mg^{2+} .

Mechanical agitation caused during the treatment procedure could facilitate structural changes within the samples. Even if not reflected in the SOM properties directly after treatment, such influences could have acted as a driving force to enhance the structural changes during aging, with long-lasting effect.

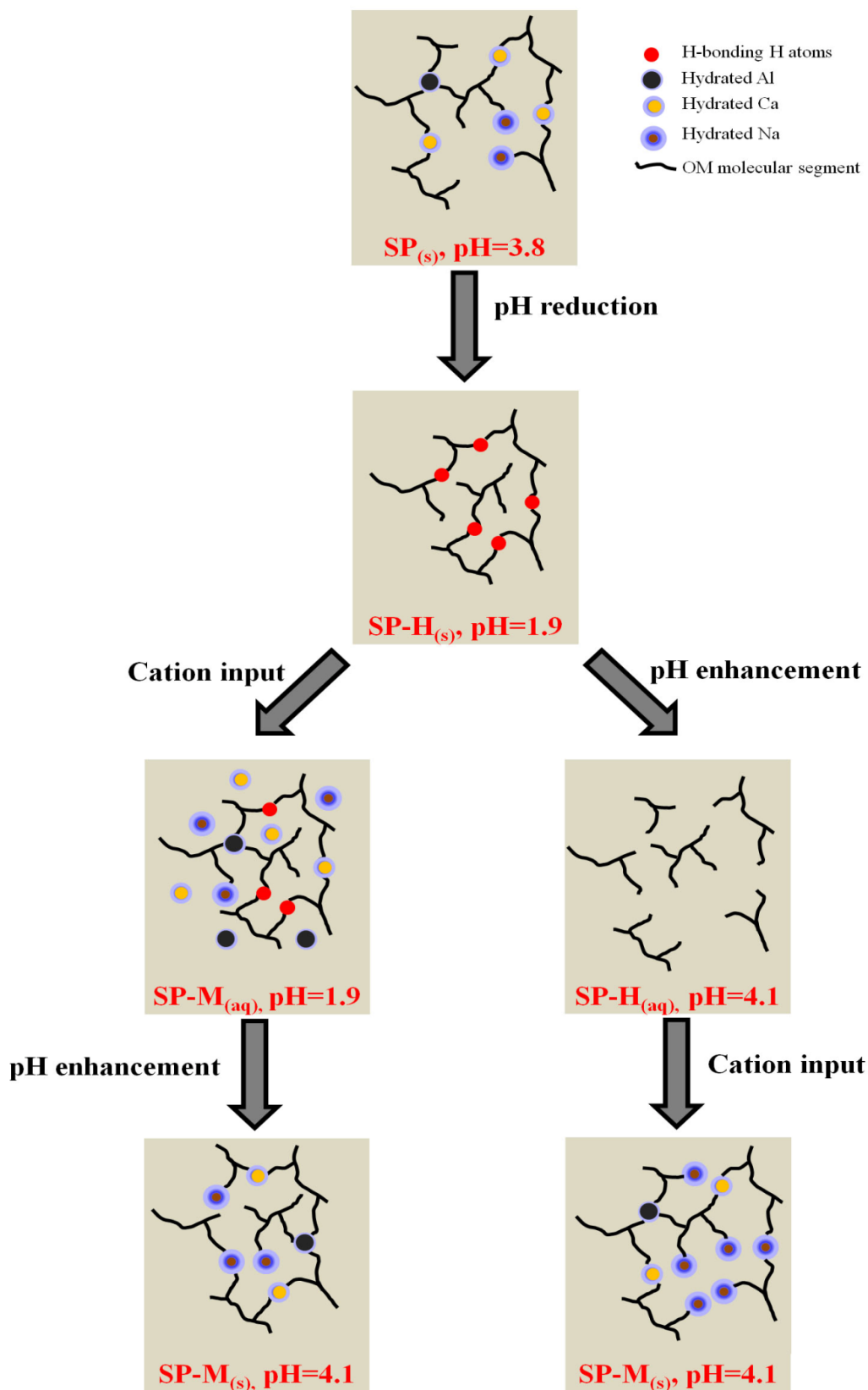


Figure 1. Model structures describing the supramolecular structure of the peat OM at different stages of interaction (chapter 3). Suffixes show the physical state to which the models refer.

As seen in chapter 3, addition of cations in the peat have created OM matrix which is more vulnerable to further structural reorientation than the untreated one, during aging in six months (change in T^* , $\Delta T^* = 5-10\text{ }^\circ\text{C}$ and $4.0\text{ }^\circ\text{C}$, respectively). Similar effect was shown in chapter 4, for the soil sample. ΔT^* by aging for 8 weeks for Soil-Mg samples varied between $4.7-8.7\text{ }^\circ\text{C}$ while that for untreated soil was $3.9\text{ }^\circ\text{C}$. This further suggests a low prominence of cross-linking, in the peat and in Soil-Mg samples, to affect structural rigidity directly after treatment significantly. However, after aging, these cation treated OM attain a more stable structure than the untreated one. On the other hand, Soil-Ca and Soil-Ba samples, which expressed significant cross-linking directly after treatment, showed lower ΔT^* values ($0.8-2.8\text{ }^\circ\text{C}$) than the untreated soil, indicating that already existing cross-links make them less vulnerable to structural changes in aging period. This evidently shows that CaB increases matrix rigidity of SOM, in general. Further, it could be attributed that the higher degree of structural reorganisation lead to more stable matrix, which can be disrupted only at higher temperature. This indicates that structural reorganisation occurs in the thermodynamically more stable direction and SOM system at certain condition can be considered as intermediate structure in a thermodynamic transformation pathway.

Another important outcome of this study is that the chemical structural quality of SOM depends on the type of mineral material on which the mineral-microbial interaction was established. Nevertheless, SOM was found to develop similar physicochemical network in organo-mineral associations, irrespective of its chemical characteristics and the nature of minerals, within a time frame of several months. Interaction with mineral surfaces may reduce the mobility of SOM, due to structural restriction at one end of segments. This may then suggest that SOM, adhered on minerals, as in case of soils, undergo less intensive

Summarising, this thesis contribute to the scientific understanding of SOM cross-links via CaB; mainly its structural requirements and effects of hydration water. The results of aging experiments points to the importance of time in defining soil characteristics, owing to the high structural mobility of SOM. Temperature and other environmental influences may enhance restructuring. This reinforces the demand of considering SOM as a physicochemical structural unit, beyond its chemical composition. Aging effects is thus one of the most important consequences of supramolecular consideration. This further gives hints to the idea of occurrence of process-relevant hotspots and hot moment (Hagedorn and Bellamy 2011).

AFM-nTA further adds to the physicochemical understanding of SOM by its potential to reveal heterogeneity and microspatial distribution of nano- and micro domains. In this way, it could visualise SOM as an assembly of several types of materials, organised in a special way at given locality, at given time.

7.5 Ongoing research and open questions

Repeated drying and wetting of cross-linked OM matrix. Selected cation treated samples described in chapter 4 are currently being analysed for the development in the nature of CaB, as the system is stressed by drying and rewetting. It is hypothesised that drying will remove water molecules in the hydration shell, step-by-step. The consecutive wetting would help intake of water molecules back, within the hydrations shell. But a following drying cycle will again displace water molecules. After several of such cycles, cations may form stronger bond with the binding partner and at one stage, it is supposed that complete removal of hydration water cause inner sphere complexation. Thus CaB become stronger and further addition of water molecules will not affect the direct CaB interactions. Additionally, TGA-DSC-MS are also conducted to get more insight into the OM structural properties.

Micro and macroscale thermoanalytical methods to assess physicochemical structure and stability of OM. It has been already seen that intrinsic mobility of OM molecular segments plays key role in biogeochemical functions (e.g. CaB- and WaMB-related processes). Mobility is determined by primary and secondary structure of the material, as seen in chapter 1. In order to attain deeper insight into the physicochemical structure and quality of OM, various thermoanalytical methods are used, including TGA-DSC-MS, low-temperature DSC and AFM-nTA. TGA-DSC-MS gives the thermal stability of OM fractions within samples and information of chemical composition of burned material at certain temperature. Low-temperature DSC, as shows in chapters 3, 6 and 7 gives more reliable information on energetical changes within samples. AFM-nTA, as shown in chapters 6 and 7, is a promising tool in analysis of soil samples from various aspects. Further, by combining all these methods, more concrete interpretation of nanoscale thermograms could be made possible. Various natural soils differing mainly in organic matter content are used.

Open questions. Studies on CaB, described in this thesis considered only low pH range at which only carboxylic groups are deprotonated. But phenolic functional groups, which dissociate at higher pH, above 8, are also able to undergo various types of interactions with multivalent cations. Thus the current experiment can be modified so that interactions at

higher pH were also targeted. This would further allow to experimentally distinguish the interaction of cations with π electron systems of aromatic ring structures (e.g. in ferrocene), from CaB.

Nanothermal analysis and force mapping techniques are able to enhance research on soil systems by adding to the attempts to understand structural heterogeneity of the system. Further, hints of WaMB were produced, when compared with bulk DSC measurements. However, a direct assessment of these condition- (e.g. moisture content) dependant processes needs further containment in the experimental set up. Currently, practical difficulties exist in controlling the moisture condition of the sample. A change in moisture cannot be avoided, as the measurements are done in aerated hood. One possible solution could be to create dry atmosphere in the AFM hood, by filling up of inert gases. Moreover, to be able to understand the real process behind each thermomechanical event noted by AFM-nTA, the current data set needs to be expanded by collecting thermograms of defined thermal processes in well-defined materials.

Furthermore, inclusion of additional PFQNM parameters such as Young's modulus will be more informative about nanomechanical properties. However, the currently available nanothermal probes do not allow this, due to incompatibility of tip and soil samples, with respect to their hardness. A technical improvement in this direction could add further to the combination of nanomechanical, morphological and thermal analysis. Further additions with Nano-SIMS (nanoscale secondary ion mass spectroscopy) and chemical force microscopy (CFM) could be designed. The former would give information on elemental composition and binding state with spatial resolution of sub-100 nm whereas the latter one would give more insight into chemical composition, based on chemical interaction forces. However, a big step in the technical field has to be covered in order to be able to relocate the same nanoregion which was previously investigated by nano-SIMS or CFM, for thermal analysis. Currently relocation of ROI, selected using SEM, under AFM is done by navigating along the surface, based on edges and shapes of relatively larger structures of the soil samples. This method is not accurate, when considering in nano scale, due to the limitation of human eye and CCD camera of the AFM navigator. Therefore, it is demanding to have a computer-controlled method.

References

- Aquino, A. J. A., D. Tunega, G. E. Schaumann, G. Haberhauer, M. H. Gerzabek and H. Lischka (2011). The functionality of cation bridges for binding polar groups in soil aggregates. *International Journal of Quantum Chemistry* 111: 1531-1542.
- Atkins, P. and J. De Paula (2006). *Physical Chemistry*, Oxford University Press.
- Bloom, P. R. and U. Skyllberg (2011). Soil pH and pH buffering. *Handbook of Soil Sciences: Properties and Processes*. P. M. Huang, Y. Li and M. E. Sumner. New York, CRC Press, Taylor and Francis group. 2: 19 (1)- 19(14).
- Conte, P. and A. Piccolo (1999). Conformational Arrangement of Dissolved Humic Substances. Influence of Solution Composition on Association of Humic Molecules. *Environmental Science and Technology* 33(10): 1682-1690.
- Engbreton, R. R. and R. van Wandruszka (1998). Kinetic Aspects of Cation-Enhanced Aggregation in Aqueous Humic Acids. *Environmental Science and Technology* 32(4): 488-493.
- Hagedorn, F. and P. Bellamy (2011). Hot Spots and Hot Moments for Greenhouse Gas Emissions from Soils. *Soil Carbon in Sensitive European Ecosystems*, John Wiley & Sons, Ltd: 13-32.
- Hurrass, J. and G. E. Schaumann (2005). Is glassiness a common characteristic of soil organic matter? *Environmental Science and Technology* 39(24): 9534-9540.
- Jaeger, F., E. Grohmann and G. E. Schaumann (2005). Do swelling and microbial activity affect pore size distribution in humous soil samples? *Geophysical Research Abstracts* 7(SSS9: Quantification of soil structure and soil porosity changes caused by natural and anthropogenic affects): EGU05-A-02313; SSS9-1MO3P-0262.
- Kucerik, J., J. Schwarz, A. Jaeger, M. Bertmer and G. Schaumann (in preparation). Character of transitions causing physicochemical aging of a sapric histosol.
- Lu, Y. and J. J. Pignatello (2004). Sorption of apolar aromatic compounds to soil humic acid particles affected by aluminum(III) ion cross-linking. *Journal of Environmental Quality* 33(4): 1314-1321.
- Odum, E. P. (1969). *The Strategy of Ecosystem Development*. 164: 262-270.
- Piccolo, A. (2002). The supramolecular structure of humic substances: A novel understanding of humus chemistry and implications in soil science. *Advances in Agronomy* 75: 57-134.
- Schaumann, G. E. (2005). Matrix relaxation and change of water state during hydration of peat. *Colloids and Surfaces A: Physicochemical and Engineering Aspects* 265(1-3): 163-170.
- Schaumann, G. E. (2006). Soil organic matter beyond molecular structure. 2. Amorphous nature and physical aging. *Journal of Plant Nutrition and Soil Science* 169(2): 157-167.
- Schaumann, G. E. and O. Antelmann (2000). Thermal characteristics of soil organic matter measured by DSC: A hint on a glass transition. *Journal of Plant Nutrition and Soil Science* 163(2): 179-181.
- Schaumann, G. E. and M. Bertmer (2008). Do water molecules bridge soil organic matter molecule segments? *European Journal of Soil Science* 59(3): 423-429.
- Schaumann, G. E., D. Diehl, M. Bertmer, A. Jaeger, P. Conte, G. Alonzo and J. Bachmann (2013). Combined Proton NMR wideline and NMR Relaxometry to study SOM-water interactions of cation-treated soils. *Journal of Hydrology and Hydromechanics* 61(1): 50-63.
- Schaumann, G. E., D. Gildemeister, D. Diehl, Y. Kunhi Mouvenchery and S. Spielvogel (submitted 2013). Cation specific formation and aging of cross-links in soil organic matter (SOM). *Journal of Soils and Sediments*.

- Schaumann, G. E. and E. J. LeBoeuf (2005). Glass transitions in peat - their relevance and the impact of water. *Environmental Science and Technology* 39(3): 800-806.
- Schaumann, G. E. and S. Thiele-Bruhn (2011). Molecular modelling of soil organic matter: Squaring the circle? *Geoderma* 169: 55-68.
- Thomas, L. C. (2001). Use of multiple heating rate DSC and modulated temperature DSC to detect and analyze temperature-time-independent transitions in materials. *American Laboratory* 33(1): 26

Annex I

Supporting information to chapter 3

Restructuring of a peat in interaction with multivalent cations: Effect of cation
type and aging time

Kunhi Mouvenchery, Y., Jäger, A., Aquino, A.J.A., Tunega, D, Diehl, D.,

Bertmer, M., Schaumann, G.E. (2013) PLoS ONE 8(6): e65359.

[doi:10.1371/journal.pone.0065359](https://doi.org/10.1371/journal.pone.0065359)

Sample	Amount of sorbed cation, M / mmol _c kg ⁻¹	CEC _{eff} / mmol _c kg ⁻¹	DOC / mgkg ⁻¹	Contact angle / °	Step transition temperature, T* / °C	¹ H NMR relaxation characteristics		¹ H NMR wideline characteristics	
						T _{2,fast} / ms	Contribution of fast-relaxing water to the total T ₂ / %	Intensity of Lorentzian line, related to the total signal / %	Change in intensity of Lorentzian line after heating / %
SP		123 ± 12	2.3 ± 0.1	109 ± 3	56.0 ± 0.3	319 ± 16	12 ± 6	48.0 ± 0.2	2.1 ± 0.2
SP-H		256 ± 3	1.58 ± 0	127 ± 1	57.5 ± 0.5	150 ± 17	26 ± 3	44.5 ± 0.2	2.4 ± 0.2
SP-Al@1.9	2.5 ± 3.7	197.2 ± 3.4	1.1 ± 0	128 ± 5	55.3 ± 0.2	141 ± 17	24 ± 1	48.2 ± 0.2	2.0 ± 0.2
	2.8 ± 1.7	164.4 ± 2.1	1.6 ± 0	131 ± 2	55.9 ± 0.2	155 ± 8	26 ± 1	48.3 ± 0.2	1.7 ± 0.2
	2.8 ± 2.6	181.6 ± 2.2	1.1 ± 0	130 ± 5	55.6 ± 0.2	144 ± 1	26 ± 1	46.2 ± 0.2	2.4 ± 0.2
	3.3 ± 0.5	209.3 ± 1.7	1.1 ± 0.1	124 ± 2	55.2 ± 0.1	157 ± 2	23 ± 0	48.0 ± 0.2	2.6 ± 0.2
	5.4 ± 0.6	250.2 ± 3.1	1.34 ± 0	136 ± 1	57.1 ± 0.3	148 ± 1	23 ± 0	45.7 ± 0.2	3.2 ± 0.2
SP-Ca@1.9	5.9 ± 0.2	194.4 ± 1.0	1.5 ± 0	126 ± 1	55.2 ± 0.1	146 ± 7	25 ± 0	47.2 ± 0.2	2.1 ± 0.2
	6.6 ± 0.1	184.4 ± 3.1	2.1 ± 0.1	125 ± 2	55.4 ± 0.1	153 ± 0	23 ± 0	48.1 ± 0.2	2.3 ± 0.2
	6.6 ± 0.1	190.7 ± 8.9	1.5 ± 0	132 ± 2	55.9 ± 0.4	151 ± 2	24 ± 0	47.9 ± 0.2	2.2 ± 0.2
	6.2 ± 0.1	203.9 ± 1.6	1.6 ± 0.1	127 ± 2	55.6 ± 0.2	150 ± 2	22 ± 0	48.1 ± 0.2	2.2 ± 0.2
SP-Na@1.9	5.7 ± 0.4	221.9 ± 2.6	1.6 ± 0	125 ± 3	56.6 ± 0.3	155 ± 1	21 ± 1	45.8 ± 0.2	2.1 ± 0.2
	20.7 ± 3.4	167.6 ± 6.4	1.4 ± 0.1	121 ± 1	55.6 ± 0.2	158 ± 1	23 ± 0	49.3 ± 0.2	1.9 ± 0.2
	16.8 ± 2.4	139.8 ± 12	1.0 ± 0	120 ± 2	55.4 ± 0.2	165 ± 1	23 ± 1	46.7 ± 0.2	2.1 ± 0.2
	18.0 ± 0.9	163.0 ± 3.9	1.6 ± 0	131 ± 1	56.2 ± 0.1	156 ± 2	22 ± 1	48.4 ± 0.2	1.9 ± 0.2
	16.5 ± 1.3	196.6 ± 4.7	1.6 ± 0	129 ± 1	56.6 ± 0.5	169 ± 2	22 ± 0	47.4 ± 0.2	1.6 ± 0.2
	19.2 ± 0.8	216.9 ± 9.5	1.5 ± 0.1	128 ± 0	56.4 ± 0.2	150 ± 1	22 ± 1	46.1 ± 0.2	2.0 ± 0.2

Table S1. All the investigated parameters for untreated (SP), resin-treated (SP-H) and cation treated samples with different cations and cation concentration where cation treatment was carried out at pH 1.9.

Sample	Amount of sorbed cation, M / mmol _c kg ⁻¹	CEC _{eff} / mmol _c kg ⁻¹	DOC / mgkg ⁻¹	Contact angle / °	Step transition temperature, T* / °C	¹ H NMR relaxation characteristics		¹ H NMR wideline characteristics	
						T _{2,fast} / ms	Contribution of fast-relaxing water to the total T ₂ / %	Intensity of Lorentzian line, related to the total signal / %	Change in intensity of Lorentzian line after heating / %
SP-Al@4.1	4.4 ± 0.4	214.4 ± 7.6	1.6 ± 0	139 ± 1	57.1 ± 0.1	73 ± 1	36 ± 0	46.8 ± 0.2	2.2 ± 0.2
	7.0 ± 0.2	57.4 ± 7.9	1.7 ± 0	130 ± 1	55.8 ± 0.1	72 ± 1	31 ± 2	43.7 ± 0.2	2.3 ± 0.2
	11.8 ± 0.3	113.9 ± 5.3	1.4 ± 0	134 ± 1	55.8 ± 0.2	75 ± 2	40 ± 2	43.7 ± 0.2	2.3 ± 0.2
	14.5 ± 0.1	62.9 ± 3.4	1.4 ± 0.1	135 ± 1	55.8 ± 0.1	79 ± 0	42 ± 0	45.4 ± 0.2	2.2 ± 0.2
	13.8 ± 1	216.8 ± 1.7	1.5 ± 0	127 ± 1	56.4 ± 0.3	82 ± 3	31 ± 4	45.6 ± 0.2	2.3 ± 0.2
SP-Ca@4.1	9.4 ± 4.7	243.5 ± 8.8	1.5 ± 0	133 ± 2	56.7 ± 0.1	61 ± 1	32 ± 6	43.3 ± 0.2	2.1 ± 0.2
	13.1 ± 1.3	181.0 ± 1.3	1.5 ± 0	132 ± 1	56.2 ± 0.1	58 ± 1	35 ± 2	43.8 ± 0.2	2.1 ± 0.2
	21.2 ± 2.6	198.3 ± 8.8	1.6 ± 0	122 ± 1	55.4 ± 0.1	62 ± 1	29 ± 1	47.6 ± 0.2	2.1 ± 0.2
	27.2 ± 2.5	184.8 ± 8.2	1.6 ± 0	125 ± 2	56.6 ± 0.2	71 ± 2	31 ± 3	43.6 ± 0.2	2.2 ± 0.2
	27.6 ± 8.2	201.8 ± 5.7	1.7 ± 0	128 ± 1	55.9 ± 0.1	67 ± 2	28 ± 3	42.9 ± 0.2	2. ± 0.2
SP-Na@4.1	25.7 ± 5.1	196.1 ± 1.2	1.7 ± 0	120 ± 2	55.5 ± 0.1	73 ± 1	32 ± 2	45.8 ± 0.2	2.4 ± 0.2
	30.5 ± 1.3	189.9 ± 2.8	1.7 ± 0	127 ± 1	54.3 ± 0.2	60 ± 1	37 ± 6	47.5 ± 0.2	1.0 ± 0.2
	37.7 ± 0.9	196.8 ± 2.7	1.6 ± 0	135 ± 1	56.5 ± 0.2	70 ± 1	29 ± 2	44.6 ± 0.2	2.2 ± 0.2
	37.7 ± 1.0	201.3 ± 3.8	1.7 ± 0	123 ± 1	56.8 ± 0.1	71 ± 4	34 ± 4	42.8 ± 0.2	1.9 ± 0.2
	38.5 ± 0.8	191.1 ± 4.3	1.7 ± 0	134 ± 1	55.8 ± 0.2	60 ± 1	30 ± 7	44.2 ± 0.2	2.1 ± 0.2

Table S2. All the investigated parameters for cation treated samples with different cations and cation concentration where cation treatment was carried out at pH 4.1.

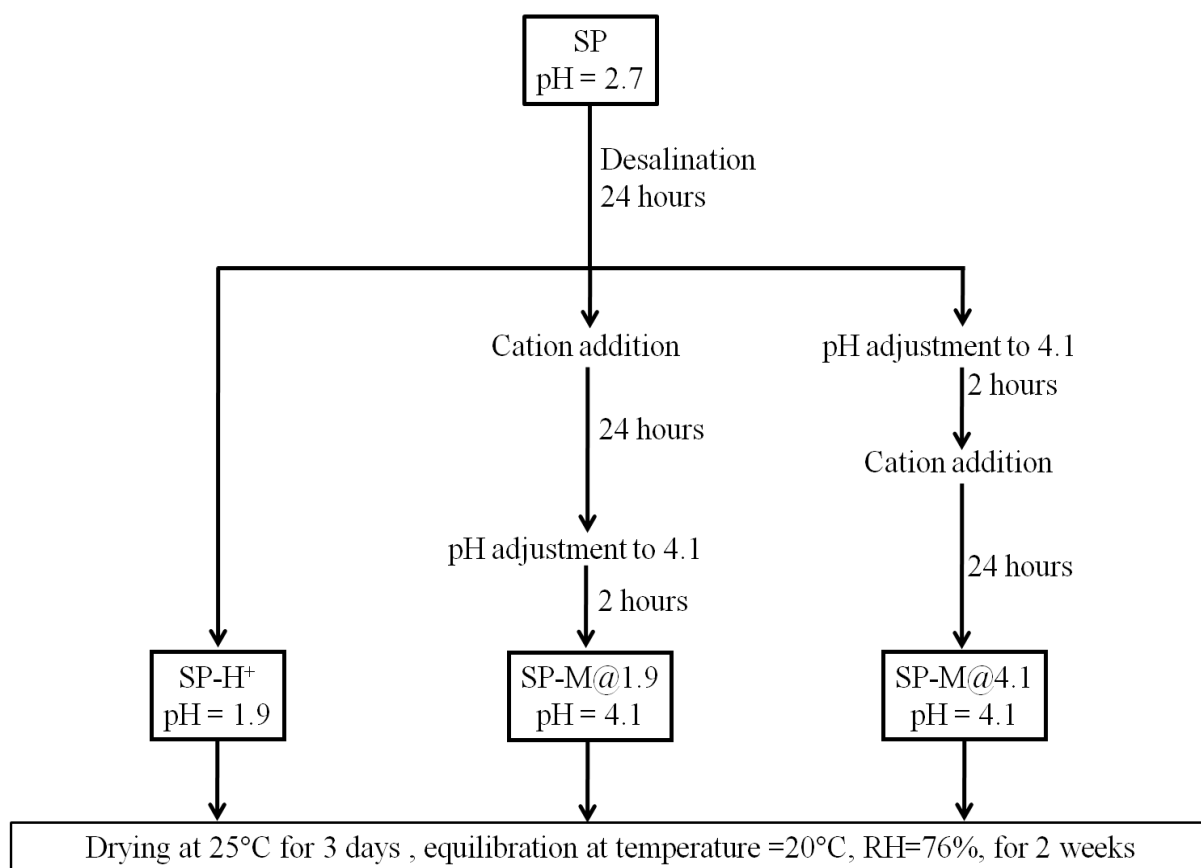


Figure S1. Schematic diagram describing the experimental procedure adopted for treatment of peat with exchange resin and with different cations.

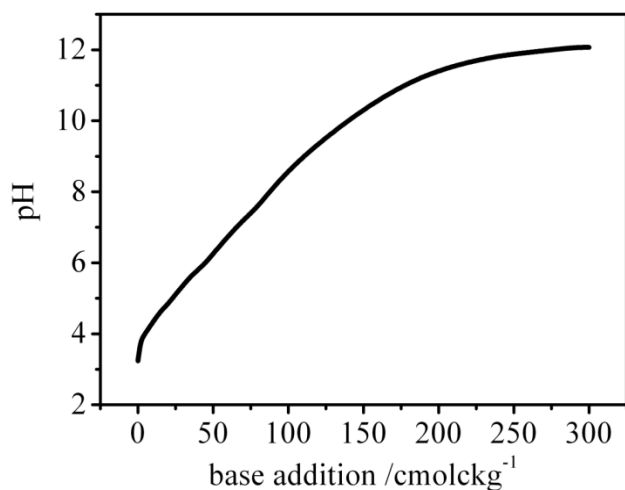


Figure S2. Titration curve of the original peat. Aqueous suspension of peat was titrated against 0.1 M NaOH with time interval of 90 minutes between each titration step. This interval was selected to record stable pH.

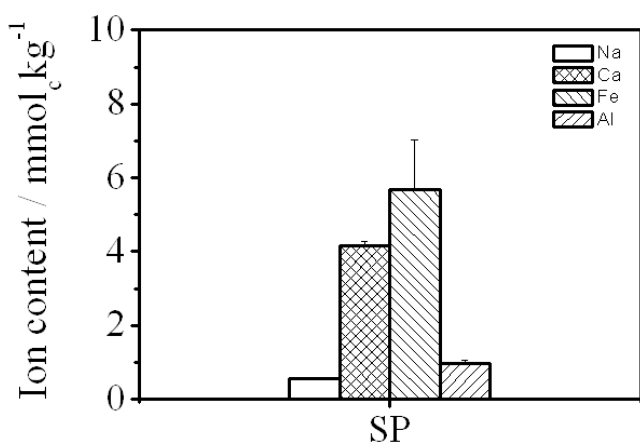


Figure S3. Cation composition of colloidal particles deposited after ultracentrifugation of aqueous extract of untreated peat.

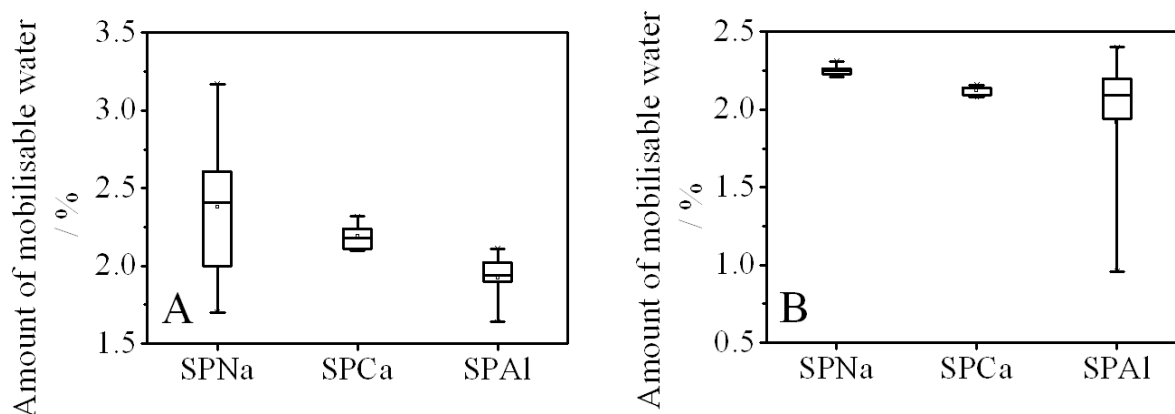


Figure S4. Amount of mobilisable water in treated peat with respect to the type of loaded cations, after cation treatment at pH 1.9 A) and at 4.1 B) before aging.

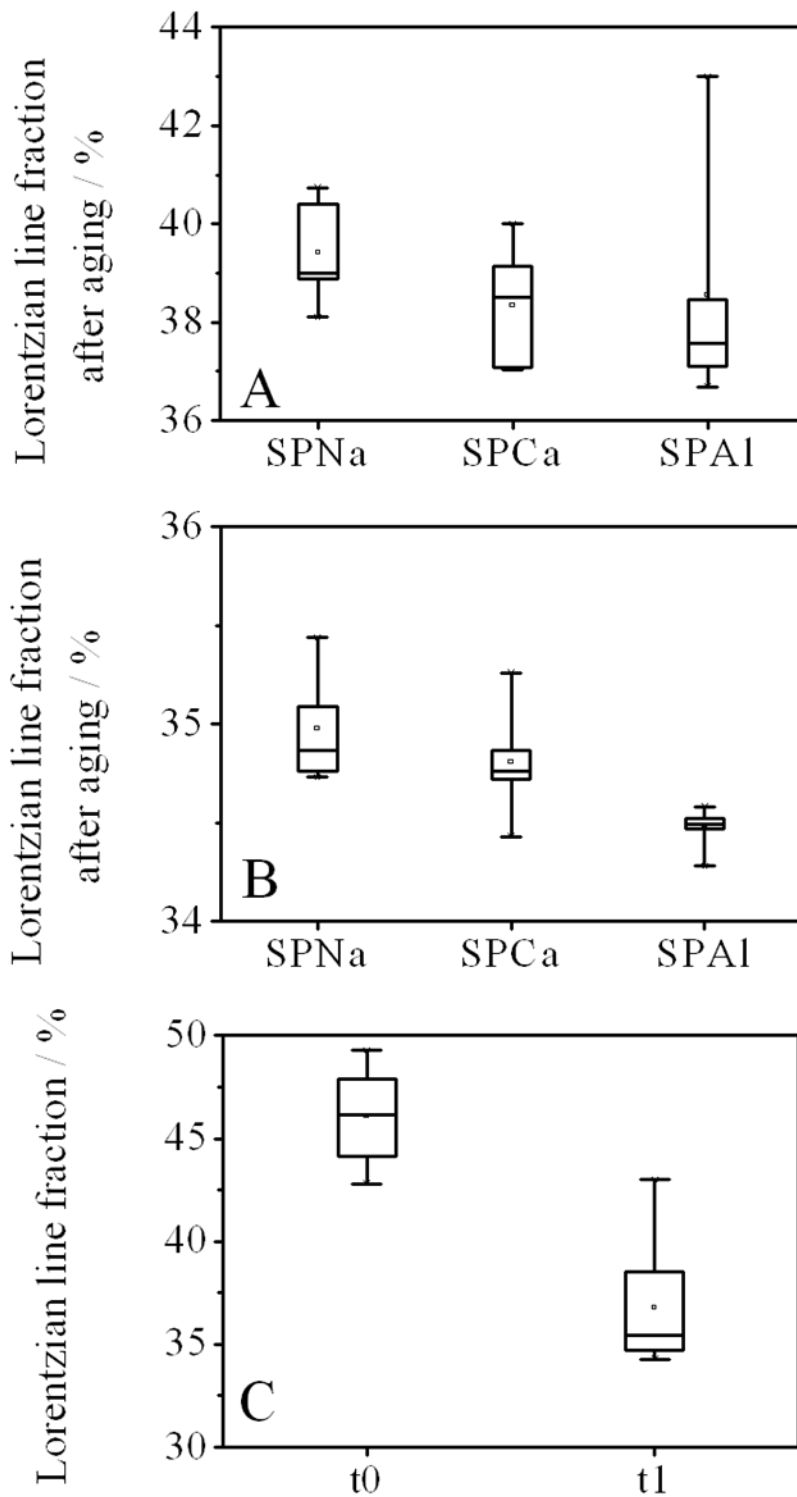


Figure S5. Lorentzian line fraction of ^1H wideline (amount of mobile water) after aging, shown with respect to cation types for SP-M@1.9 (A) and for SP-M@4.1(B). Lorentzian line fraction for all the treated samples before (t_0) and after (t_1) aging are shown in (C).

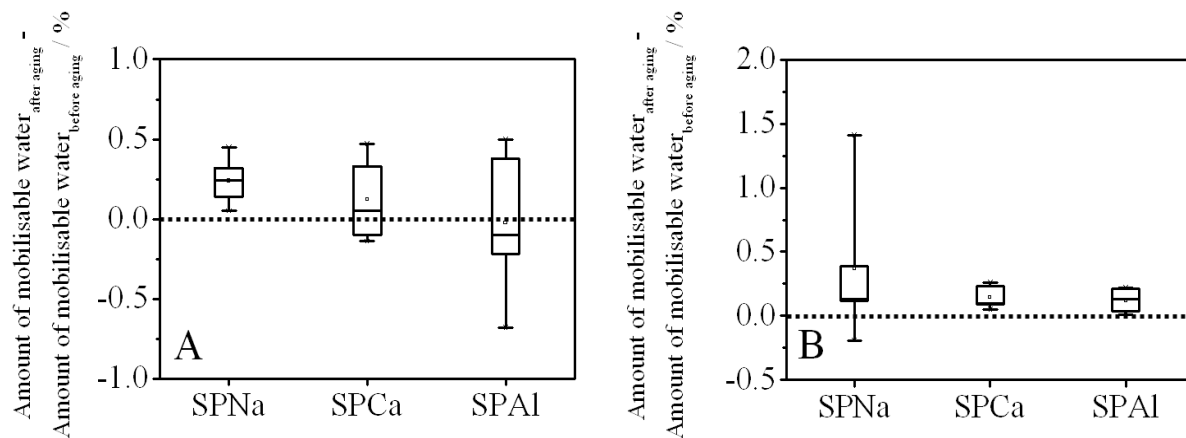


Figure S6. Change in amount of mobilisable water after aging for cation addition at pH 1.9 (A) and at 4.1 (B), with respect to the loaded cation type. Dashed line along zero distinguishes the increase and decrease in amount of mobile water after aging.

Annex II

Supporting information to chapter 7

Linking Atomic Force Microscopy with nanothermal analysis to assess
microspatial distribution of materials in young soils

Kunhi Mouvenchery, Y., Miltner, A., Schurig, C., Kästner, M,
Schaumann, G.E. (submitted, 2013) *Geochimica et Cosmochimica Acta*

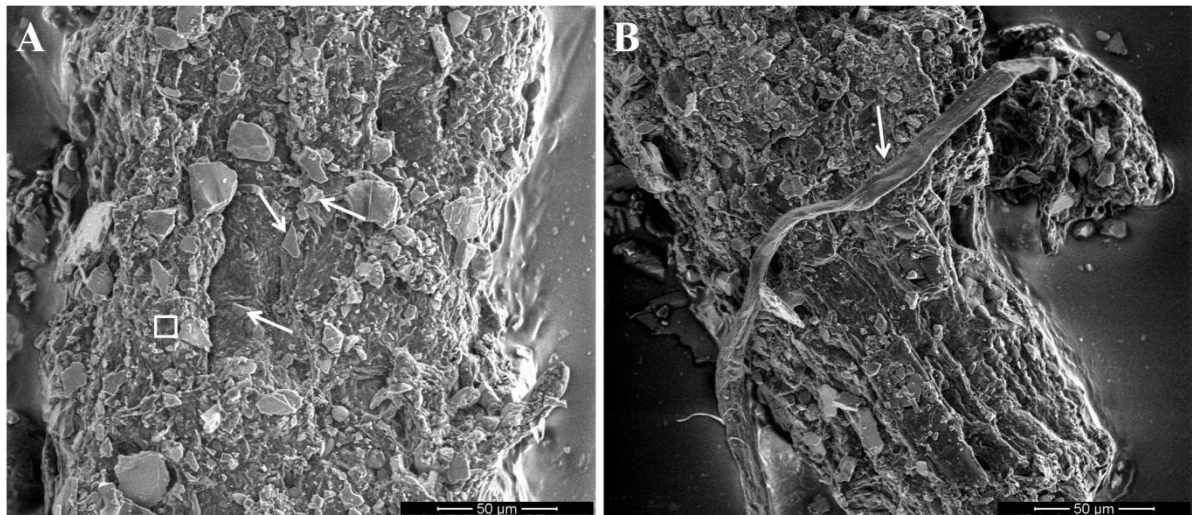


Figure S1. ESEM images of test- plant material showing A) mineral particles (indicated by arrows) and investigated ROI (indicated by square) and B) fungal hypha, indicated by arrow.

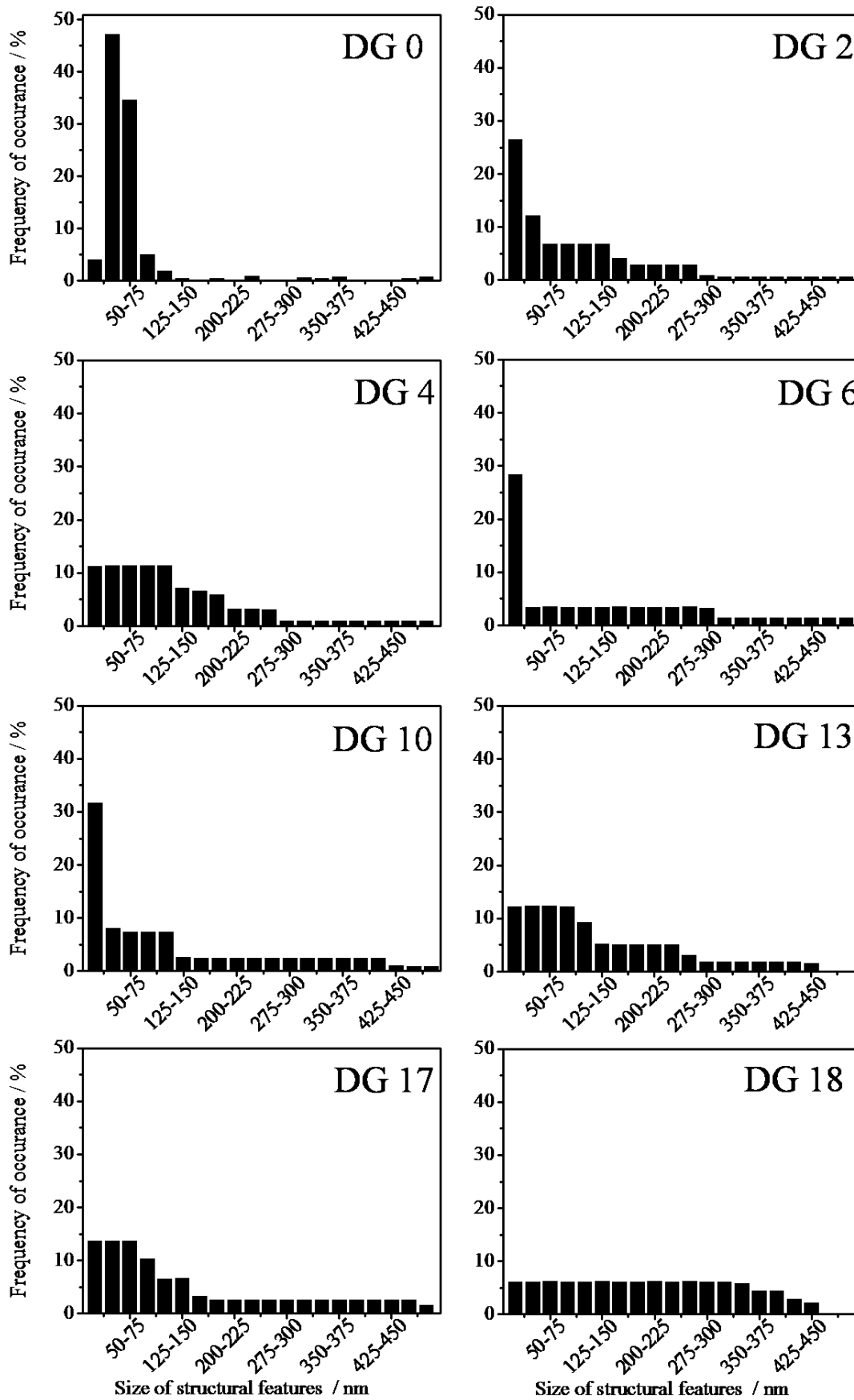


Figure S2. Size distribution of structural features for each soil, averaged over four images of each soil sample

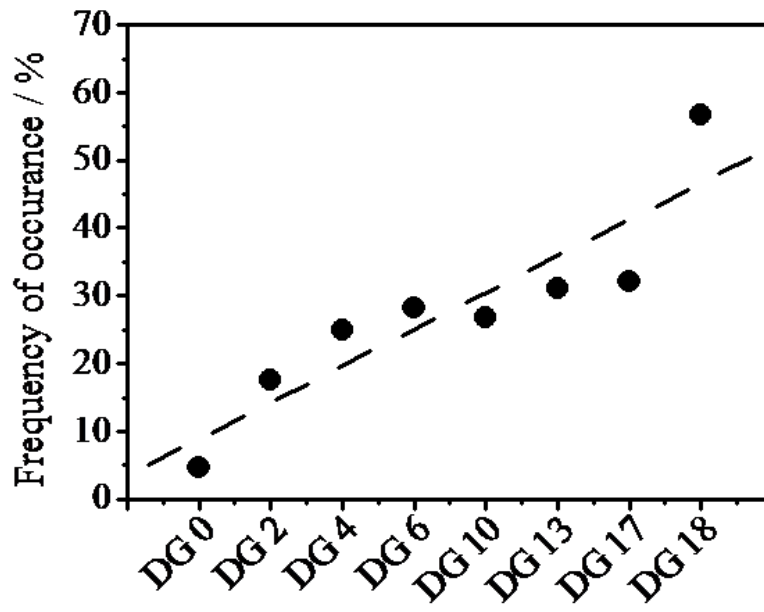


Figure S3. Development of the abundance of 200-500 nm large structural features with increasing glacier-soil distance.

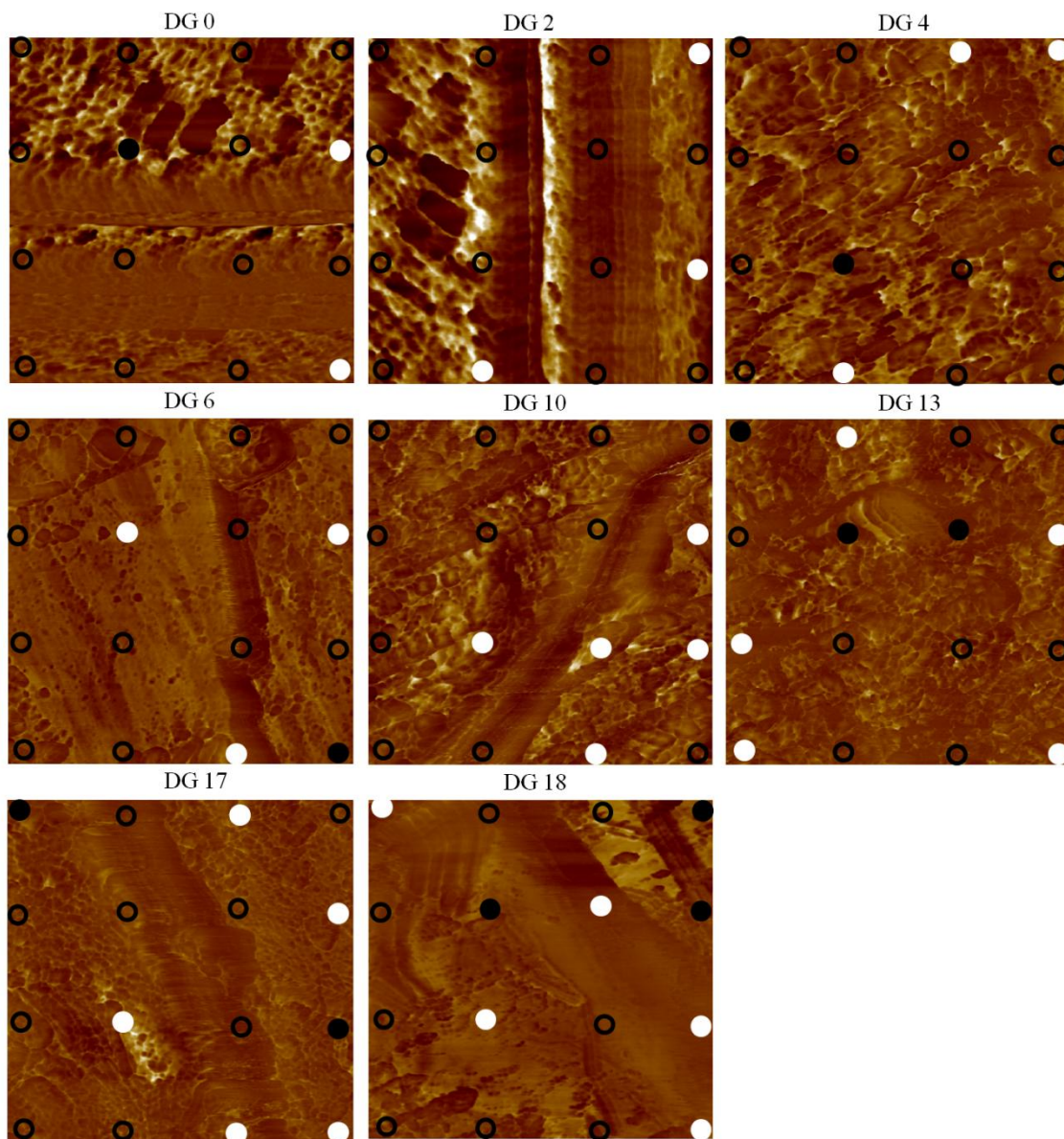


Figure S4. Distribution of thermogram types on the 4x4 grid on the adhesion images. Open, black and white circles represent type I, II and III thermograms, respectively. Color scale: darkest and lightest points correspond to force of 0 nN and 50 nN, respectively.

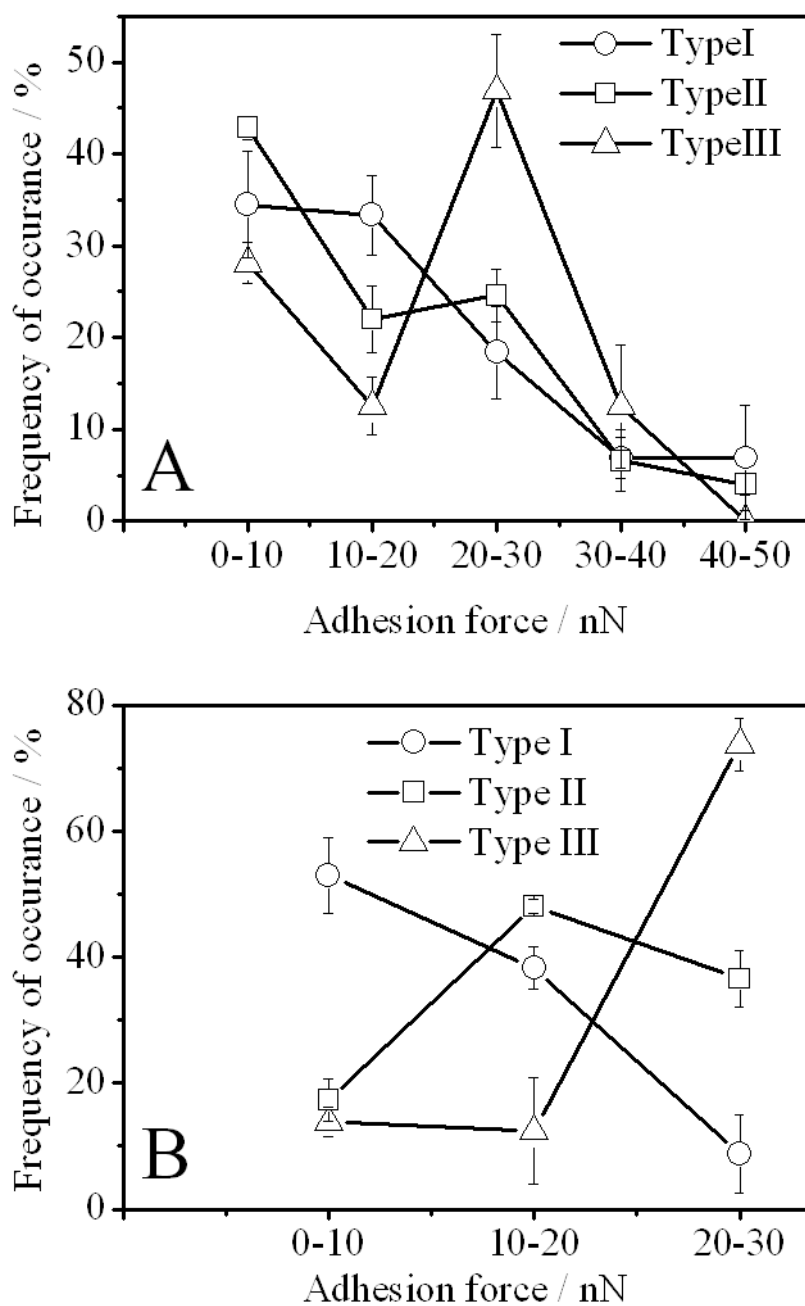


Figure S5. Relative abundance of thermogram types at locations with given adhesion force ranges given as percentages of the total abundance of each thermogram type, A) on the points along 4x4 grids on each AFM image and B) over the features of size 200 nm to 500 nm which were hypothesized to be potential candidates for microbial cell envelope fragments. Error bars show the ROI-ROI variability, across all soil samples.

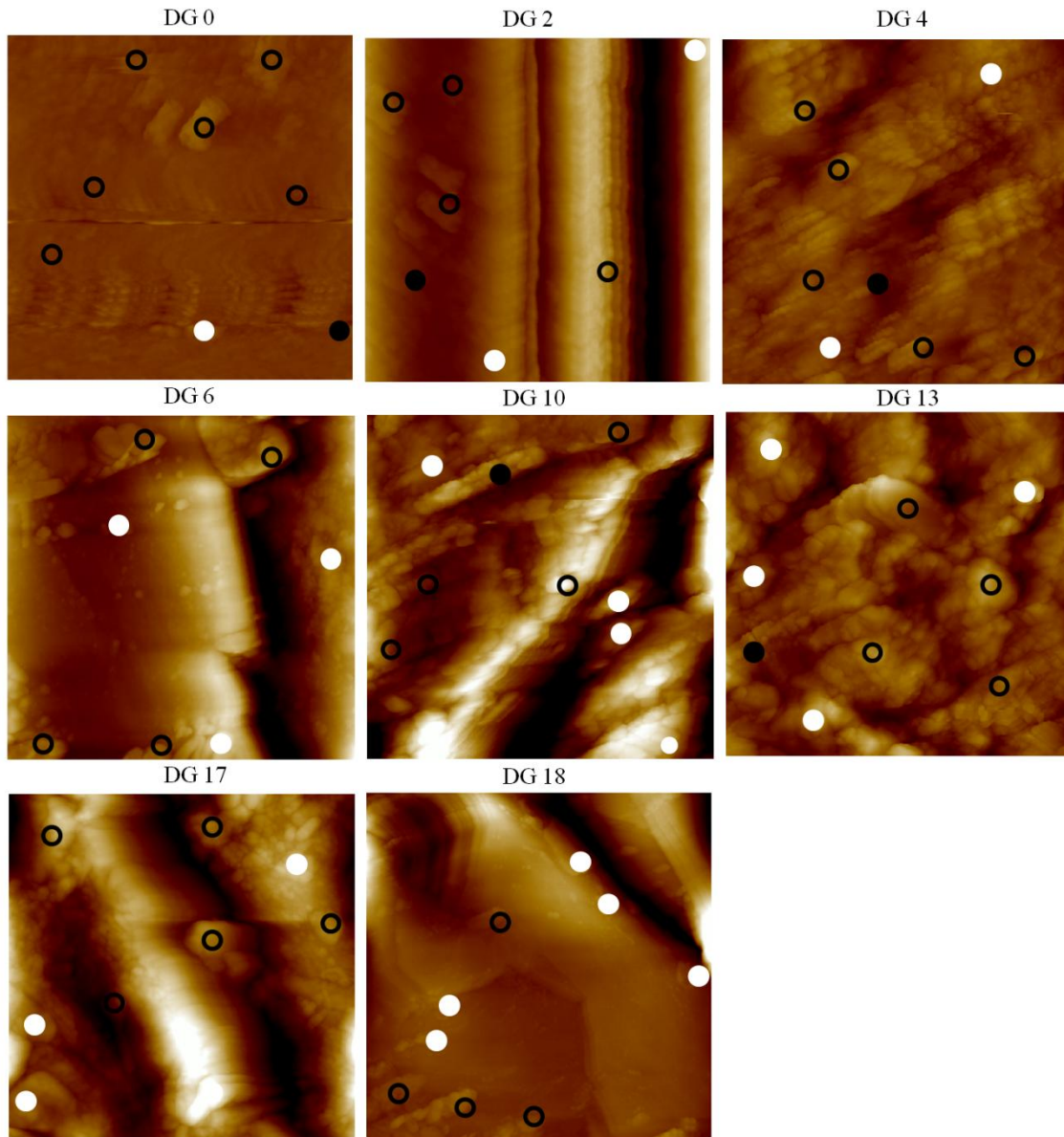


Figure S6. Distribution of thermogram types over features that were potential candidates for the hypothesized microbial fragments on height images. Open, black and white circles represent type I, II and III thermograms, respectively. Color scale: Darkest and lightest points correspond to depth of 80 nm and height of 80 nm, respectively, from the mean plane.

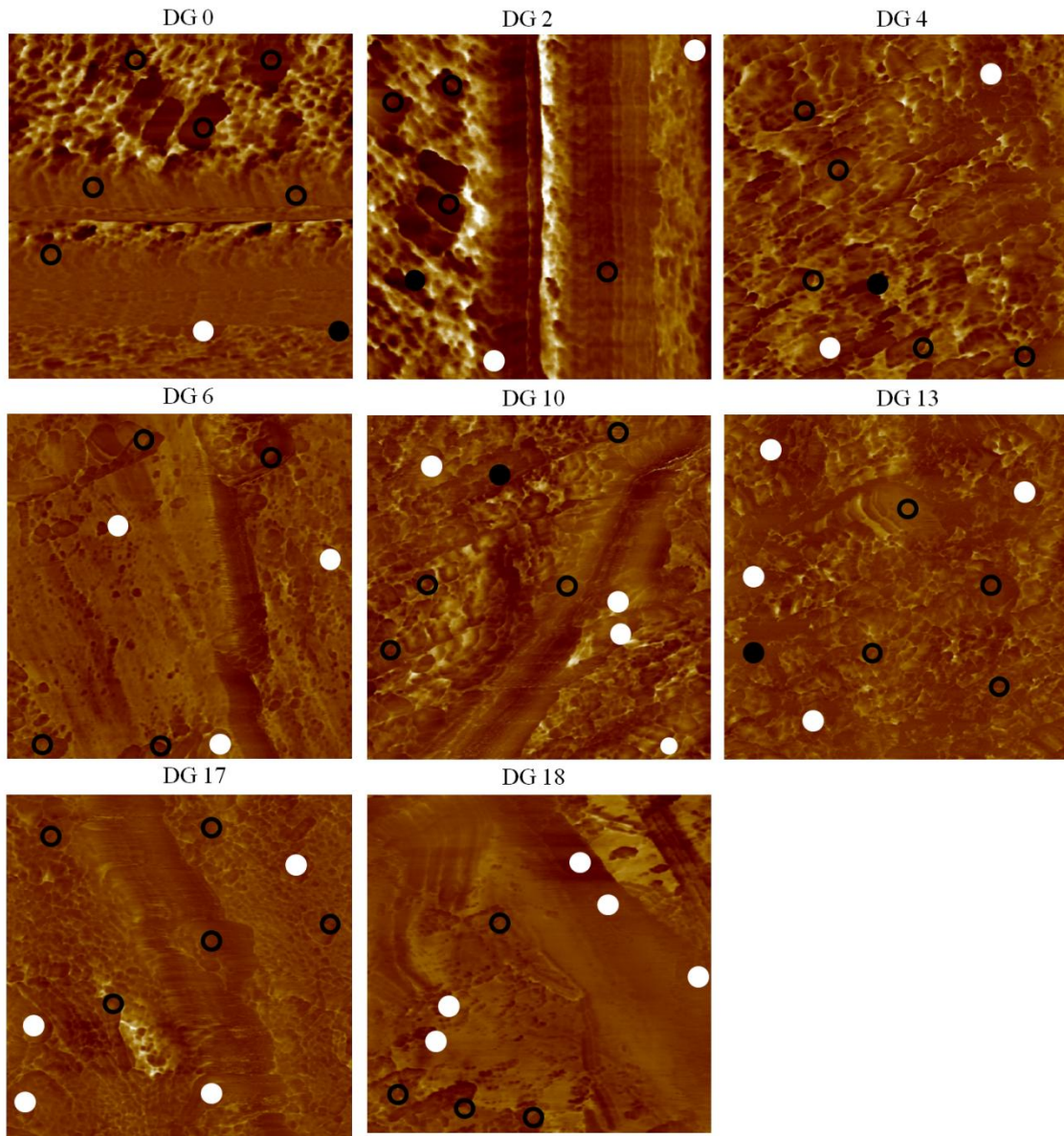


Figure S7. Distribution of thermogram types over adhesion images showing adhesive force for various material types. Open, black and white circles represent type I, II and III thermograms, respectively. Color scale: darkest and lightest points correspond to force of 0 nN and 50 nN, respectively.

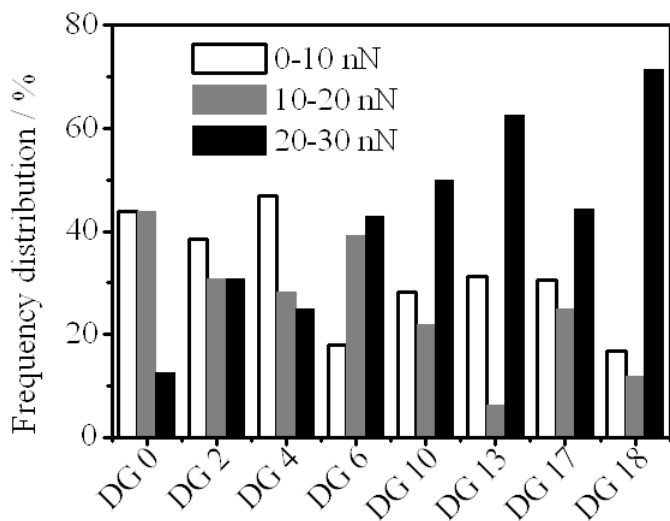


Figure S8. Development of adhesive force ranges revealed by selected features of 200 nm to 500 nm size, which were considered to be the potential candidates for microbial cell envelope fragments, with glacier-soil distance. The histograms were constructed over four replicate images per sample.

Annex III

List of abbreviations

AFM	atomic force microscopy
AFM-nTA	atomic force microscopy - nanothermal analysis
CA	contact angle
CaB	cation bridge
CEC	cation exchange capacity
CEC _{eff}	effective cation exchange capacity
DOC	dissolved organic carbon
DSC	differential scanning calorimetry
EDX	energy-dispersive X-ray spectroscopy
FA	fulvic acid
HA	humic acid
HPSEC	high pressure size exclusion chromatography
HS	humic substance
k	Langmuir coefficient
LPSEC	low pressure size exclusion chromatography
NMR	nuclear magnetic resonance
NOM	natural organic matter
OM	organic matter
PFQNM	peak force quantitative nanomechanical force mapping
Q _{max}	maximum sorbable amount in Langmuir sorption
R _a	average surface roughness
ROI	region of interest
SEM	Scanning electron microscopy
SOM	soil organic matter
T*	WaMB transition temperature
T ₂	spin-spin relaxation time
WaMB	water molecule bridges

Curriculum Vitae

Contact

Name: Yamuna Kunhi Mouvenchery
Address: Triftweg 23, 76829-Landau, Germany
Email: shyamayamuna@gmail.com
Telephone: 0049 6341 280 31574

Personal data

Date of birth: 07.03.1986
Place of birth: Peralassery, India
Nationality: Indian

Employment history

Date: October 2009 - present
Position: Scientific staff
Employer: Universität Koblenz-Landau, Landau, Germany

Date: August 2008 - October 2009
Position: Project assistant
Employer: National Chemical Laboratory, Pune, India

Education

Date: June 2006 – April 2008
Qualification: MSc. (Hydrochemistry)
University: Cochin University of Science and Technology, Kerala, India

Date: June 2003 – April 2006

Qualification: BSc. (Chemistry)

University: Kannur University, Kerala, India

Secondary school: Mambaram Higher Secondary School, Kerala, India

Year of school leaving: 2003

Publications

- Kunhi Mouvenchery, Y., Jäger, A., Aquino, A.J.A., Tunega, D, Diehl, D., Bertmer, M., Schaumann, G.E. (2013) Restructuring of a peat in interaction with multivalent cations: Effect of cation type and aging time. *PLoS ONE* 8(6): e65359. doi:10.1371/journal.pone.0065359.
- Shchegolikhina A; Kunhi Mouvenchery, Y; Woche, S.K; Bachmann, J; Schaumann, G.E; Marschner, B (2013). Cation treatment and drying temperatures effects on nonylphenol and phenanthrene sorption isotherms of a sandy soil. *Journal of Plant Nutrition and Soil Science*. 000: 1-9
- Kunhi Mouvenchery, Y; Miltner, A; Schurig, C; Kaestner, M; Schaumann, G.E (submitted 2013). Linking Atomic Force Microscopy with nanothermal analysis to assess microspatial distribution of materials in young soils. *Geochimica et Cosmochimica Acta*.
- Schaumann, G. E; Gildemeister, D; Kunhi Mouvenchery, Y; Diehl, D; Spielvogel (submitted 2013) Interactions between cations and water molecule bridges in soil organic matter. *Journal of Soils and Sediments*. 10.1007/s11368-013-0746-7
- Schaumann, G.E; Kunhi Mouvenchery, Y (2012) Potential of AFM-Nanothermal Analysis to study the microscale thermal characteristics in soils and natural organic matter (NOM). *Journal of Soils and Sediments*. 12.
- Kunhi Mouvenchery, Y; Kučerík, J; Diehl, D; Schaumann, G.E (2012) Cation-mediated cross-linking in natural organic matter - a review. *Reviews in Environmental Science and Bio/technology*. 11.
- Rieger, M; Schaumann, G. E; Kunhi Mouvenchery, Y; Reinhard, N; Seidel, M; Baumann, T (2012) Antibody-Labeled Nanoparticles for the Visualization of Surface-

immobilized Benzo[a]Pyrene Using NMR Relaxometry and Magnetic Resonance Imaging. *Journal of Analytical and Bioanalytical Chemistry*. 403.

Oral presentations

- Kunhi Mouvenchery, Y; Miltner, A; Schaumann, G.E. Nano and microspatial distribution of mineral and organic minerals in young soils as assessed by AFM-nanothermal analysis; SPP 1315 Annual Meeting 2012. Dornburg, Germany
- Kunhi Mouvenchery, Y; Miltner, A; Schaumann, G.E. Nanoscale thermal behaviour of microbially derived organic materials in soils: SPP 1315 Workshop 2012. Bayreuth, Germany

Poster presentations

- Kunhi Mouvenchery, Y; Schaumann, G.E. Development in proton mobility and organic matter quality during maturation of artificial soils. SPP1315 Annual Meeting 2012. Dornburg, Germany
- Kunhi Mouvenchery, Y; Schaumann, G.E. Are surface properties of microbes governing mineral-microbial interactions? SPP1315 Annual Meeting 2012. Dornburg, Germany
- Kunhi Mouvenchery, Y; Schaumann, G.E. AFM-Nanothermal Analysis to study the nano- and microscale thermal characteristics in soils and natural organic matter (NOM). SPP 1315 Annual Meeting 2011. Dornburg, Germany
- Kunhi Mouvenchery, Y; Schaumann, G.E. Water molecular bridges and cation bridges as validated by three different independent instrumental techniques- NMR, DSC and AFM-NTA. SPP 1315 Annual Meeting 2011. Dornburg, Germany
- Kunhi Mouvenchery, Y; Schaumann, G.E. Multivalent cations and soil organic matter- Effects of Reaction Conditions on Binding and on Properties of Resulting Complex. German Soil Science Society Annual Seminar 2011. Berlin, Germany
- Kunhi Mouvenchery, Y; Schaumann, G.E. Cross-linking Effects of Multivalent Cations on Soil Organic Matter. Conference “Co-Evolution of soil and organic substances” 2011. Landau. Germany